NATIONAL ADVISORY COMMITTEE FOR AERONAUTICS

TECHNICAL NOTE

No. 1304

WIND-TUNNEL INVESTIGATION OF THE BOUNDARY LAYER AND WAKE AND THEIR RELATION TO AIRFOIL CHARACTERISTICS - NACA 65_1-012 AIRFOIL WITH A TRUE CONTOUR FLAP AND A BEVELED-TRAILING-EDGE FLAP

By Robert A. Mendelsohn

Langley Memorial Aeronautical Laboratory
Langley Field, Va.

Washington

June 1947

NATIONAL ADVISORY COMMITTEE FOR AERONAUTICS

TECHNICAL NOTE NO. 1304

WIND-TUNNEL INVESTIGATION OF THE BOUNDARY LAYER AND WAKE AND THEIR RELATION TO AIRFOIL CHARACTERISTICS - NACA 65_1-012 AIRFOIL WITH A TRUE CONTOUR FLAP AND A BEVELED-TRAILING-EDGE FLAP

By Robert A. Mendelsohn

SUMMARY

Two-dimensional flow tests were conducted in the $2\frac{1}{2}$- by 6-foot test section of the Langley stability tunnel on an NACA 65_1-012 airfoil with a true contour flap and a beveled-trailing-edge flap to determine lift, drag, hinge moment, boundary layer, and wake characteristics. Lift and hinge-moment data are presented for various angles of attack and flap angles, and a limited amount of drag and pressure-distribution data is given. Measured velocity and static-pressure profiles at various positions on the airfoil and behind the trailing edge are presented. Theoretical boundary-layer parameters, computed from measured pressure distributions, are compared with the values determined from velocity profiles.

Measurements indicated that the static-pressure gradient through a boundary layer may be large in regions where the airfoil has a small radius of curvature and that a static-pressure rise exists at the vertical position of minimum wake velocity for a region just behind the trailing edge.

The theoretical and measured boundary-layer parameters were in good agreement except near the trailing edge. Methods for more accurately predicting the boundary layer in this region appear to be necessary before satisfactory estimations of hinge moments from calculated boundary layers may be made. There is also a possibility that estimates of profile drag based on the boundary-layer thickness at the trailing edge may be considerably in error because of failure of the theory to predict accurately the boundary layer at the trailing edge and because of failure to take into account the vertical static-pressure gradient of the wake.

INTRODUCTION

Because flap hinge moments are critically affected by boundary-layer conditions, it would be desirable to have reliable estimates of boundary-layer parameters before an attempt is made to determine their effect on hinge moments. The present investigation was made to obtain data on the boundary-layer characteristics in order to check the results against values computed from theory. In addition to determinations of boundary-layer velocity and static-pressure profiles, measurements were made of lift, profile drag, hinge moment, and pressure distribution. For comparison with test data, theoretical boundary-layer parameters are given for the same conditions as those used in several of the tests, measured pressure distributions being used for the calculations. For one model configuration, the theoretical vertical static-pressure gradient was also estimated.

SYMBOLS

The coefficients and symbols used are defined as follows:

c_l airfoil section lift coefficient (l/qc)

c_d airfoil section drag coefficient (d/qc)

c_h flap section-hinge-moment coefficient (h/qc_f^2)

P pressure coefficient at wing surface $\left(\frac{p - p_o}{q}\right)$

P' pressure coefficient in air stream $\left(\frac{p' - p_o}{q}\right)$

P'' pressure coefficient at edge of boundary layer or wake $\left(\frac{p'' - p_o}{q}\right)$

l section lift per unit span

d section drag per unit span

h flap section hinge moment, positive when tending to deflect flap downward

c chord of airfoil

c_f chord of flap behind hinge

q free-stream dynamic pressure $\left(\frac{\rho}{2} U_o^2\right)$

p static pressure at airfoil surface

p' static pressure in air stream

p'' static pressure at edge of boundary layer or wake

p_o free-stream static pressure

u local velocity

U velocity just outside boundary layer or wake

U_o free-stream velocity

ρ density of air

x distance from airfoil leading edge along chord line

y distance above airfoil surface or distance above projected chord line of flap when $\frac{x}{c} > 1.0$

δ' distance above surface to edge of boundary layer

α angle of attack

ϕ trailing-edge angle

δ flap deflection, positive downward

δ^*/c nondimensional displacement thickness $\left(\int_0^{\frac{\delta'}{c}} \left(1 - \frac{u}{U}\right) d\left(\frac{y}{c}\right)\right)$

θ/c nondimensional momentum thickness $\left(\int_0^{\frac{\delta'}{c}} \left[\frac{u}{U} - \left(\frac{u}{U}\right)^2\right] d\left(\frac{y}{c}\right)\right)$

$\overline{\theta}/c$ alternate definition of nondimensional momentum thickness $\left(\frac{\theta}{c} - \frac{1}{2}\left(\frac{U_o}{U}\right)^2 \int_0^{\frac{\delta'}{c}} (p' - p'') \, d\left(\frac{y}{c}\right)\right)$

H boundary-layer-shape parameter $\left(\frac{\delta^*/c}{\theta/c}\right)$

$\bar{H}$ alternate definition of boundary-layer-shape parameter $\left(\frac{\delta^*/c}{\bar{\theta}/c}\right)$

Subscripts:

U uncorrected value

l value at survey station

t tab

m one-half difference between upper- and lower-surface value

$c_{l_\alpha} = \left(\frac{\partial c_l}{\partial \alpha}\right)_\delta$

$c_{l_\delta} = \left(\frac{\partial c_l}{\partial \delta}\right)_\alpha$

$c_{h_\alpha} = \left(\frac{\partial c_h}{\partial \alpha}\right)_\delta$

$c_{h_\delta} = \left(\frac{\partial c_h}{\partial \delta}\right)_\alpha$

$c_{h_{\delta_t}} = \left(\frac{\partial c_h}{\partial \delta_t}\right)_{\alpha,\delta}$

The subscripts outside the parenthesis denote the variables held constant when the partial derivatives are taken.

APPARATUS AND MODELS

A 4-foot-chord airfoil model of NACA 65_1-012 contour was mounted in the $2\frac{1}{2}$- by 6-foot test section of the Langley stability tunnel as shown in figure 1. The airfoil completely spanned the test section and was sealed at the walls except for a gap of 1/16 inch on each side of the flap to allow freedom for hinge-moment measurements. The airfoil was made of laminated mahogany finished with paint and

sanded to an aerodynamic smoothness. Fitted in the upper surface only were a series of static pressure orifices. Two flaps were used with this airfoil; one having the original contour ($\phi = 6^\circ$) is referred to as the basic flap, and one having flat sides with a 25° bevel is referred to as the modified flap. (See fig. 2.) Both flaps had fabric seals. The flaps were connected by means of a shaft to a hinge-moment balance which was rotated for changes in flap deflection. Changes in angle of attack were accomplished by rotation of end disks in which the model was fitted.

Boundary-layer velocity and static-pressure profiles were measured by means of "mice" consisting of a number of total-pressure and static-pressure tubes of 0.040-inch outside-diameter hypodermic tubing. Three sizes of total-pressure mice were used, each consisting of six total-pressure tubes flattened to have an opening of 0.006 inch and each having the tubes spaced to survey a definite range above the airfoil surface. A static-pressure "mouse" consisting of six static-pressure tubes, spaced to measure the static-pressure profile from the surface to a point 2 inches above the surface, was used. Each of the tubes was calibrated against a tube for which the characteristics were known.

Wake profiles were measured with the mice mounted on an arm fastened to the flap as illustrated in figure 1(a). In order to reduce interference as much as possible, all rubber leads were brought straight back to a streamline strut mounted vertically behind the airfoil.

Boundary-layer transition was obtained at the desired location by means of transition strips glued to both the upper and lower airfoil surfaces. The strips were made of "Scotch" cellulose tape having, fixed to one side, a $\frac{1}{4}$-inch band of sawdust which had been filtered through a $\frac{1}{16}$-inch mesh screen.

Lift was measured by means of an integrating manometer connected to static orifices in the floor and ceiling of the tunnel.

TESTS

For the boundary-layer, wake, and static-pressure tests, the Langley stability tunnel was run at a dynamic pressure of 24.9 pounds per square foot which, for standard sea-level conditions, corresponded to a velocity of approximately 99 miles per hour and to a Reynolds number of approximately 3.68×10^6. Hinge-moment, lift, and drag tests were run at a higher dynamic pressure (39.7 pounds per square foot) in order to increase the forces so that greater accuracy could be

obtained. This dynamic pressure corresponds to a velocity of approximately 125 miles per hour and to a Reynolds number of 4.64×10^6.

The following table presents a summary of the tests made and the model configurations used:

Type of tests	α_U (deg)	δ (deg)	Location of transition
Boundary layer	0	0	Nose
Do	0	0	0.50c
Do	±6	0	Free
Do	0	±6	Nose
Force	Range	Range	Free

Because a symmetrical airfoil was used, measurements were made on only the upper surface, and the tests at a negative angle of attack or flap deflection were used as the equivalent of lower-surface measurements for positive angles of attack and flap angles.

In order to obtain velocities through the boundary layer as accurately as possible, static-pressure profile surveys were made in order that the static pressure corresponding to the actual position of the total-pressure tube above the airfoil surface could be used in the calculations. The total and static pressures in the boundary layer were measured relative to the total pressure in the free stream. The positions of the tubes above the surface were measured by means of a microscope which read to the nearest 0.001 inch. A tube-height correction was then applied for the effective center location as given in reference 1.

TUNNEL CORRECTIONS

Tunnel corrections were applied to only the angle-of-attack, hinge-moment, lift, and drag data. No corrections were applied to the pressure-distribution or boundary-layer data. Because the model chord was large compared with the tunnel height, it was found necessary to apply a correction to the angle of attack for lift caused by flap deflection. Thus, the hinge-moment and lift data, presented against flap deflection, are derived from cross plots and

are given without test-point symbols. The equations used in correcting the data are:

$$\alpha = 1.0915\ \alpha_U + 0.0068\ \delta \tag{1}$$

$$c_l = 0.8885\ c_{l_U} \tag{2}$$

$$c_d = 0.98\ c_{d_U} \tag{3}$$

$$c_h = c_{h_U} + 0.0181\ c_l \tag{4}$$

RESULTS AND DISCUSSION

In the discussion that follows, the airfoil with the true-contour ($\phi = 6^\circ$) flap will be referred to as the basic-flap model and the same airfoil with a beveled ($\phi = 25^\circ$) flap will be referred to as the modified-flap model.

Pressure distributions.- Before pressure-distribution tests were made, a boundary-layer survey revealed that transition occurred behind the theoretical minimum-pressure point for $\alpha_U = 0^\circ$, $\delta = 0^\circ$. This transition location was attributed to the low Reynolds number of the tests and to the low turbulence level of the tunnel. Since for the boundary-layer calculations that were to be made, it was necessary to know the position of transition, roughness strips were used to cause transition at a desired location for most of the test configurations.

Pressure distributions are given in figure 3 for several angle-of-attack and flap configurations. The pressure distribution for $\alpha_U = 0^\circ$, $\delta = 0^\circ$, basic-flap model, transition at 0.50c, (fig. 3(a)) shows good agreement with a theoretical curve computed by a method similar to that of reference 2. The theoretical pressures are somewhat lower near the leading edge and somewhat higher behind 0.60c than the test values. A distortion in the measured pressure distribution is caused by the flap gap. Movement of the transition tape to the leading edge had little effect on the pressure distribution for this model configuration.

A comparison of the pressure distributions for the basic-flap and modified-flap models indicates that, for all configurations

tested, the modified-flap model had a more negative static-pressure gradient from the hinge line to the bevel than the basic-flap model; behind the bevel, however, the static-pressure gradient was less negative.

Boundary-layer and wake profiles.- Static-pressure profiles for various positions along the airfoil and behind the trailing edge are presented in figures 4 to 13. The assumption of a constant static pressure through a boundary layer, used in most boundary-layer calculations, is shown to be closely approached except in regions where small radii of curvature exist, such as are found at 0.937c on the modified flap. (See fig. 9(k).)

With the assumption that, for small distances above the airfoil, the streamlines are concentric arcs and that changes in static pressure will be a function of the centrifugal force of air particles traversing a curved path, computations of the variation of static pressure with distance above the airfoil surface were made. Since this computation determined only the change in static pressure above the surface, the increments were subtracted from the values determined by the surface orifices, and these values are shown plotted in figure 4. For most positions the computed static-pressure gradients above the surface were almost the same as the measured gradients. Above the surface the measured pressures faired into the values determined from surface orifices except in regions where there existed a surface discontinuity or a high curvature.

Velocity profiles for various positions along the airfoil and behind the trailing edge are presented in figures 14 to 33. The velocity profiles at 0.021c for the conditions with transition tape at the leading edge (figs. 15, 18, 19, 25, 28, and 29) show that the tape has a marked effect on the local profile shape. The distortion is soon damped out, however, and a normal turbulent profile develops. Laminar separation is not indicated.

Just ahead of the flap gap for $\alpha_U = 0^\circ$, $\delta = -6^\circ$, with transition at the leading edge, the velocity close to the surface begins to decrease, then to increase again as the gap is passed. (See figs. 18 and 28.) Because of the negative pressure gradient, no separation has taken place and the boundary layer becomes more stable as it progresses rearward. For $\alpha_U = 0^\circ$, $\delta = 6^\circ$, however, although no separation is shown at the flap gap, the boundary layer becomes less stable as the trailing edge is approached because of the positive static-pressure gradient. On the modified flap, for all configurations except $\alpha_U = 0^\circ$, $\delta = 6^\circ$, the boundary layer behind the gap becomes more stable until the bevel is reached because of the favorable static-pressure gradient. Beyond the bevel, the

positive static-pressure gradient causes an approach to separation. The velocity profiles of the modified flap show a greater tendency toward separation than those of the basic flap, but in no case is separation indicated.

For $\alpha_J = 6^\circ$, $\delta = 0^\circ$ and for $\alpha_J = 0^\circ$, $\delta = 6^\circ$ (figs. 22, 23, 32, and 33) the velocity profiles behind the trailing edge show the rapid rise and spreading of the wake region as the distance is increased. Just behind the airfoil there is a rapid increase in the minimum velocity in the wake, and the profile gradually approaches a symmetrical shape.

The velocity profiles in the wake of both airfoils, for the angle of attack and flap-deflection configurations (figs. 22, 23, 32, and 33) indicate that, for positive angles of attack and flap angles, the velocity at the edge of the boundary layer of the upper surface was slightly higher than the velocity at the edge of the boundary layer of the lower surface. Similar results have been reported in reference 3 and do not necessarily indicate that infinite velocities occur around the trailing edge since the velocity profiles at the trailing edge show that the surface velocity is probably zero. Because of the difference in velocity between the upper and lower surface at the trailing edge, the wake curvature is believed to be affected. This curvature may be illustrated by figure 34, which is a plot of vertical position of minimum velocity in the wake against chordwise position x/c. The figure shows the rapid change in wake-center direction occurring close to the trailing edge. For both angle of attack and flap-deflection configurations, the wake center is shown to rise above a plane formed by the trailing edge and extending in the direction of the free stream.

Figure 35 is a plot of the static pressures at the vertical position of minimum velocity in the wake against chordwise position x/c. A static-pressure rise is indicated immediately behind the trailing edge for both the basic and modified flap. This rise was observed in the tests of reference 3 and for the zero-lift condition was attributed to "curvature of the streamlines which contract as they flow past the trailing edge." In a nonviscous fluid the maximum contraction of the streamlines flowing from the airfoil would occur at the trailing edge, but in a viscous fluid, because of the sudden reduction in skin friction as the air passes the airfoil, the maximum contraction of the streamlines occurs somewhat behind the trailing edge. Although this contraction of the streamlines behind the trailing edge would be associated with a pressure drop in accordance with Bernoulli's theorem, account must be taken of the fact that the air is changing direction rapidly, and requires a rise in pressure to balance the centrifugal forces. When the

airfoil is producing lift, the difference in velocity between the upper and lower surface at the edge of the boundary layer of the region behind the trailing edge apparently influences the wake curvature, and, consequently, causes a change in pressure rise as indicated by figures 34 and 35. The greater pressure rise from the modified flap than from the basic flap may be caused by the more rapid change of direction of the streamlines behind the trailing edge.

Boundary-layer parameters.- Figures 36 and 37 show a comparison between measured and theoretical boundary-layer parameters for both the basic and modified NACA 65_1-012 flap models. The boundary-layer parameters were computed from the measured-velocity profiles by the method given in the appendix. By using the measured pressure distributions, the theoretical results were obtained by a modification of the method of reference 4 for conditions with transition at the leading edge and by the method of reference 5 for other transition locations. The modification consisted in solving an integrated form of the equations of Gruschwitz and von Karman by an iteration process which accounted for the chordwise variation of skin friction. The following table summarizes the configurations presented and indicates the method used in calculating the boundary-layer parameters:

Flap	Condition		Assumed transition location	Reference for computation method
	α_U (deg)	δ (deg)		
Basic	-6	0	0.80c	5
Modified	-6	0	0.938c	5
Both	6	0	Nose	4
Both	0	-6	Nose	4
Both	0	6	Nose	4
Both	0	0	Nose	4
Both	0	0	0.50c	5

In the theoretical calculations the assumption was made that the nondimensional momentum thickness θ/c is continuous through the transition point, the value of H changes suddenly from a laminar to a turbulent value, and the nondimensional displacement thickness δ^*/c is discontinuous through the transition point.

For most of the model conditions, the computed values of δ^*/c and θ/c compare well with measured values forward of $x/c = 0.80$, the position of the flap gap. Behind the 0.80c position, several of the model configurations show large variations from theory. For the basic-flap model at $\alpha_U = 0^\circ$, $\delta = 6^\circ$ (fig. 36) with transition at the nose, the calculated values of the boundary-layer thickness are considerably smaller than the measured values behind the hinge. From the velocity profiles and the rapid increase in the value of H, it may be seen that separation is being approached. The boundary-layer parameters of the modified-flap model for the same airfoil configuration compare very well with theory until the bevel is reached, at which location the tests indicate separation tendencies. Although a very high value of H is reached (2.35), final separation is not shown by the velocity profiles at the trailing edge (fig. 33). Since reference 5 predicts separation when H reaches a value between 1.8 and 2.6, the possibility exists that the mouse tubes near the surface, which measure an average flow, will not always indicate when separation has taken place. The theoretical boundary layer on the lower surface for the same configuration compares well with the measured values except over the region between the hinge line and the bevel. For this region, tests indicate a thinner boundary layer than theory.

In general, a comparison of measured and theoretical boundary-layer parameters indicates that for sudden changes in pressure gradient or airfoil profile, large errors in computed boundary-layer characteristics are possible.

For both flaps, the assumed laminar value of H (equals 2.15 from reference 6) was not reached but, in general, the assumed turbulent value of H (equals 1.4 from reference 5) was reached. Although there is considerable scatter of the test points, in a favorable pressure gradient and for a turbulent boundary layer, the value of H appears to remain essentially constant. (See figs. 36 and 37.)

From the measurements at $\alpha_U = 0^\circ$, $\delta = 0^\circ$, transition at 0.50c, the value of H does not appear to change suddenly through the transition point even when transition is induced by a roughness strip. The change from laminar to turbulent profile seems to start some distance ahead of the tape and to become fully developed as the tape is reached. No measurements were made at the transition position because of the presence of the tape and measurements ahead and behind were too limited to get a quantitative indication of the transition range.

In order to get an indication of what is happening to the boundary layer beyond the trailing edge, the assumption was made

that the peak of the wake velocity-profile curves defined a line where the upper- and lower-surface boundary layers joined. Based on this assumption, a positive angle of attack or flap-deflection configuration on either basic or modified-flap model indicated an increase in the boundary-layer parameters for the lower-surface wake behind the trailing edge. This result is caused by a mixing action in which the lower energy air from the upper surface mingles with the air from the lower surface, which tends to make the wake patterns symmetrical. Because of this mixing action, no real dividing line exists between the upper- and lower-surface wake and defining a streamline in the wake region becomes difficult.

Profile drag.- Although the profile-drag coefficient should be unique for a given configuration regardless of the station at which a wake profile is measured, computations indicated that, if the wake-profile measuring plane was close to the trailing edge, various values could be obtained, depending upon the assumptions made in deriving the profile-drag equations. A summary of the computation methods used, the assumptions involved, and the profile-drag equation follows:

Method	Assumptions	Equation
1	Linear variation of H with $\log_e (U_o/U)$; no static-pressure gradient in wake (reference 8)	$c_d = \frac{2\theta_1}{c}\left(\frac{U}{U_o}\right)_1^{\frac{H_1+5}{2}}$
2	Linear variation of $\bar{H}$ with $\log_e (U_o/U)$ static-pressure gradient in wake (Developed from reference 3.)	$c_d = \frac{2\bar{\theta}_1}{c}\left(\frac{U}{U_o}\right)_1^{\frac{H_1+5}{2}}$
3	Nonlinear variation of $\bar{H}$ with $\log_e (U_o/U)$ static-pressure gradient in wake (Developed from reference 8.)	$c_d = \frac{2\bar{\theta}_1}{c}\left(\frac{U}{U_o}\right)_1^{\bar{H}_1+2} (\Theta) \int_{1.0}^{\bar{H}_1} \log_e\left(\frac{U_o}{U}\right) d\bar{H}$
4	Melville Jones' wake method (reference 7)	$c_d = 2\int_{-\frac{\delta'}{c}}^{\frac{\delta'}{c}} \frac{u}{U_o}\left[1 - \sqrt{\left(\frac{u}{U_o}\right)^2 + P'}\right] d\left(\frac{y}{c}\right)$

The results obtained by the various methods are shown in table I.

In reference 8 a linear relation between $\log_e U_o/U$ and H, based on a very limited amount of test data (three test points), is used to relate the profile drag to the boundary layer and local velocity near the trailing edge. This equation is

$$c_d = 2\frac{\theta_1}{c}\left(\frac{U}{U_o}\right)_1^{\frac{H_1+5}{2}} \tag{5}$$

Figure 38 presents a plot of the relation $\log_e \frac{U_o}{U}$ against H for both the basic- and modified-flap model for various model configurations. Shown in the figure is a line representing a linear relation of the function from the trailing edge to infinity, assumed in reference 8 to obtain equation (5). The present data indicate nonlinearity of the curves, especially in the region close to the trailing edge (high values of H). This nonlinearity in the trailing-edge region is believed to be a function of the pressure rise previously described. Since equation (5), which is used in calculating profile drag of an airfoil by estimating the boundary layer at the trailing edge from theoretical considerations, assumes a linear relation between $\log_e \frac{U_o}{U}$ and H, further tests of flow characteristics existing in this region appear to be desirable.

Table I presents the estimated profile-drag coefficients of the basic and modified-flap model for several model configurations calculated from wake-velocity profiles at several positions behind the trailing edge. The drags calculated by equation (5) show large variations with distance from the trailing edge because of static-pressure gradients in the wake. This difficulty was pointed out in reference 8, and an alternate definition of the nondimensional momentum thickness θ/c and shape parameter H was given in appendix III of reference 8 which accounted for the static-pressure gradient. Thus,

$$\frac{\bar{\theta}}{c} = \frac{\theta}{c} - \frac{1}{2}\left(\frac{U_o}{U}\right)^2 \int_0^{\frac{\delta'}{c}} (P' - P'')\, d\left(\frac{y}{c}\right) \tag{6}$$

$$\bar{H} = \frac{\delta^*/c}{\bar{\theta}/c} \tag{7}$$

Table I shows that application of these alternate definitions considerably reduces the variation of computed drag coefficient with distance of wake measurement from the trailing edge.

In view of the nonlinearity of the relation between $\log_e \frac{U_o}{U}$ and H as pointed out previously, drag coefficients were calculated by use of the measured variation of the velocity function from the following relation:

$$c_d = 2\frac{\bar{\theta}_1}{c}\left(\frac{U}{U_o}\right)_1^{\bar{H}_1+2(e)} \int_{1.0}^{\bar{H}_1} \log_e\left(\frac{U_o}{U}\right) d\bar{H} \qquad (8)$$

Also, drag coefficients were computed by the Melville Jones' method (reference 7). Though considerable variation of drag coefficient with distance from the trailing edge is still present, because of the inaccuracies in the method of measuring wake patterns in two parts, no great increase in accuracy appears to be obtained by the use of equation (8). A comparison of the drag coefficients calculated by the alternate definition of the boundary-layer parameters with those computed by the Melville Jones' method indicates that, for angle of attack and aileron-deflection configurations, the drag will be overestimated for measurements near the trailing edge. Some of this variation may be caused by the difficulty in determining accurately the velocity at the edge of the boundary layer.

This investigation indicates that for profile-drag determinations, measurements very close to the body should be avoided and that, in using equations which relate the profile drag to the measured boundary-layer or wake characteristics near the trailing edge, the static-pressure gradient should be taken into account. In addition, a theoretical calculation of profile drag which involves an estimation of the boundary-layer thickness at the trailing edge could be considerably in error because of the failure to take the vertical static-pressure gradient into account and because of the possibility, as discussed in the section on boundary-layer parameters, that theory will fail to predict accurately the boundary layer at the trailing edge.

Force and hinge-moment data.- Force and hinge-moment data for the basic-flap model and the modified-flap model are presented in figures 39 to 41 for the free-transition condition. A summary of hinge-moment and lift parameters measured from these data are as follows:

Flap	C_{h_α}	C_{h_δ}	C_{l_α}	C_{l_δ}
Basic	-0.0047	-0.0111	0.107	0.058
Modified	.0048	-.0047	.093	.044

With free transition, the minimum profile drag of both the basic- and the modified-flap model is the same since transition occurs at the same position for both flaps. With change in lift coefficient, however, the modified-flap model has the greater profile drag.

The basic-flap model has a considerably higher lift-curve slope than the modified-flap model because of the large difference in trailing-edge angle. This trailing-edge-angle effect on the model characteristics may be considered to be caused by local changes in effective mean-line camber brought about by the fact that the boundary layer over the upper surface is different from that over the lower surface. Figure 42, which is a plot of the effective-mean line δ^*_m/c against position x/c, indicates that the modified flap has a greater effective-camber change near the trailing edge than the basic flap. This effective-camber change causes the bevel to act as a balancing tab for small changes in angle of attack or flap deflection; thus, a reduction is obtained in the variations in lift and in hinge moment with angle of attack or with flap deflection. (See figs. 39 to 41.) At large positive flap deflections, however, separation of the boundary layer occurs ahead of the bevel on the upper surface, and on the lower surface the boundary layer is very thin. The balancing effect of the upper-surface bevel is consequently lost and the balancing effect of the lower-surface bevel acts like a trim tab, as shown by the fact that the slope of the hinge-moment curve of the modified flap approaches that of the basic flap. The hinge-moment curves for both the basic and modified flap fail to pass through the origin because of inaccuracies in construction of the models. After tests were completed the basic-contour flap was found to have a slight upward curvature near the trailing edge and the modified flap was found to have 0.8° upward deflection of the bevel center line.

On the assumption that δ^*_m/c (see fig. 42) defined changes in mean-line shape which would cause experimental hinge moments to differ from those computed by thin-airfoil theory, hinge moments were estimated from figure 42 by use of an extension of reference 9. These calculations indicated that a considerable improvement in boundary-layer theory will be necessary before satisfactory estimations of flap characteristics will be possible, since departures

of flap characteristics from perfect-fluid theory are primarily caused by the boundary layer. Not only must the magnitude of the boundary-layer parameters be accurately predicted, but the rates of change in the magnitude of these boundary-layer parameters along the surface must also be accurately predicted because the flap hinge-moment characteristics are dependent on these rates of change.

CONCLUDING REMARKS

Measurements obtained from two-dimensional tests of the NACA 65_1-012 airfoil indicated that the static-pressure gradient through the boundary layer may be large in regions where the airfoil has a small radius of curvature, and a static-pressure rise at the vertical position of minimum wake velocity for some section just behind the trailing edge is shown to exist. For increase in angle of attack and flap deflection, the pressure rise behind the trailing edge was shown to increase.

Good agreement between measured boundary-layer characteristics and those calculated from measured pressure distributions was obtained for positions ahead of the flap hinge. Behind the flap hinge the agreement between measured boundary-layer characteristics and those calculated from measured pressure distributions was not so good. Because the discrepancy between measured and calculated boundary-layer parameters is greatest in the region near the trailing edge where the effect on hinge moments is the greatest, methods for more accurately predicting the boundary layer in this region appear to be necessary before satisfactory estimations of hinge moments from calculated boundary layers may be made.

In the equations which relate the profile drag to the measured boundary-layer or wake characteristics near the trailing edge the static-pressure gradient should be taken into account.

A theoretical calculation of profile drag, which involves an estimation of the boundary-layer thickness at the trailing edge, could be considerably in error because of failure of the theory in

accurately predicting the boundary layer at the trailing edge and because of the failure to take the vertical static-pressure gradient into account.

Langley Memorial Aeronautical Laboratory
National Advisory Committee for Aeronautics
Langley Field, Va., January 15, 1947

APPENDIX

SUGGESTED METHOD OF DETERMINING BOUNDARY-LAYER PARAMETERS FROM VELOCITY PROFILES BY THE USE OF A MECHANICAL INTEGRATOR

A graphical method of determining boundary-layer parameters directly from measured-velocity profiles is presented. This method was found convenient because of the great amount of labor that may be saved in determining both δ^*/c and θ/c from one plot. Since the method involves taking the difference between a moment and an area as determined by a mechanical integrator, a large-scale plot should be used to obtain satisfactory accuracy. A typical boundary-layer profile is illustrated in the following sketch:

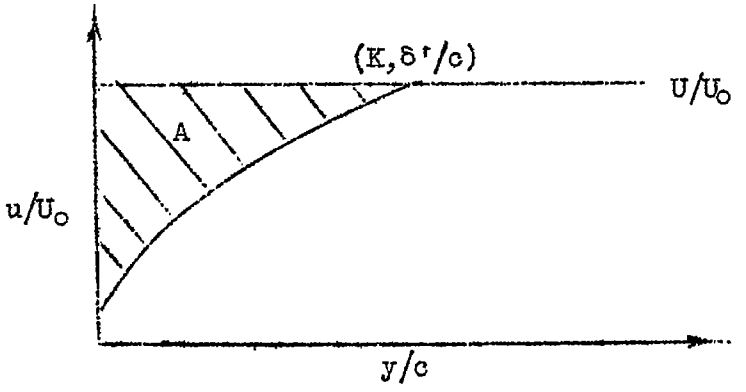

The method necessitates finding the shaded area shown in the sketch, and its moment with respect to the axis y/c. Inasmuch as

$$\frac{\delta^*}{c} = \int_0^{\frac{\delta'}{c}} \left(1 - \frac{u}{U}\right) \, d\left(\frac{y}{c}\right)$$

and $K = \frac{U}{U_o}$, then

$$\frac{\delta^*}{c} = \frac{1}{K} \int_0^{\frac{\delta'}{c}} \left(K - \frac{u}{U_o} \right) \, d\left(\frac{y}{c}\right)$$

$$\frac{\delta^*}{c} = \frac{A}{K}$$

where A is the shaded area of figure. Also, since

$$\frac{\theta}{c} = \int_0^{\frac{\delta'}{c}} \left[\frac{u}{U} - \left(\frac{u}{U}\right)^2 \right] \, d\left(\frac{y}{c}\right)$$

$$\frac{\theta}{c} = \int_0^{\frac{\delta'}{c}} \left[\frac{K^2 - \left(\frac{u}{U_o}\right)^2}{K^2} - \frac{K - \left(\frac{u}{U_o}\right)}{K} \right] \, d\left(\frac{y}{c}\right)$$

$$\frac{\theta}{c} = \int_0^{\frac{\delta'}{c}} \left[\frac{K^2 - \left(\frac{u}{U_o}\right)^2}{K^2} \right] \, d\left(\frac{y}{c}\right) - \frac{A}{K}$$

Now, if the moment of the shaded area is taken about the y/c axis,

$$M = \int_0^{\frac{\delta'}{c}} \left(K - \frac{u}{U_o} \right) \, \frac{K + \left(\frac{u}{U_o}\right)}{2} \, d\left(\frac{y}{c}\right)$$

where M is moment of shaded area or

$$M = \int_0^{\frac{\delta'}{c}} \frac{K^2 - \left(\frac{u}{U_o}\right)^2}{2} \, d\left(\frac{y}{c}\right)$$

Therefore, by substitution:

$$\frac{\theta}{c} = \frac{2M}{K^2} - \frac{A}{K}$$

REFERENCES

1. Young, A. D., and Maas, J. N.: The Behaviour of a Pitot Tube in a Transverse Total-Pressure Gradient. R. & M. No. 1770, British A.R.C., 1937.

2. Theodorsen, Theodore: Theory of Wing Sections of Arbitrary Shape. NACA Rep. No. 411, 1931.

3. Preston, J. H., and Sweeting, N. E.: The Experimental Determination of the Boundary Layer and Wake Characteristics of a Simple Joukowski Aerofoil, with Particular Reference to the Trailing-Edge Region. R. & M. No. 1998, British A.R.C., 1943.

4. Gruschwitz, E., Die turbulente Riebungsschicht in ebener Stromung bei Druckabfall und Druckansteig. Ing.- Archiv, Bd. II, Heft 3, Sept. 1931, pp. 321-346.

5. von Doenhoff, Albert E., and Tetervin, Neal: Determination of General Relations for the Behavior of Turbulent Boundary Layers. NACA ACR No. 3G13, 1943.

6. Dryden, Hugh L.: Computation of the Two-Dimensional Flow in a Laminar Boundary Layer. NACA Rep. No. 497, 1934.

7. The Cambridge University Aeronautics Laboratory: The Measurement of Profile Drag by the Pitot-Traverse Method. R. & M. No. 1688, British A.R.C., 1936.

8. Squire, H. B., and Young, A. D.: The Calculation of the Profile Drag of Aerofoils. R. & M. No. 1838, British A.R.C., 1938.

9. Perring, W. G. A.: The Theoretical Relationships for an Aerofoil with a Multiply Hinged Flap System. R. & M. No. 1171, British A.R.C., 1928.

TABLE I

SECTION DRAG COEFFICIENTS CALCULATED BY VARIOUS METHODS[1]

Station x/c	Basic-flap model, c_d				Modified-flap model, c_d			
	1	2	3	4	1	2	3	4
	$\alpha_U = 0°$; $\delta = 0°$; Transition at 0.50c							
1.000	0.0065	0.0057	0.0058	0.0060	0.0086	0.0062	0.0065	0.0065
1.013	.0062	.0054	.0054	.0057	.0078	.0067	.0068	.0064
1.025	.0062	.0056	.0056	.0059	.0074	.0064	.0065	.0067
1.050	.0057	.0056	.0056	.0057	.0067	.0063	.0063	.0064
1.100	.0056	.0054	.0054	.0056	.0062	.0062	.0062	.0064
	$\alpha_U = 0°$; $\delta = 0°$; Transition at leading edge							
1.000	0.0104	0.0098	0.0098	0.0097	0.0124	0.0100	0.0102	0.0098
1.013	.0112	.0103	.0103	.0099	.0122	.0101	.0102	.0101
1.025	.0107	.0102	.0101	.0099	.0115	.0103	.0103	.0100
1.050	.0101	.0098	.0098	.0097	.0101	.0095	.0095	.0100
1.100	.0097	.0096	.0095	.0092	.0096	.0093	.0093	.0094
	$\alpha_U = 0°$; $\delta = 6°$; Transition at leading edge							
1.000	0.0121	0.0118	0.0118	0.0114	0.0138	0.0130	0.0133	0.0118
1.013	.0125	.0122	.0122	.0113	.0133	.0123	.0125	.0115
1.025	.0126	.0124	.0124	.0118	.0129	.0122	.0122	.0113
1.050	.0119	.0118	.0117	.0113	.0120	.0117	.0117	.0105
1.100	.0114	.0116	.0112	.0110	.0098	.0097	.0097	.0101
	$\alpha_U = 6°$; $\delta = 0°$; Transition free							
1.000	0.0119	0.0115	0.0116	0.0111	0.0132	0.0123	0.0126	0.0111
1.013	.0111	.0108	.0107	.0103	.0122	.0114	.0116	.0107
1.025	.0113	.0112	.0111	.0108	.0122	.0115	.0116	.0109
1.050	.0111	.0110	.0110	.0106	.0109	.0106	.0106	.0101
1.100	.0102	.0101	.0101	.0104	.0106	.0103	.0103	.0105

[1]Method 1: $c_d = \frac{2\theta_1}{c}\left(\frac{U}{U_o}\right)_1^{\frac{H_1+5}{2}}$ (reference 8)

Method 2: $c_d = \frac{2\bar{\theta}_1}{c}\left(\frac{U}{U_o}\right)_1^{\frac{\bar{H}_1+5}{2}}$ (developed from reference 8)

Method 3: $c_d = \frac{2\bar{\theta}_1}{c}\left(\frac{U}{U_o}\right)_1^{\bar{H}_1+2}(e)^{\int_{1.0}^{\bar{H}_1}\log_e(U_o/U)d\bar{H}}$ (developed from reference 8)

Method 4: Jones' method (reference 7)

NATIONAL ADVISORY
COMMITTEE FOR AERONAUTICS

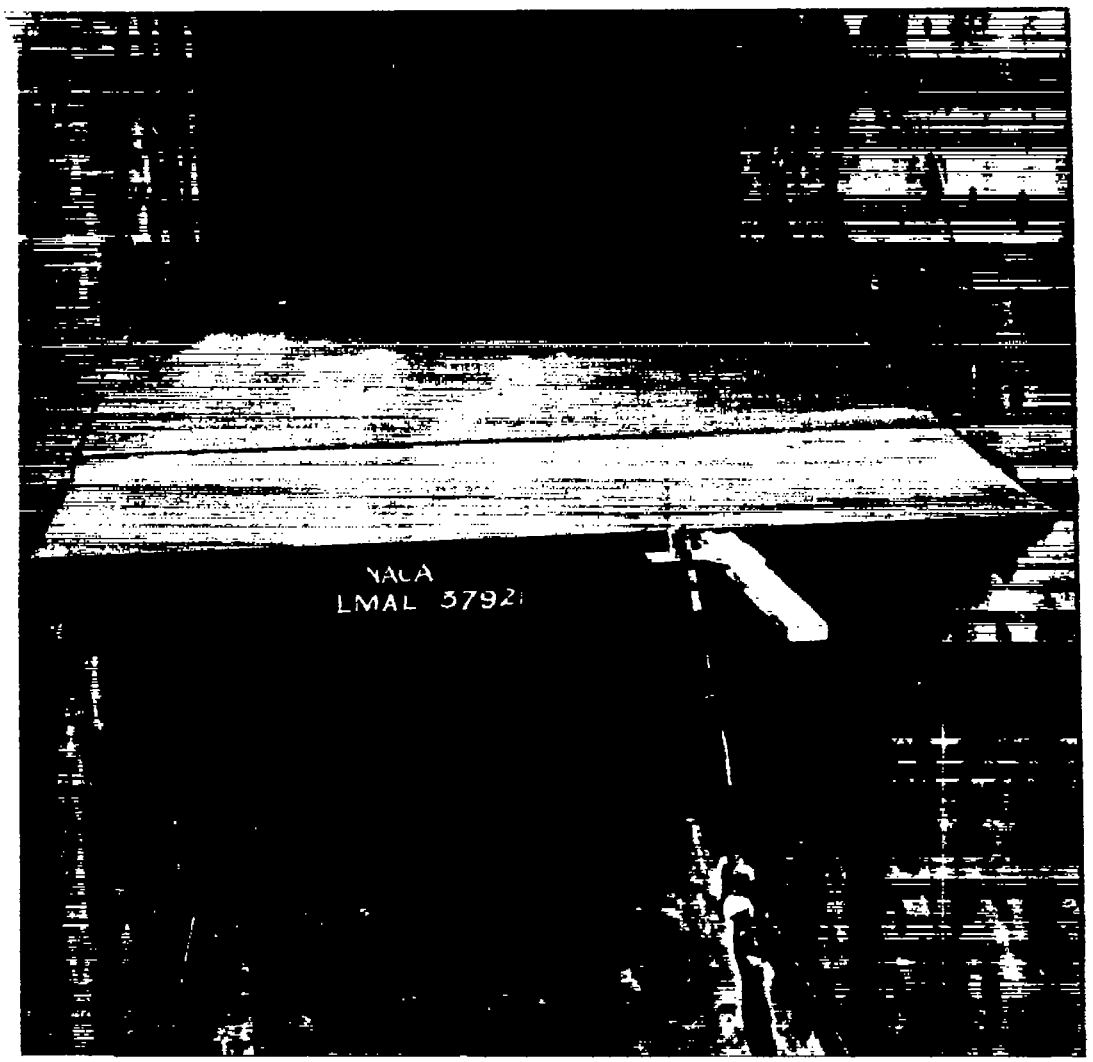

(a) Rear view.

Figure 1.- View of the NACA 65_1-012 airfoil model showing method of mounting mice. Basic-flap contour.

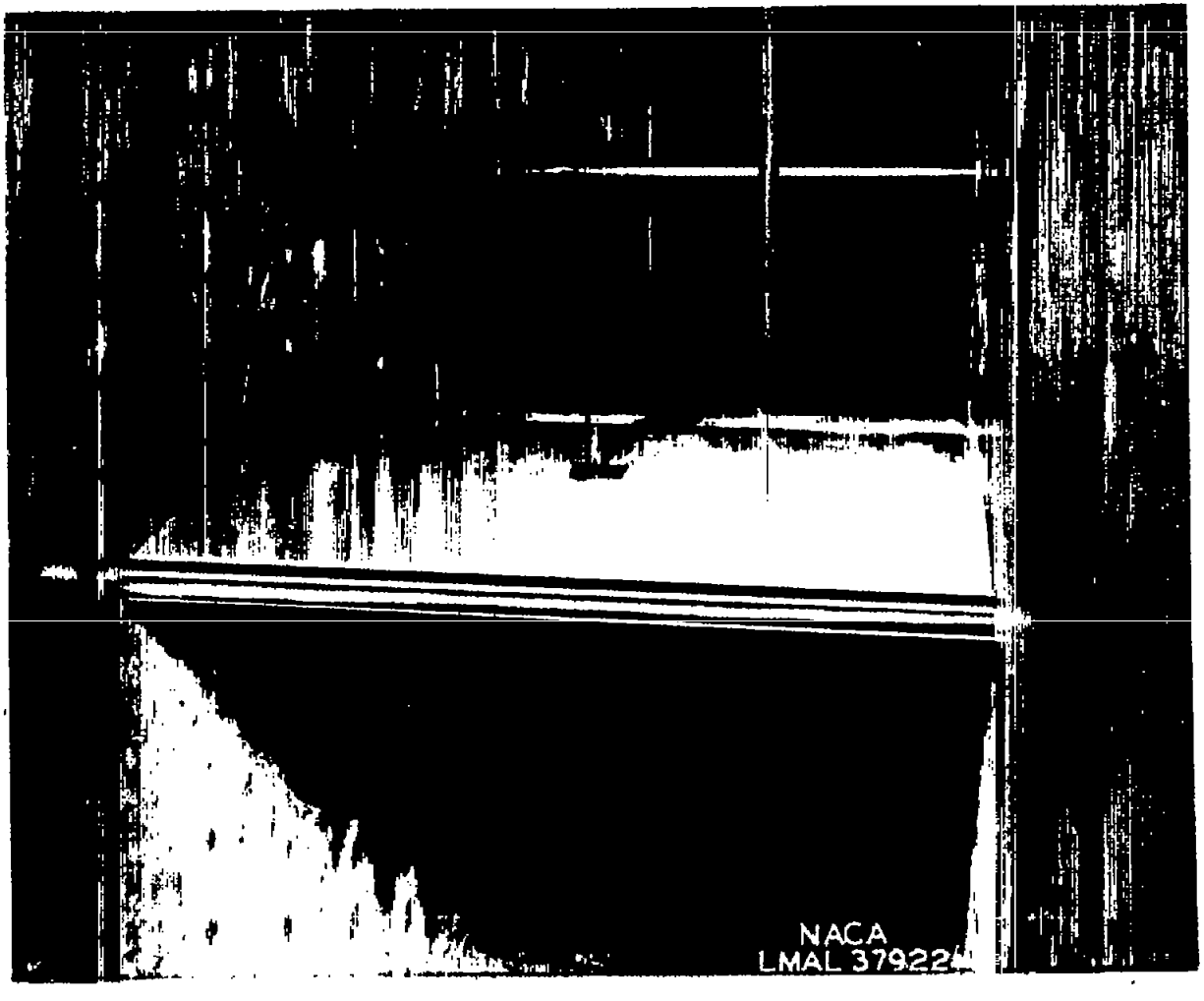

(b) Front view showing transition strips.

Figure 1.- Concluded.

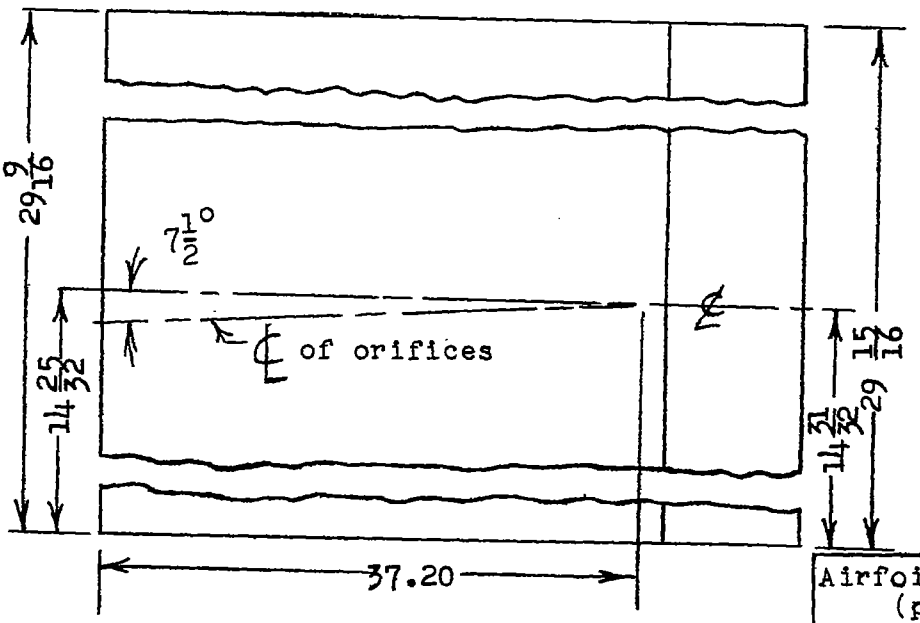

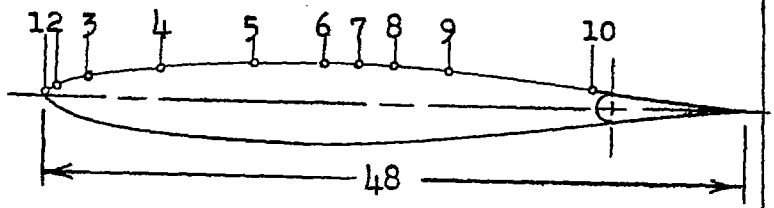

Orifice	Station
1	.17
2	2.08
3	6.29
4	16.76
5	30.02
6	40.05
7	45.00
8	50.00
9	57.45
10	77.55

NATIONAL ADVISORY
COMMITTEE FOR AERONAUTICS

Airfoil ordinates (percent c)	
Station	Ordinate
0	0
.5	.923
.75	1.109
1.25	1.387
2.5	1.875
5.0	2.606
7.5	3.172
10.	3.647
15.	4.402
20.	4.975
25.	5.406
30.	5.716
35.	5.912
40.	5.997
45.	5.949
50.	5.757
55.	5.412
60.	4.943
65.	4.381
70.	3.743
75.	3.059
80.	2.345
85.	1.630
90.	.947
95.	.356
100.	0

(a) Airfoil contour.

Figure 2.- Dimensions and pressure-orifice locations for the NACA 65_1-012 airfoil.

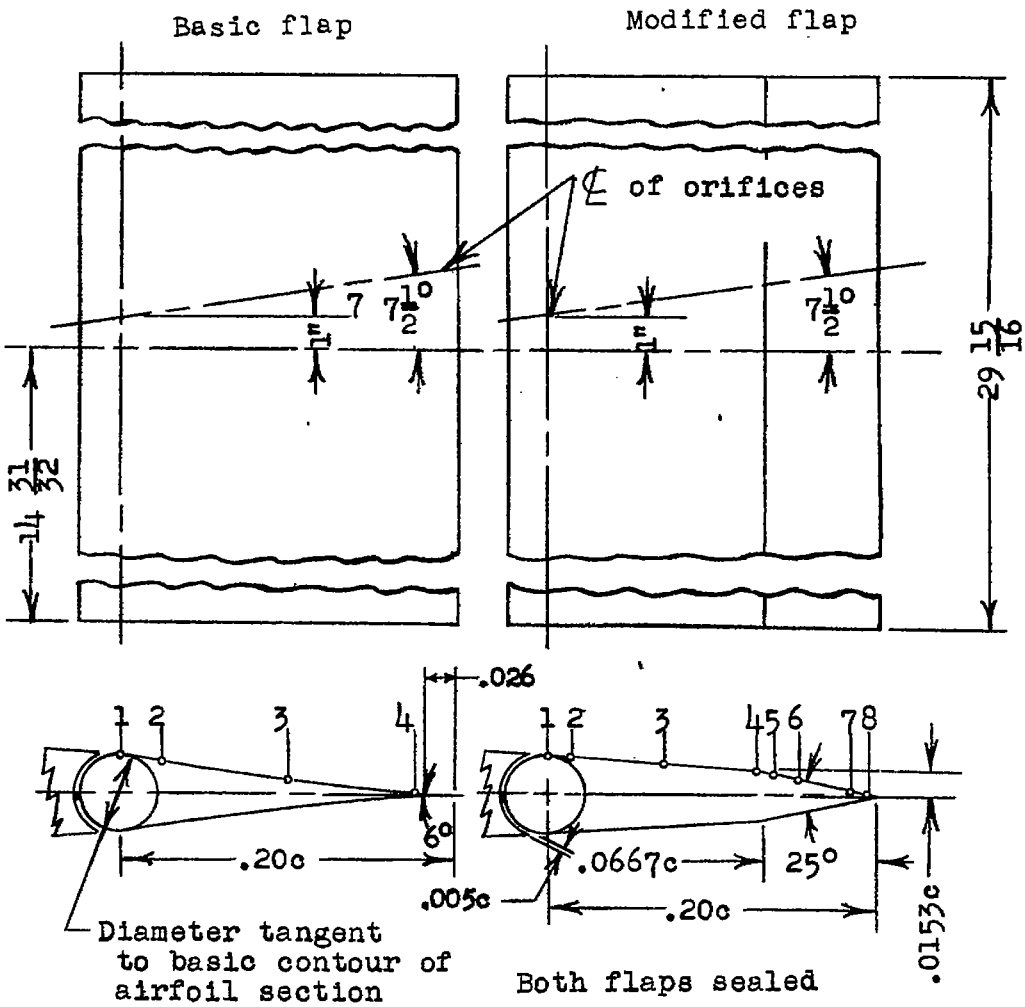

Orifice	Station from airfoil L. E. (percent c)
1	80.10
2	82.60
3	90.05
4	97.85

Orifice	Station from airfoil L.E. (percent c)
1	79.95
2	81.30
3	87.00
4	92.50
5	93.70
6	95.00
7	97.90
8	99.50

NATIONAL ADVISORY COMMITTEE FOR AERONAUTICS

(b) Flap contour.

Figure 2.- Concluded.

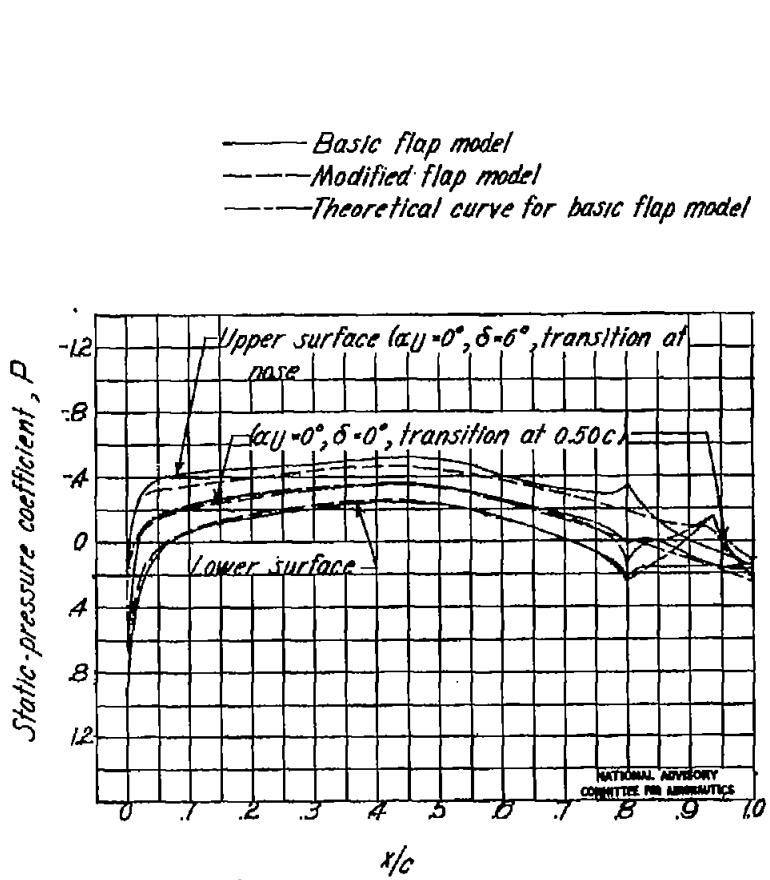

(a) $\alpha = 0^{\circ}$.

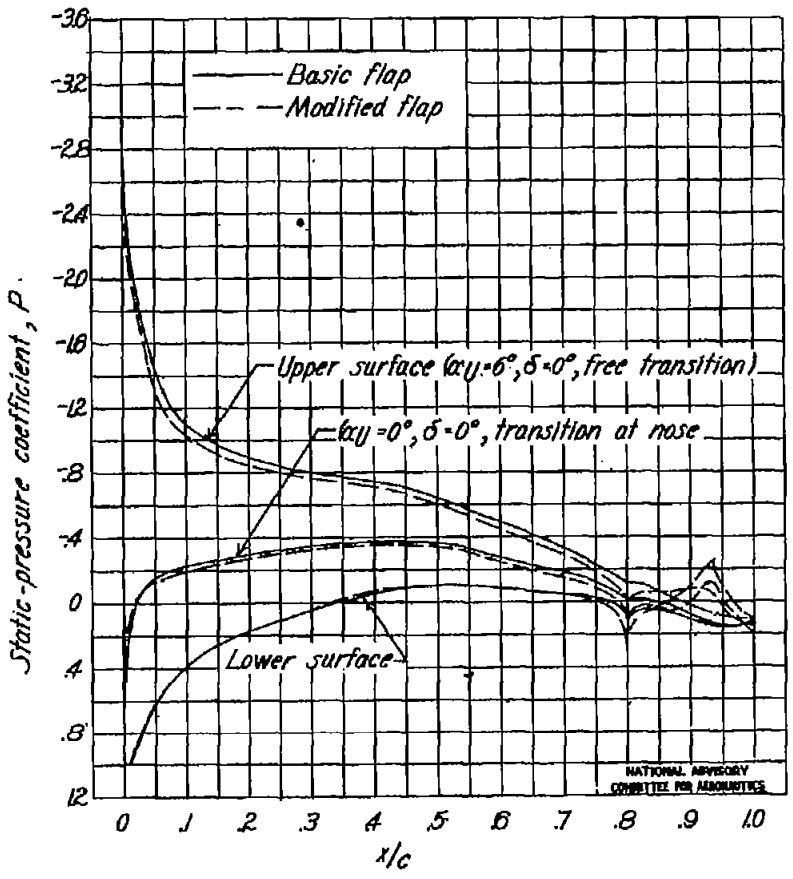

(b) $\delta = 0^{\circ}$.

Figure 3.- Pressure distributions over the NACA 65_1-012 airfoil with a basic and a modified flap.

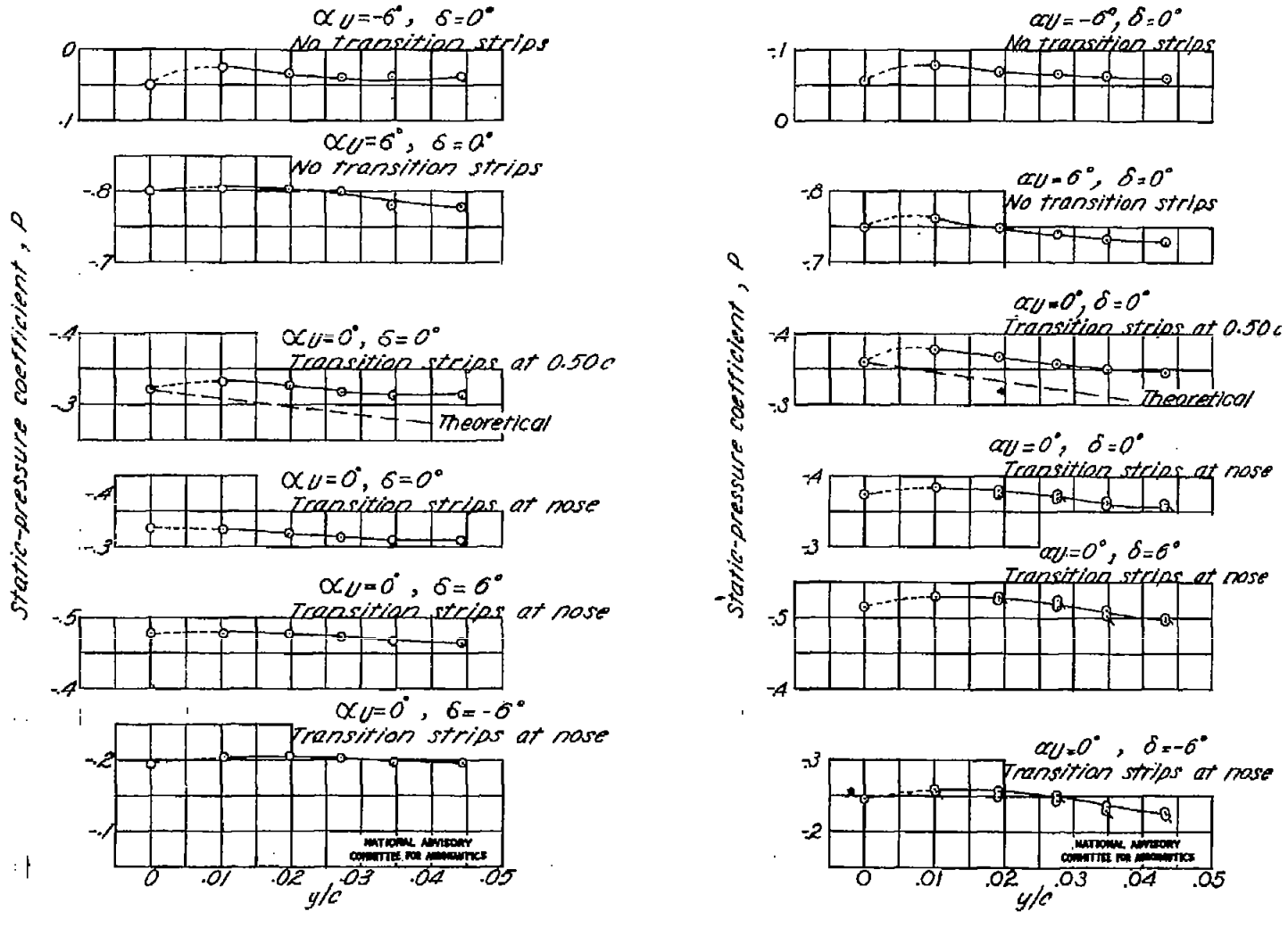

(a) $\frac{x}{c}$ = 0.300.

(b) $\frac{x}{c}$ = 0.400.

Figure 4.- Static-pressure profiles for the NACA 65_1-012 airfoil at various model configurations. Basic-flap contour.

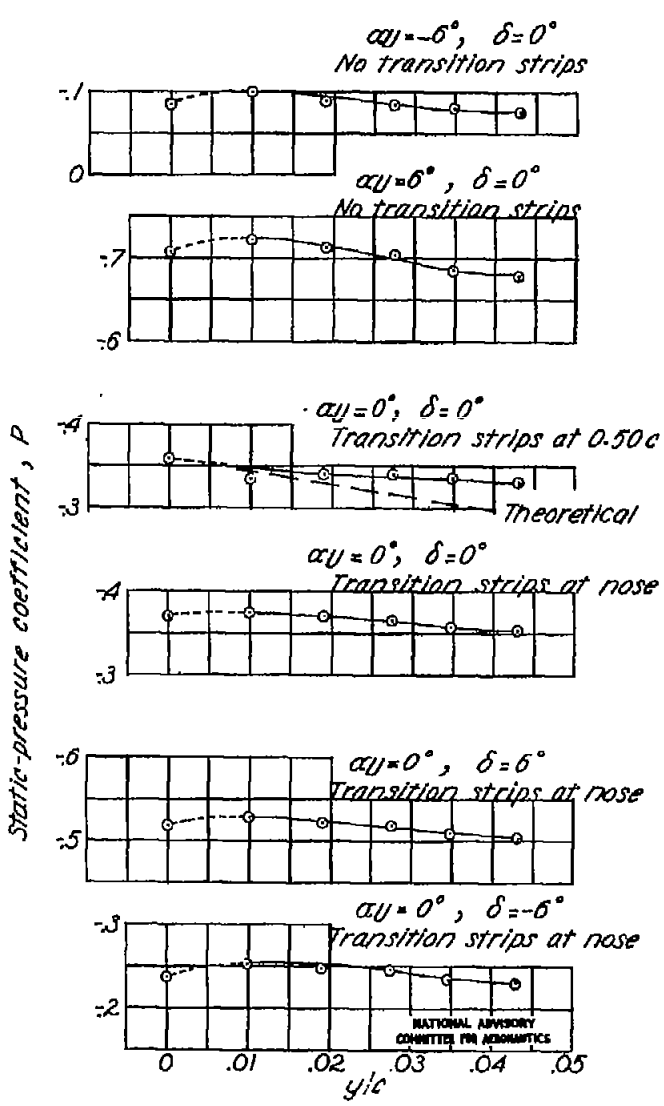

(c) $\frac{x}{c} = 0.450$.

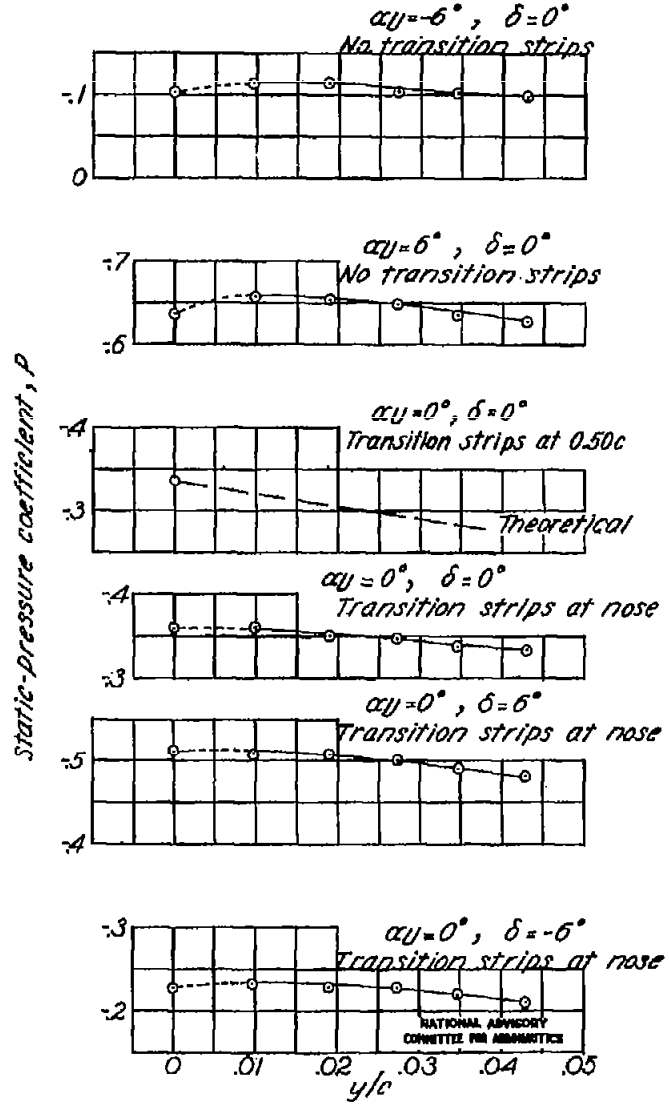

(d) $\frac{x}{c} = 0.500$.

Figure 4.- Continued.

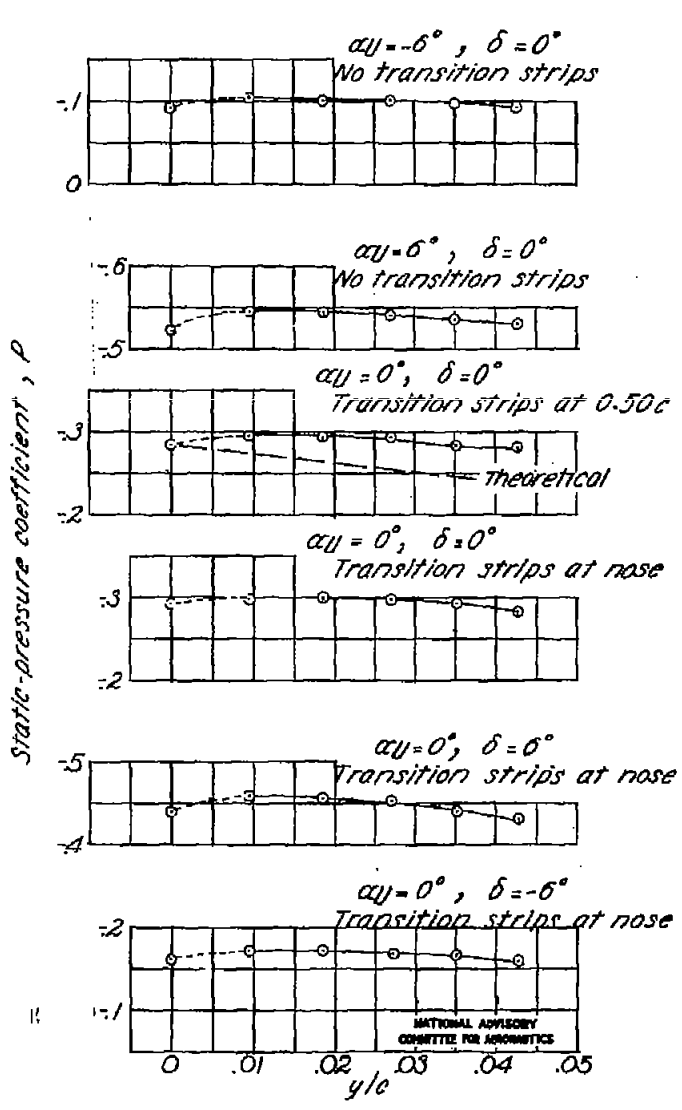

(e) $\frac{x}{c}$ = 0.575.

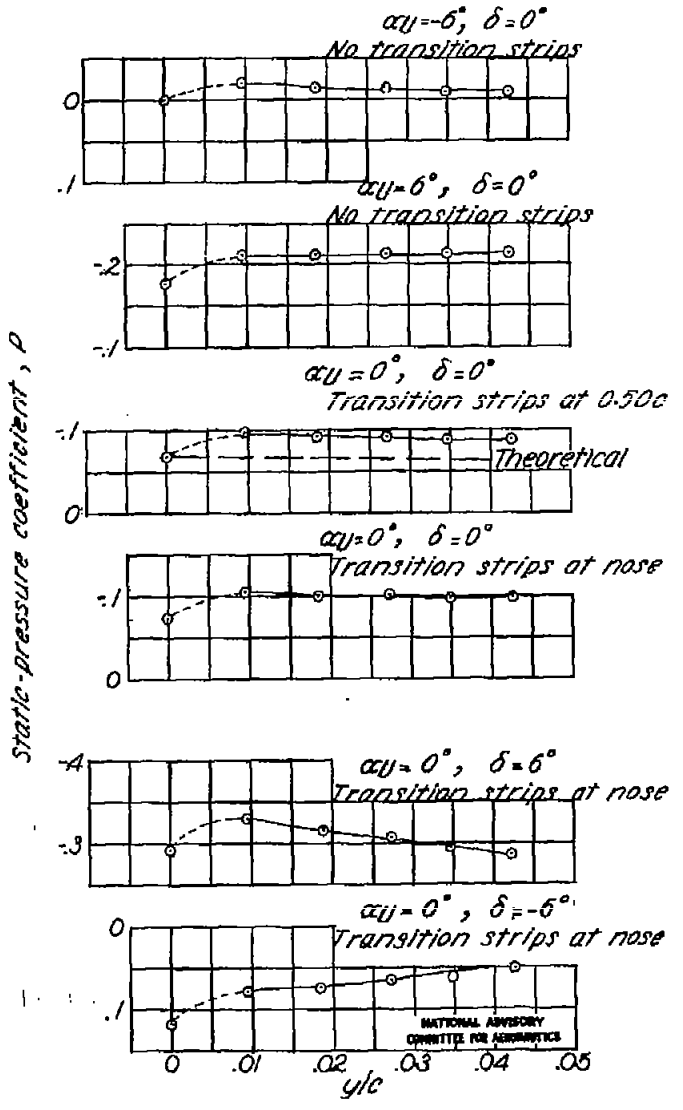

(f) $\frac{x}{c}$ = 0.775.

Figure 4.- Continued.

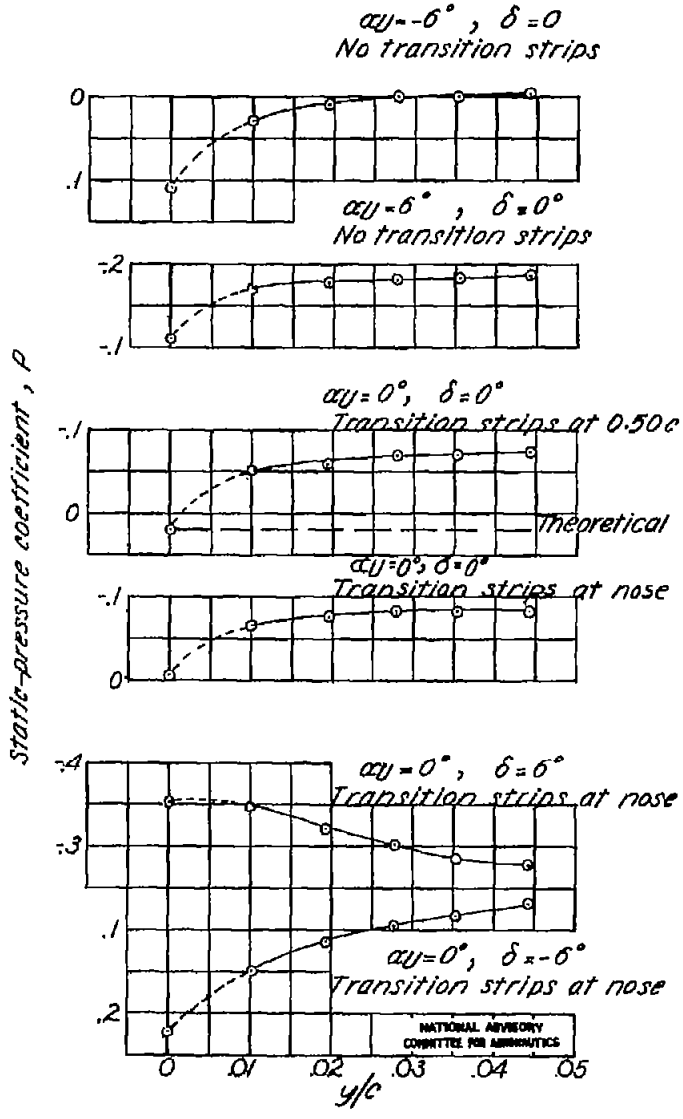

(g) $\frac{x}{c} = 0.800$.

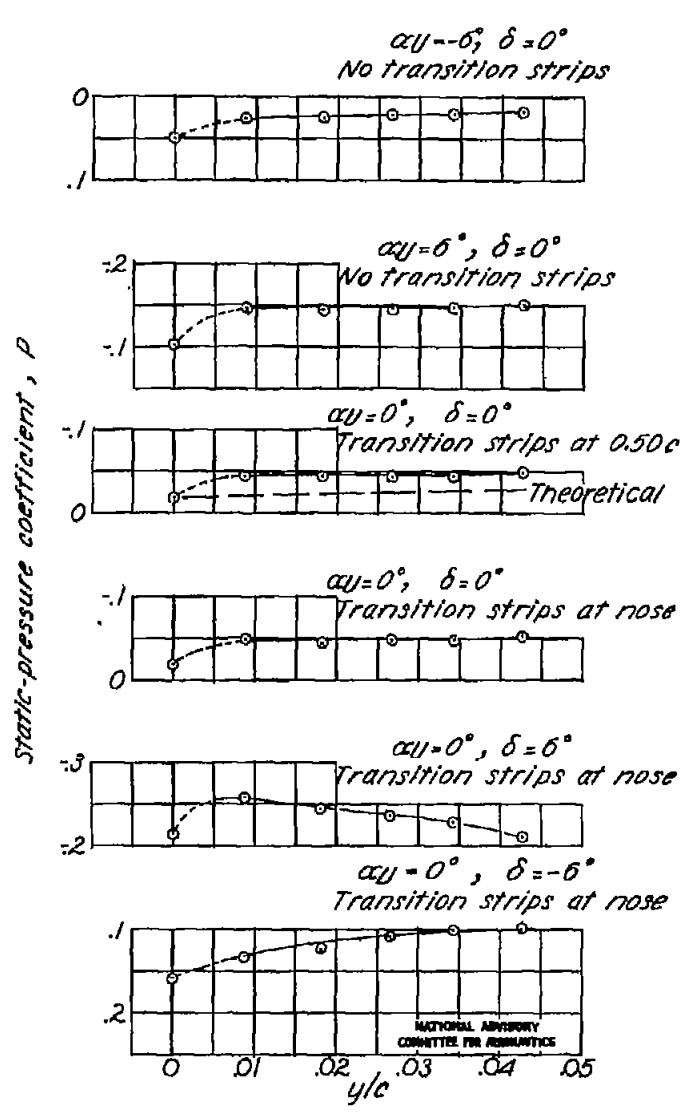

(h) $\frac{x}{c} = 0.826$.

Figure 4.- Continued.

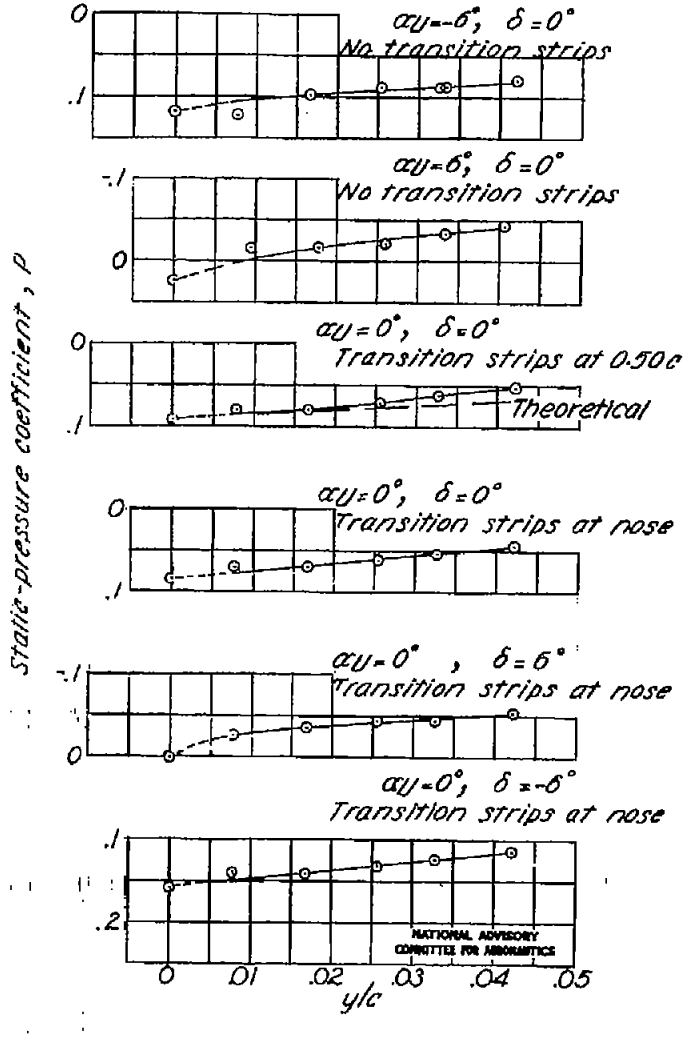

(i) $\frac{x}{c} = 0.900$.

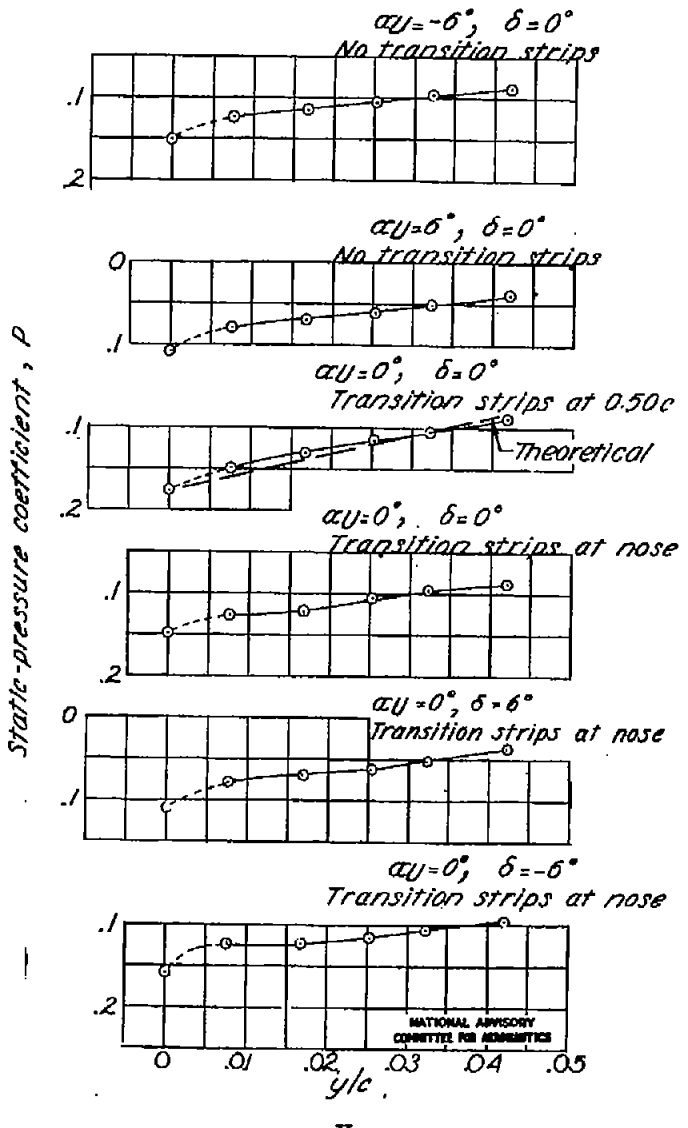

(j) $\frac{x}{c} = 0.978$.

Figure 4.- Concluded.

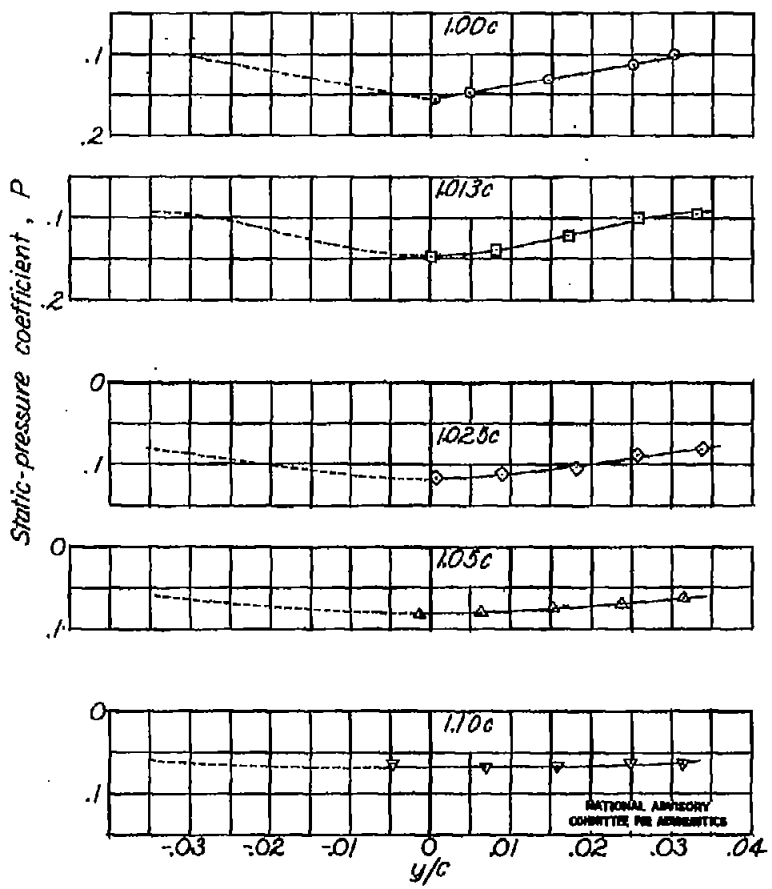

Figure 5.- Wake static-pressure profiles for the NACA 65_1-012 airfoil at $\alpha_U = 0^\circ$, $\delta = 0^\circ$, with transition strips at 0.50c. Basic-flap contour.

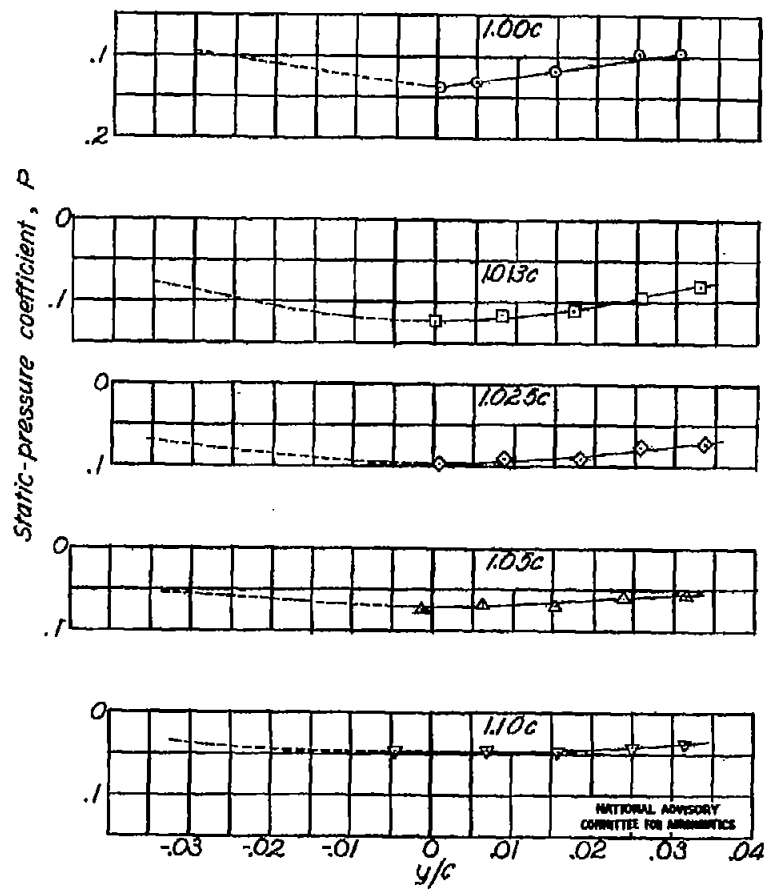

Figure 6.- Wake static-pressure profiles for the NACA 65_1-012 airfoil at $\alpha_U = 0^\circ$, $\delta = 0^\circ$, with transition strips at the leading edge. Basic-flap contour.

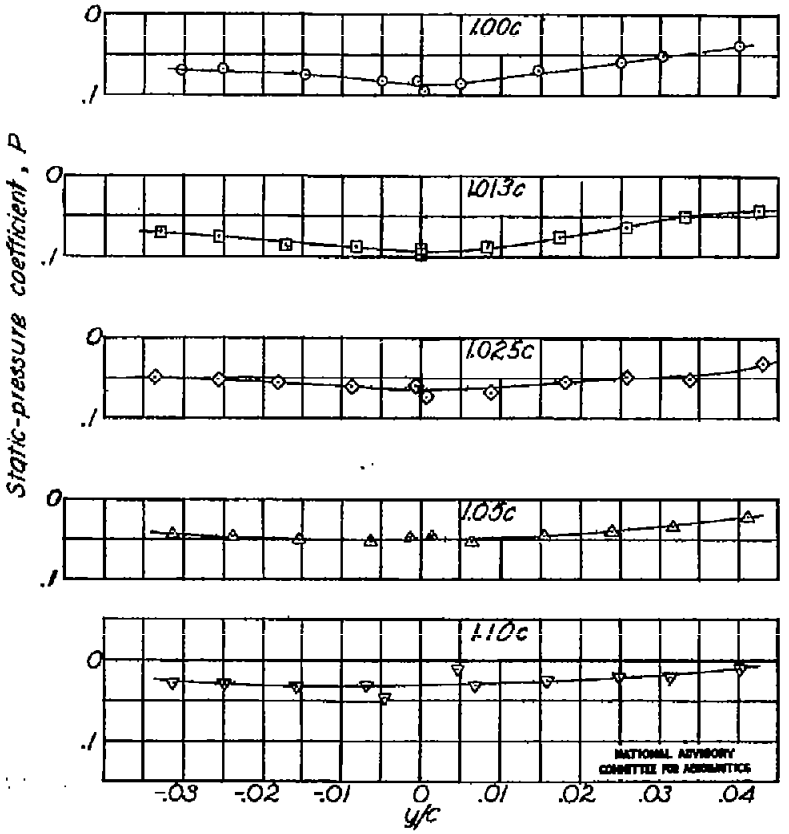

Figure 7.- Wake static-pressure profiles for the NACA 65_1-012 airfoil at $\alpha_U = 6^\circ$, $\delta = 0^\circ$, with free transition. Basic-flap contour.

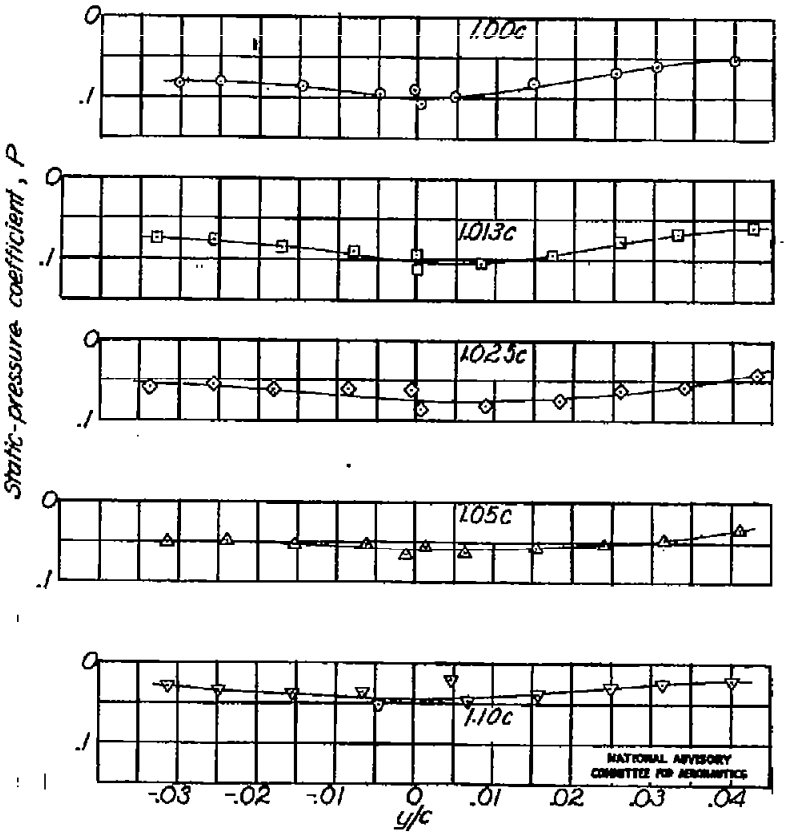

Figure 8.- Wake static-pressure profiles for the NACA 65_1-012 airfoil at $\alpha_U = 0^\circ$, $\delta = 6^\circ$, with transition strips at the leading edge. Basic-flap contour.

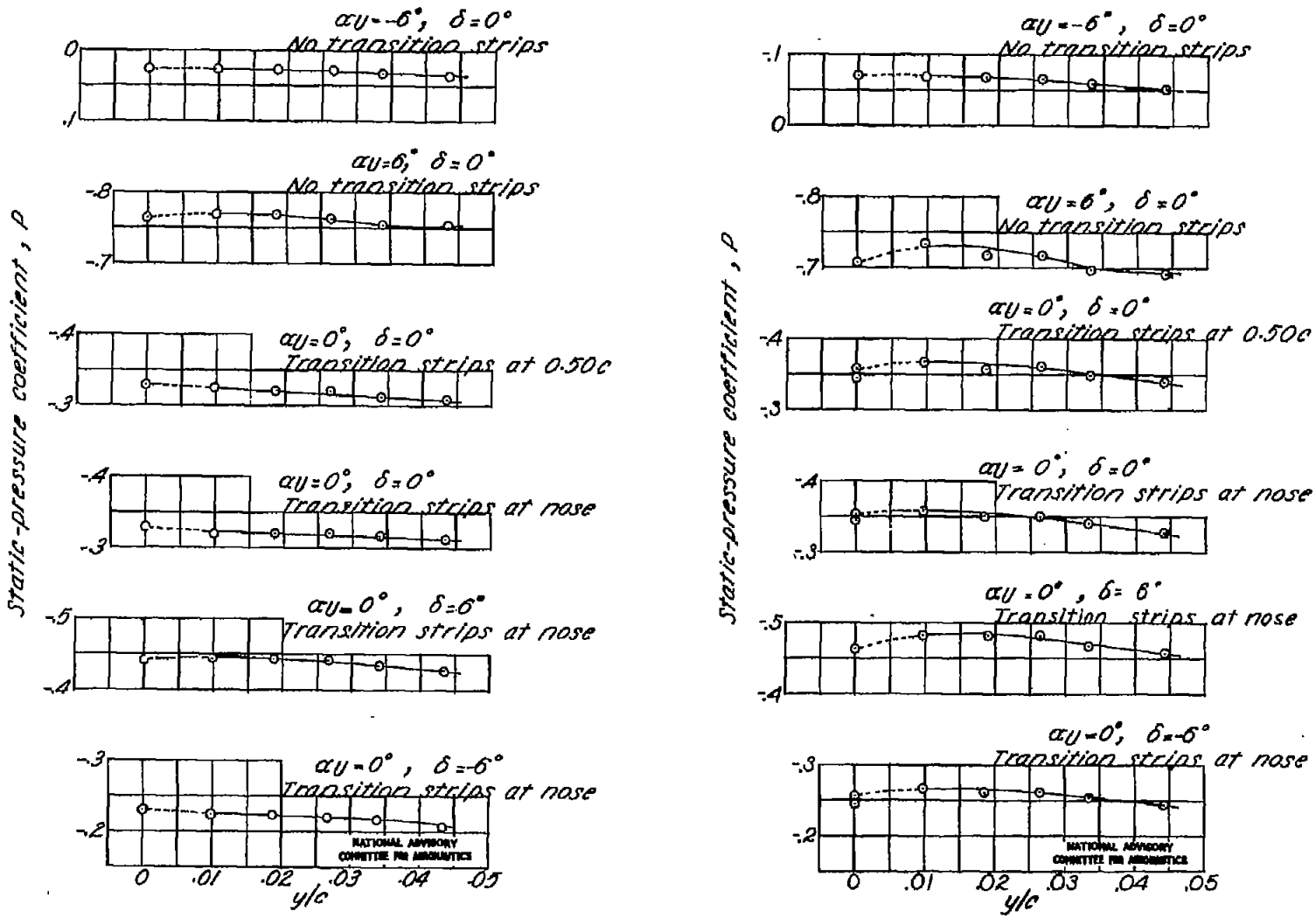

Figure 9.- Static-pressure profiles for the NACA 65_1-012 airfoil at various model configurations. Modified-flap contour.

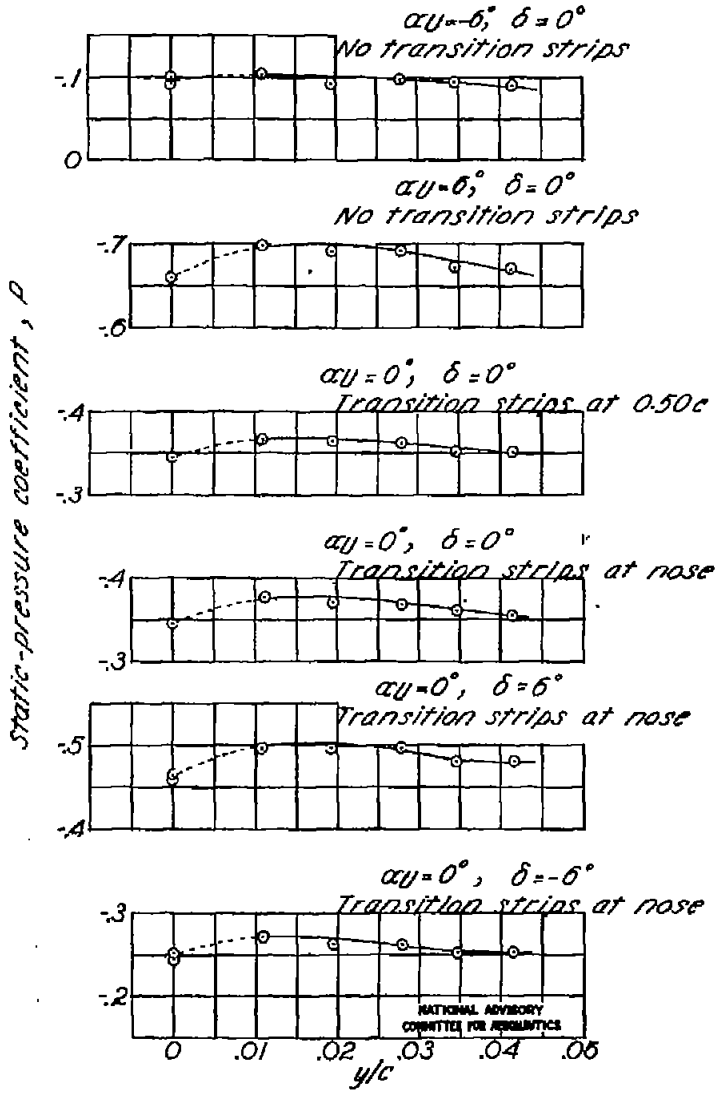

(c) $\frac{x}{c} = 0.450$

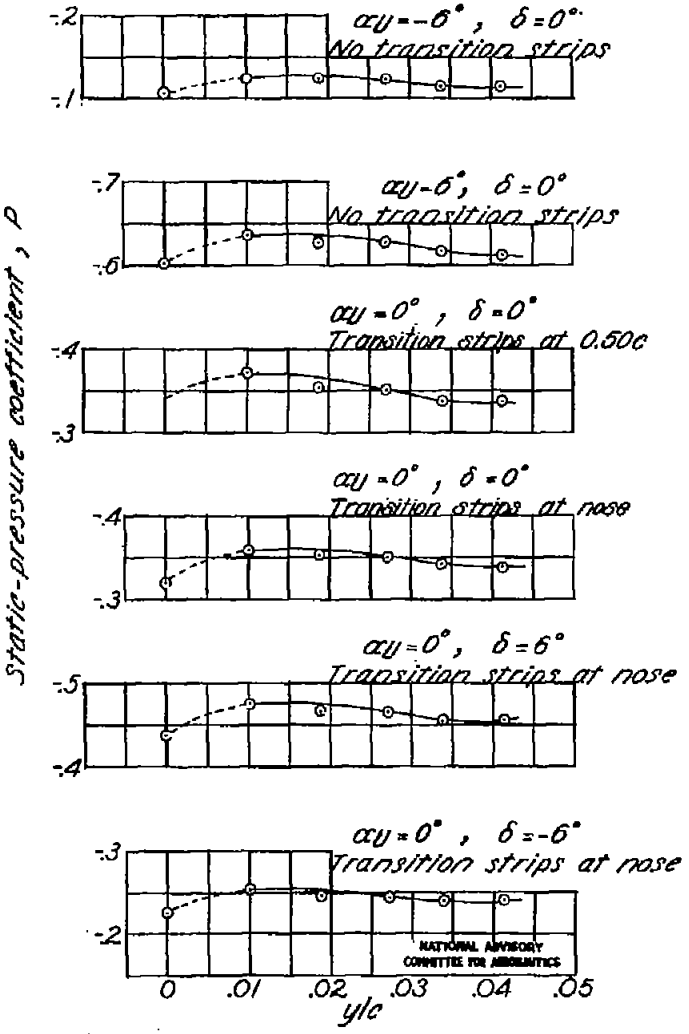

(d) $\frac{x}{c} = 0.500$.

Figure 9.- Continued.

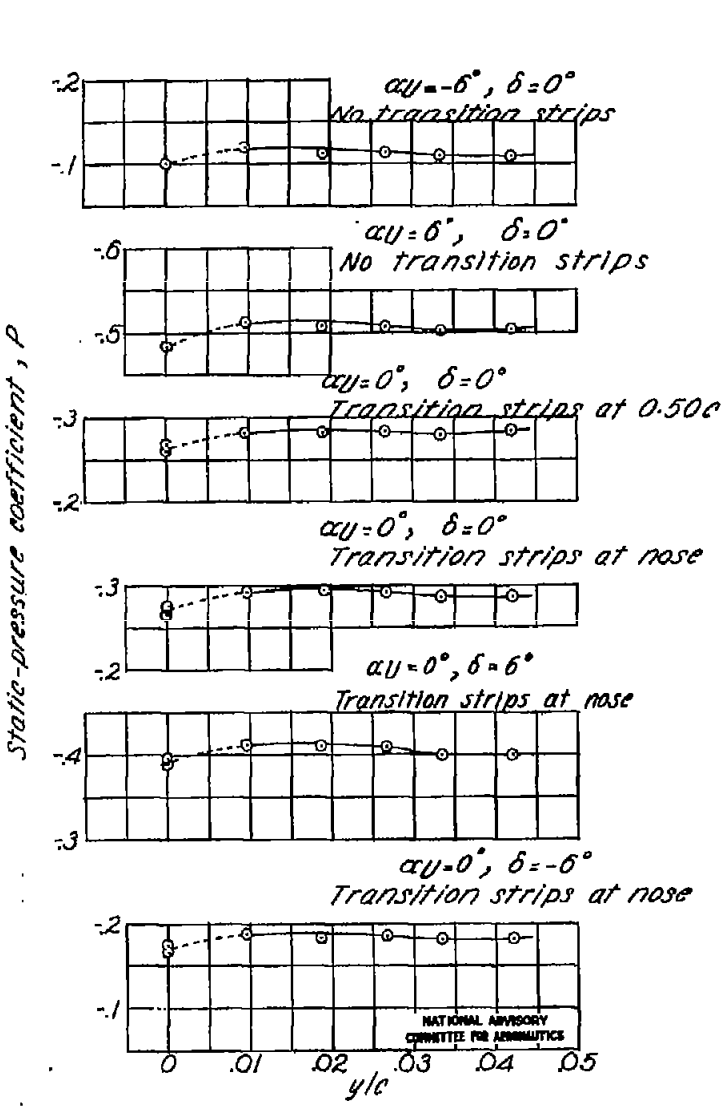

(e) $\frac{x}{c}$ = 0.575.

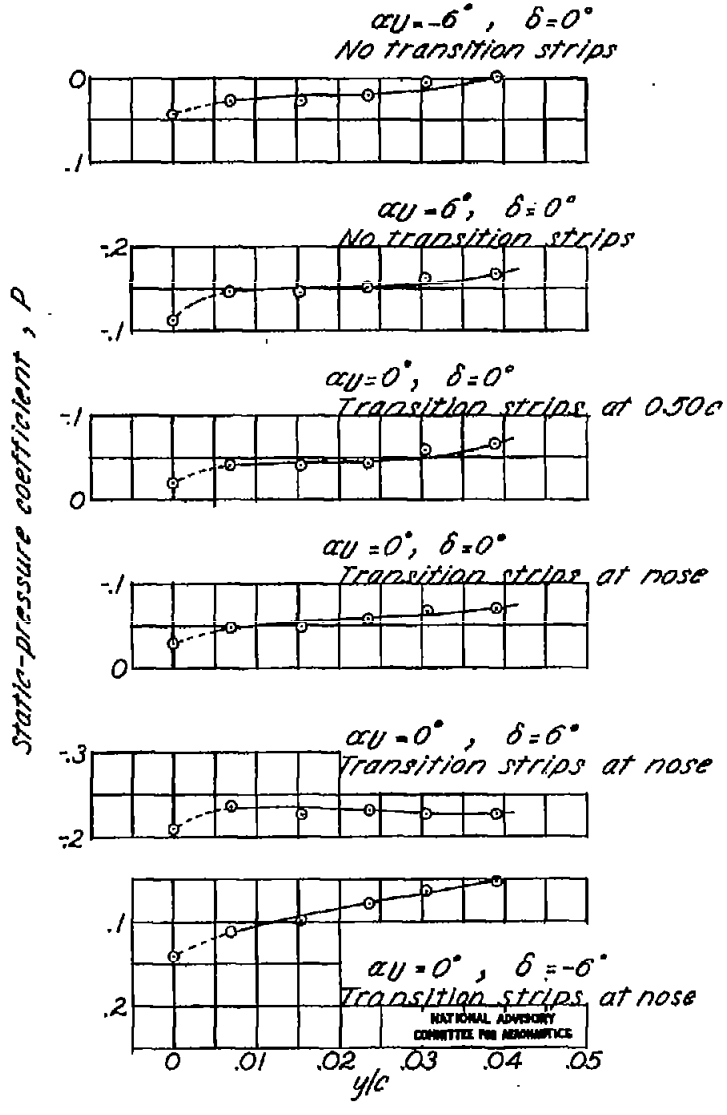

(f) $\frac{x}{c}$ = 0.775.

Figure 9.- Continued.

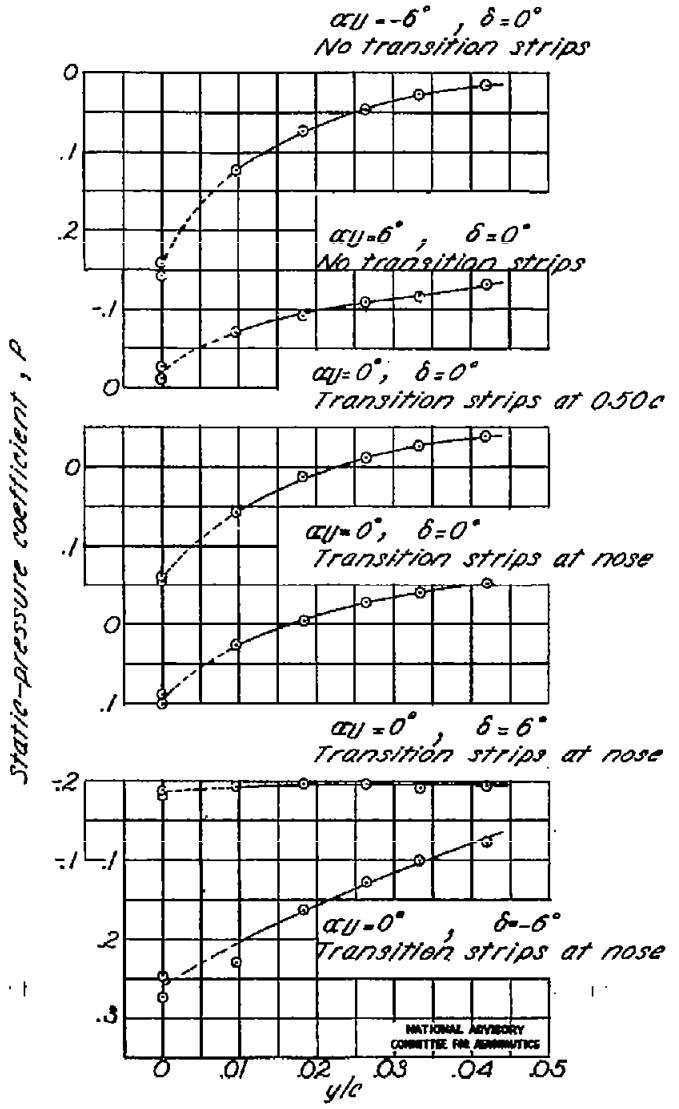

(g) $\frac{x_l}{c} = 0.800$.

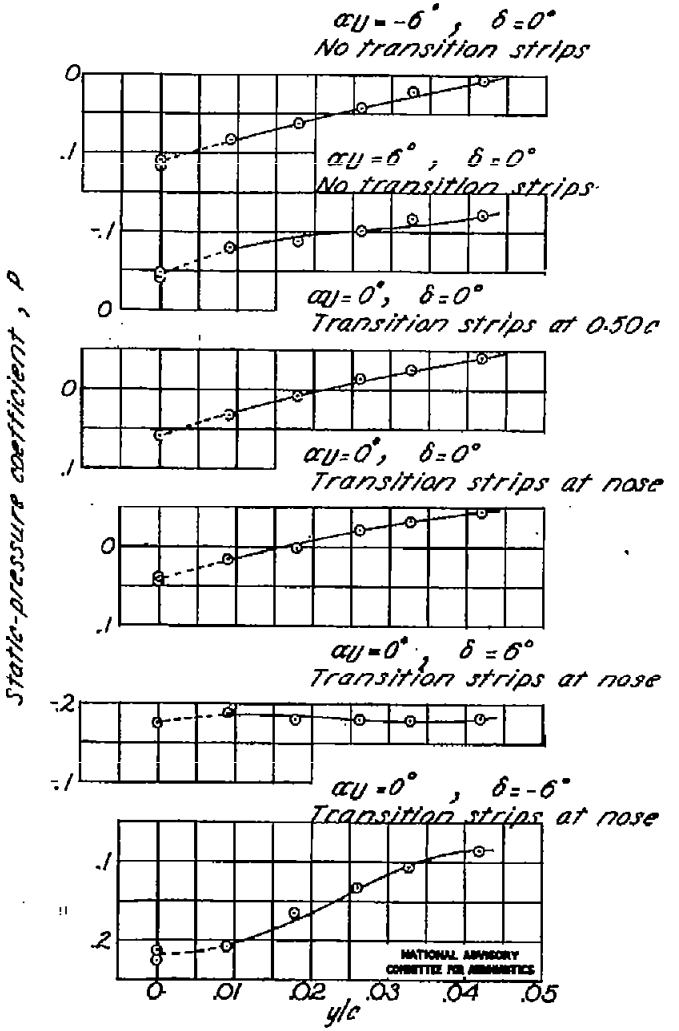

(h) $\frac{x_l}{c} = 0.814$.

Figure 9.- Continued.

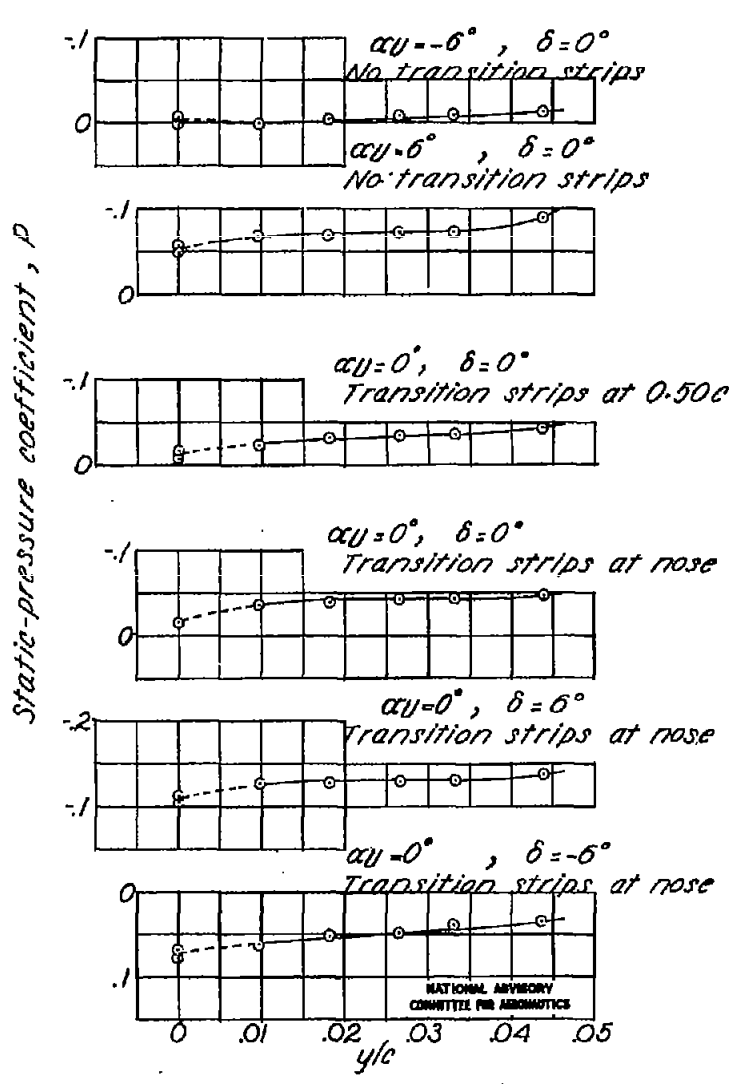

(i) $\frac{x}{c} = 0.870$.

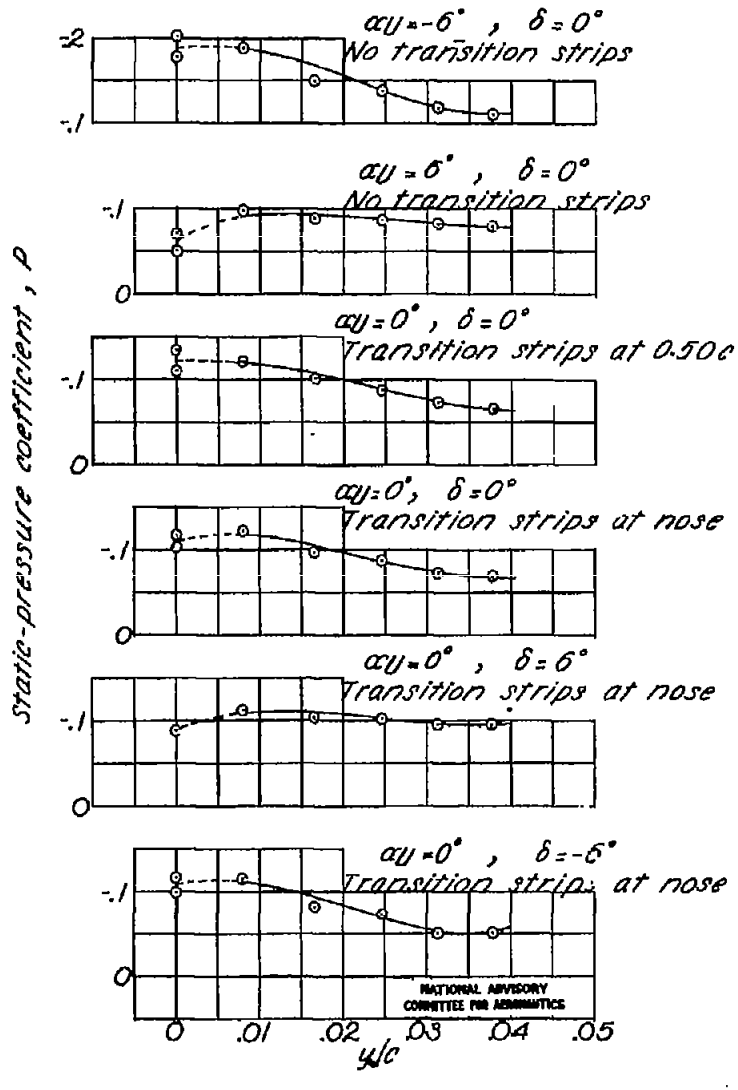

(j) $\frac{x}{c} = 0.925$.

Figure 9.- Continued.

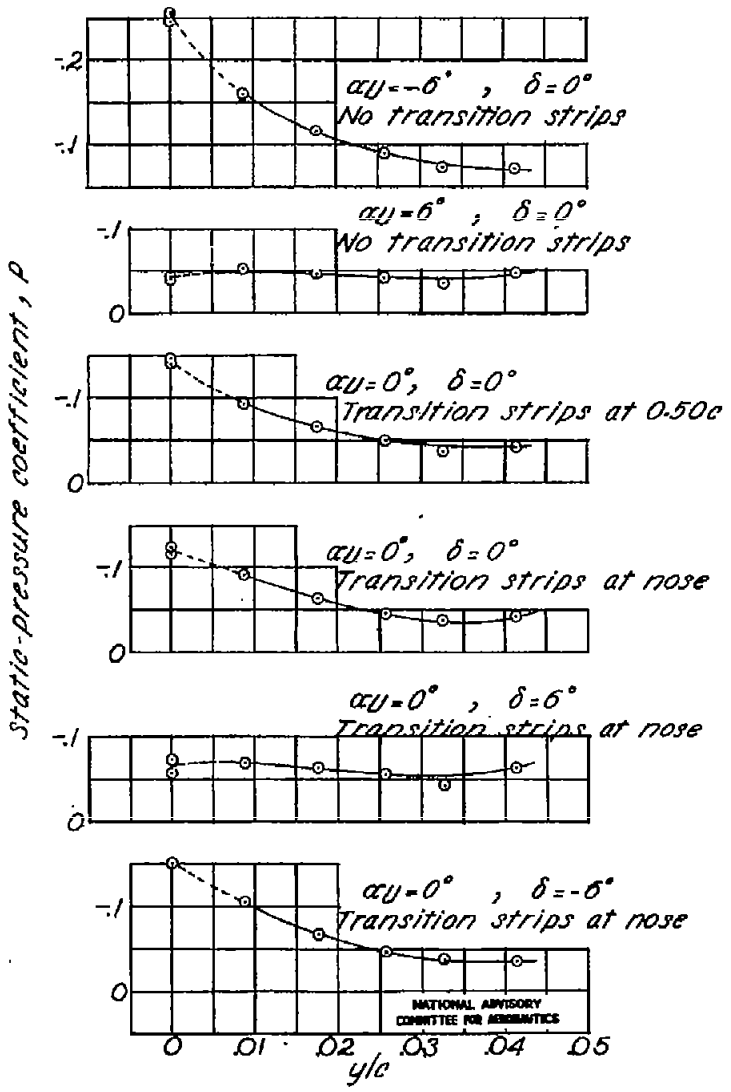

(k) $\frac{x}{c} = 0.937$.

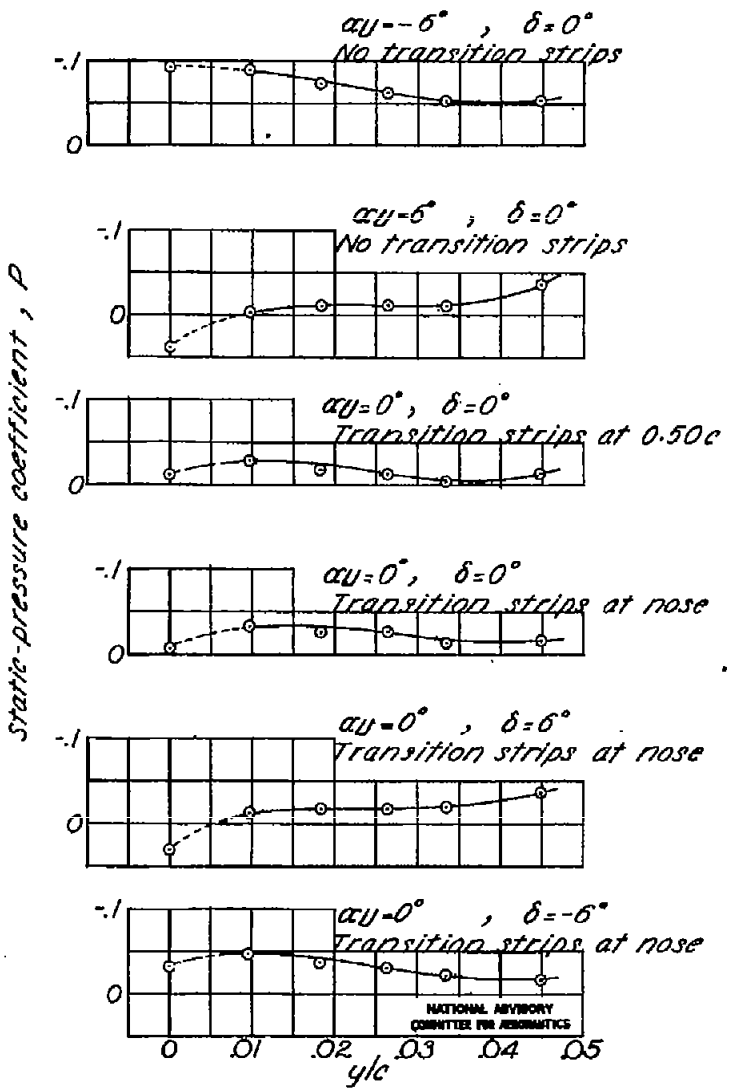

(l) $\frac{x}{c} = 0.950$.

Figure 9.- Continued.

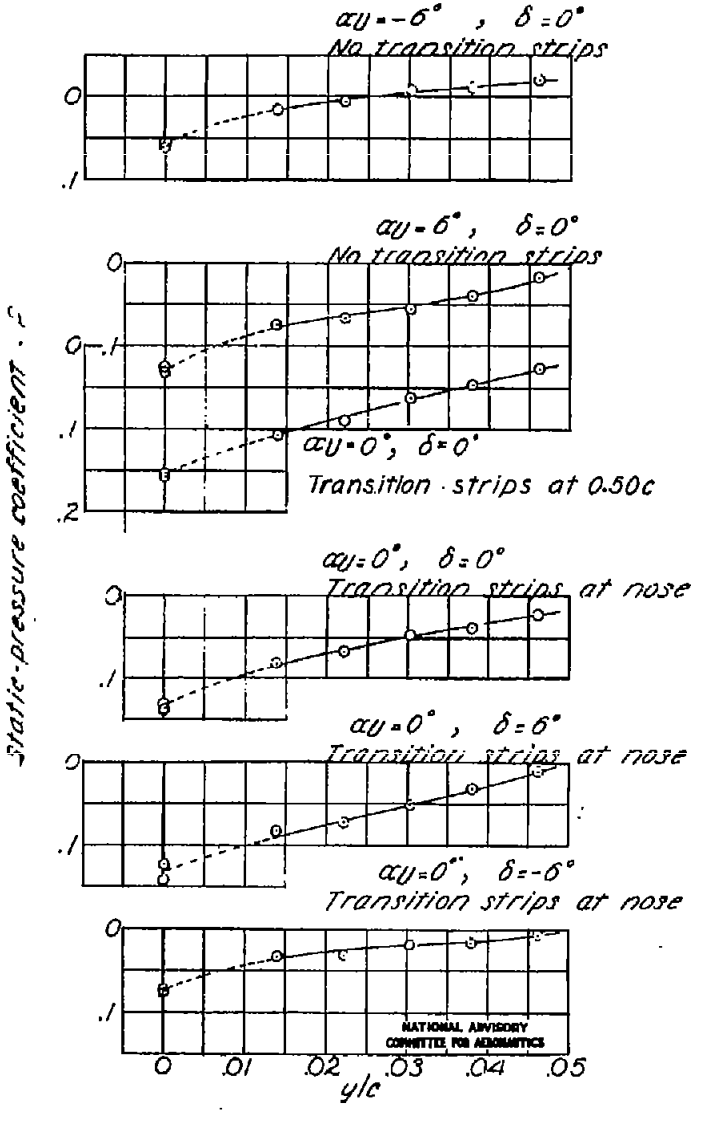

(m) $\frac{x}{c} = 0.979$.

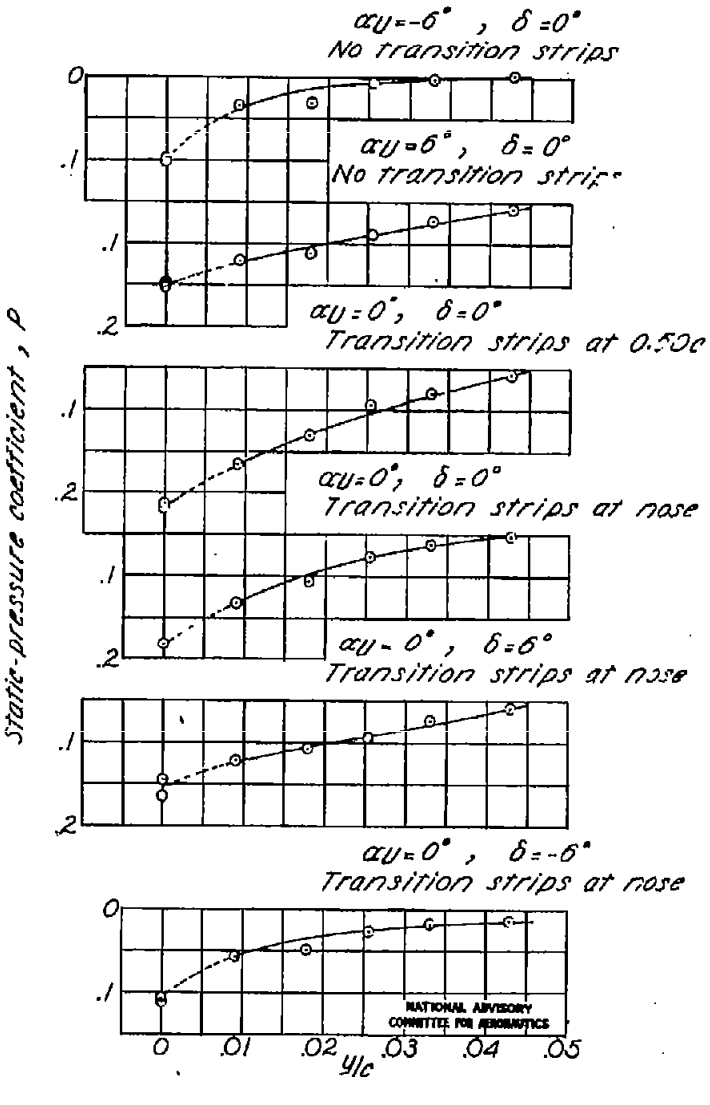

(n) $\frac{x}{c} = 0.995$.

Figure 9.- Concluded.

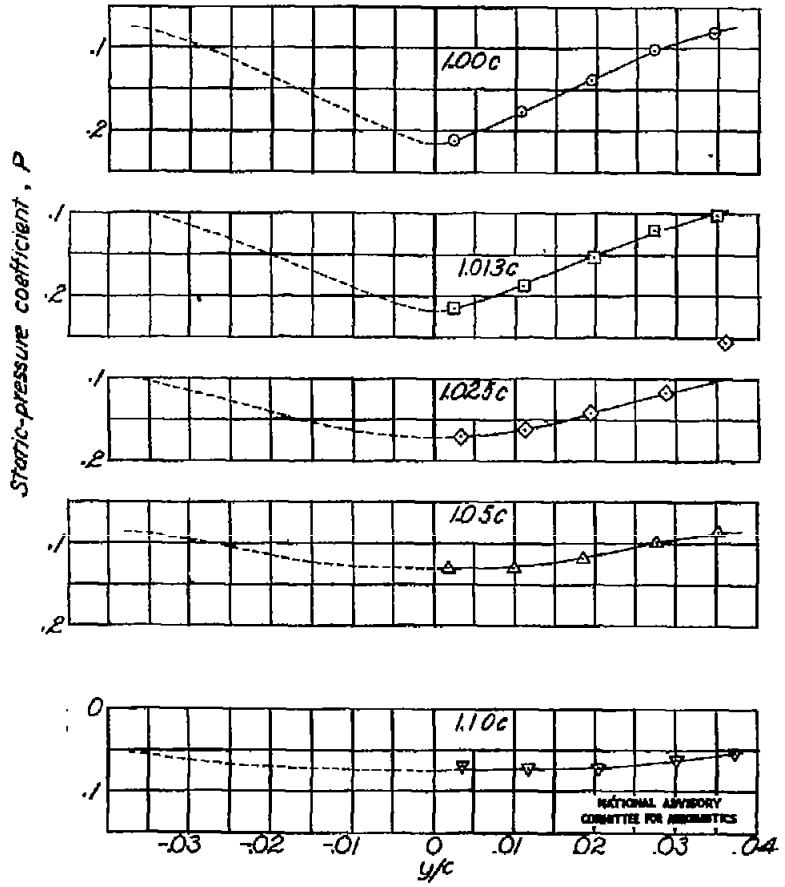

Figure 10.- Wake static-pressure profiles for the NACA 65_1-012 at $\alpha_U = 0^\circ$, $\delta = 0^\circ$, with transition strips at 0.50c. Modified-flap contour.

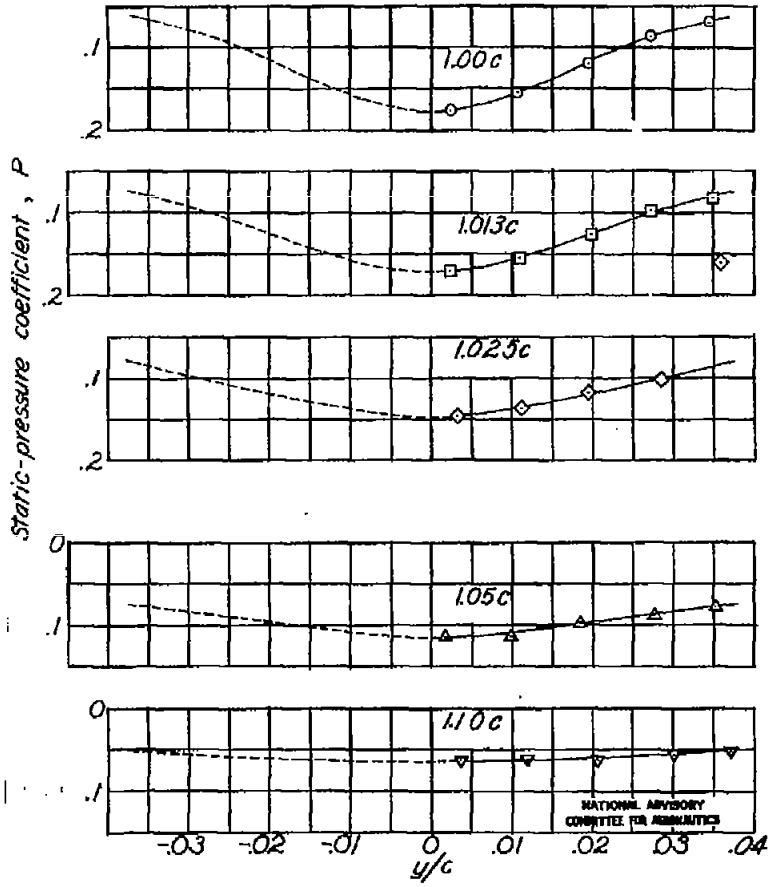

Figure 11.- Wake static-pressure profiles for the NACA 65_1-012 airfoil at $\alpha_U = 0^\circ$, $\delta = 0^\circ$, with transition strips at the leading edge. Modified-flap contour.

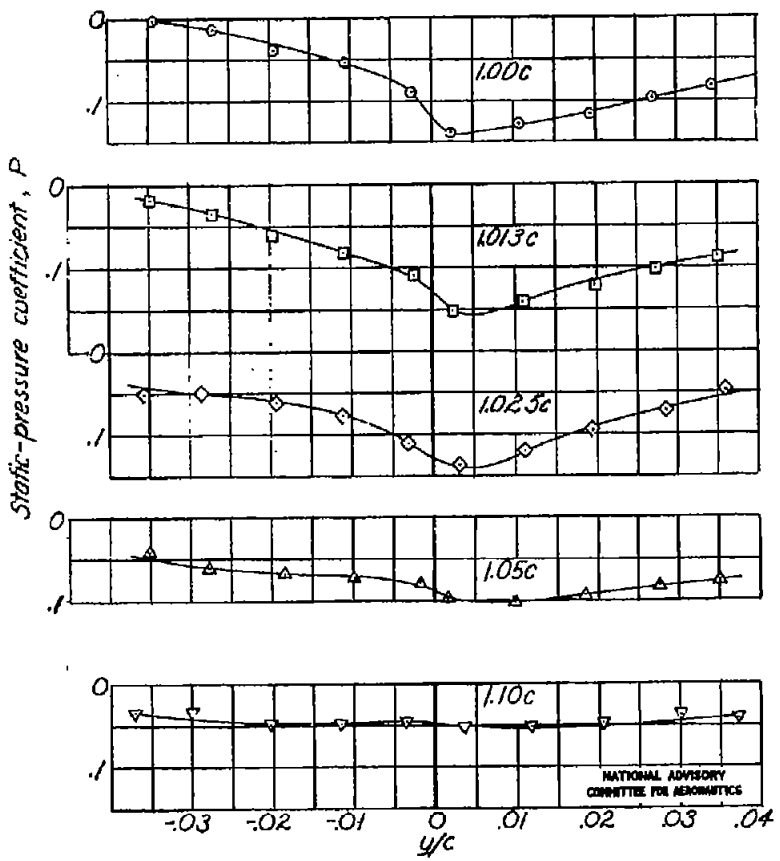

Figure 12.- Wake static-pressure profiles for the NACA 65_1-012 airfoil at $\alpha_U = 6^\circ$, $\delta = 0^\circ$, with free transition. Modified-flap contour.

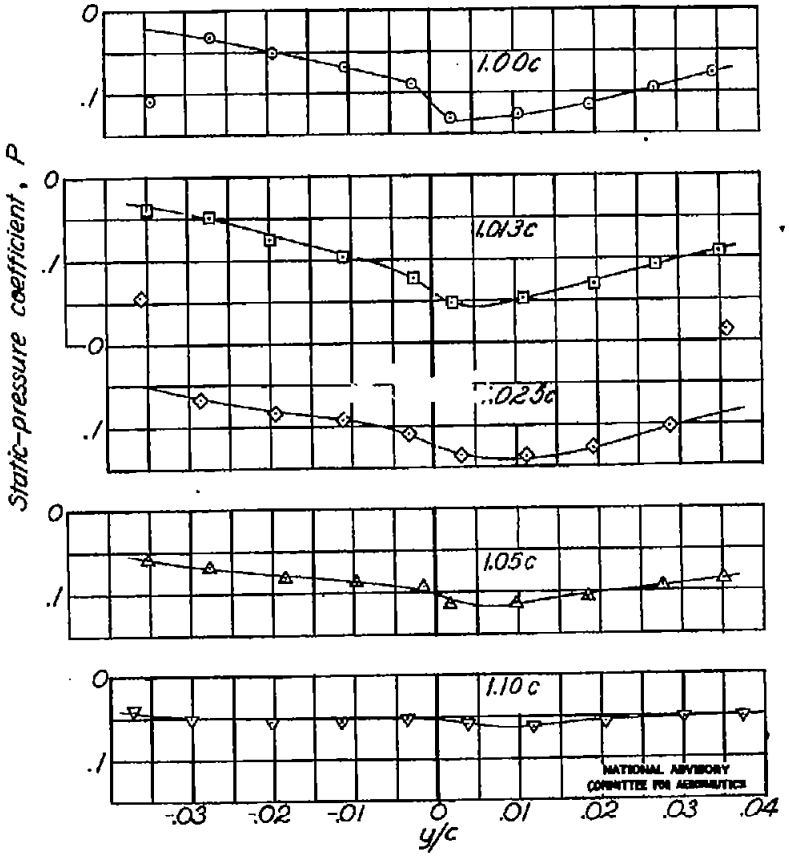

Figure 13.- Wake static-pressure profiles for the NACA 65_1-012 airfoil at $\alpha_U = 0^\circ$, $\delta = 6^\circ$, with transition at the leading edge. Modified-flap contour.

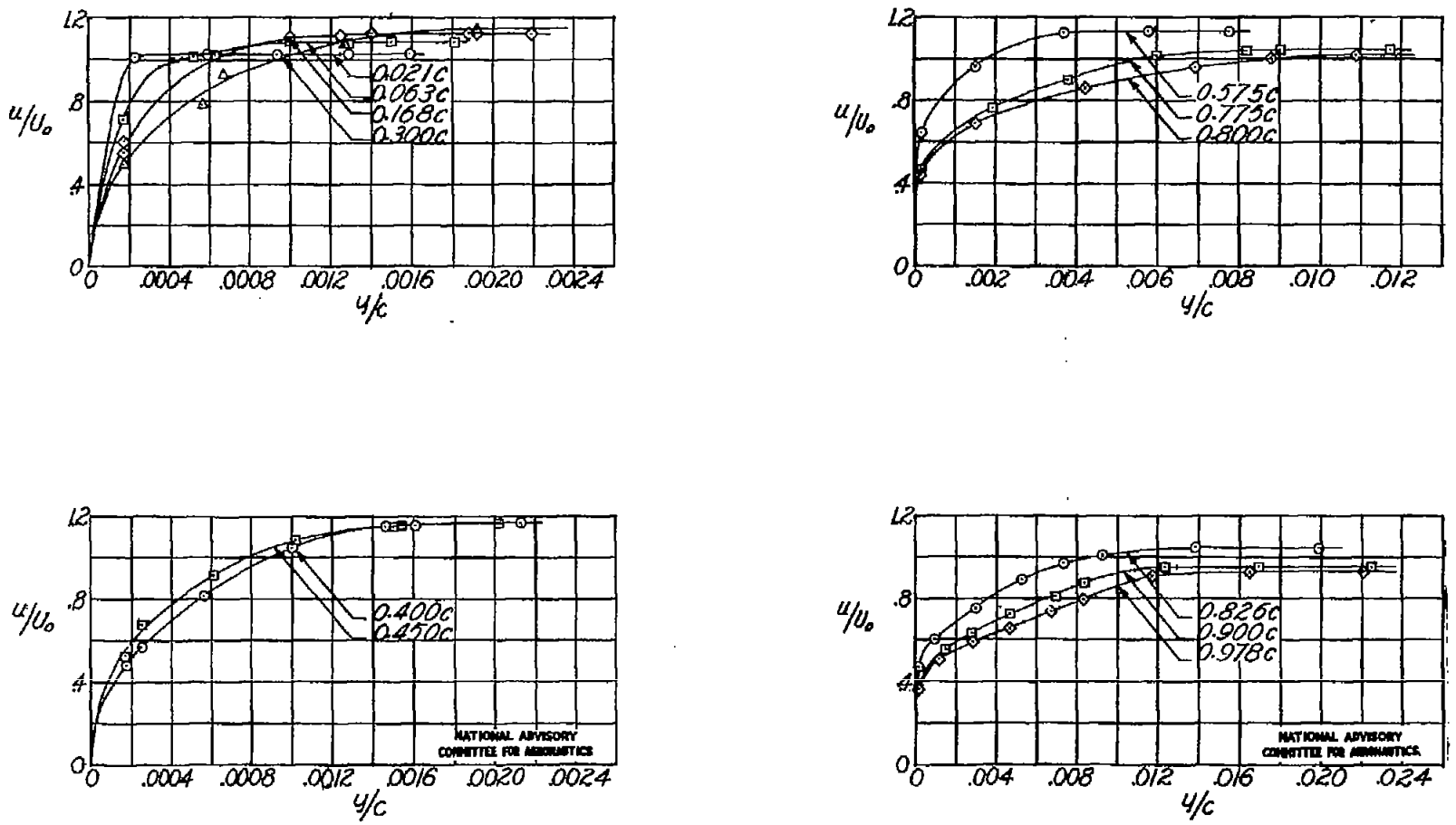

Figure 14.- Velocity profiles for the NACA 65_1-012 airfoil at $\alpha_U = 0^\circ$, $\delta = 0^\circ$, with transition strips at 0.50c. Basic-flap contour.

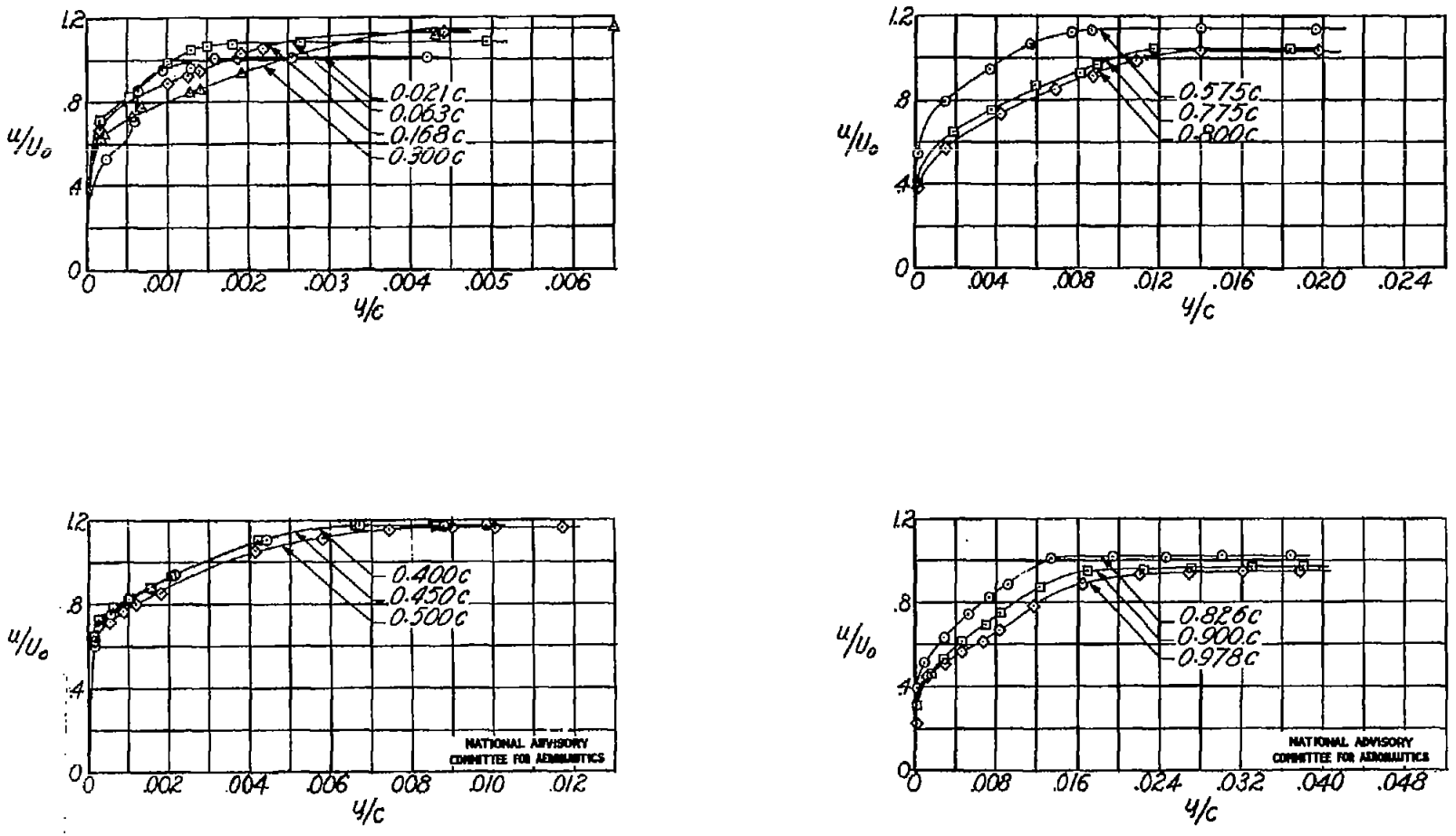

Figure 15.- Velocity profiles for the NACA 65_1-012 airfoil at $\alpha_U = 0^\circ$, $\delta = 0^\circ$, with transition strips at the leading edge. Basic-flap contour.

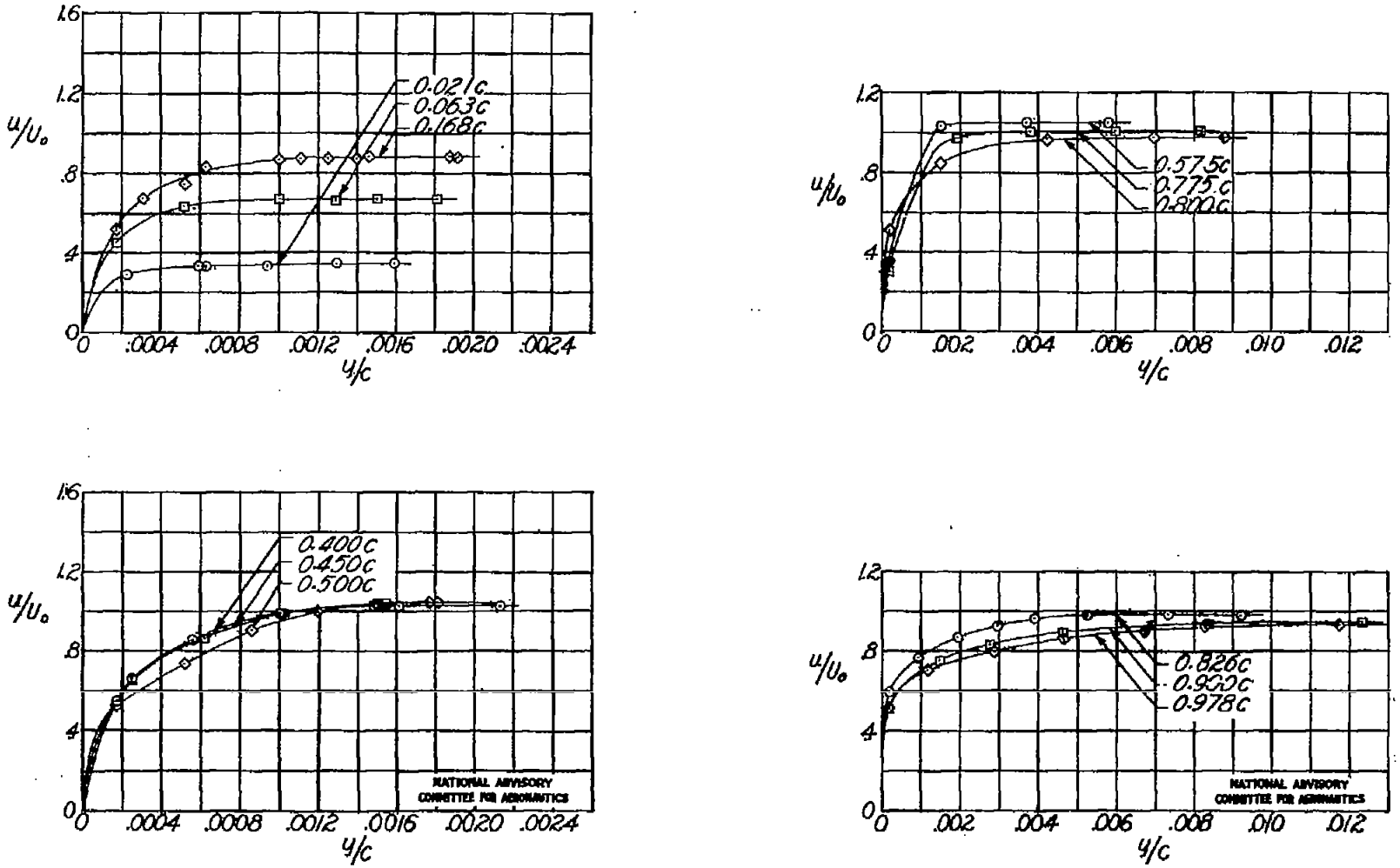

Figure 16.- Velocity profiles for the NACA 65_1-012 airfoil at $\alpha_U = -6^\circ$, $\delta = 0^\circ$, with free transition. Basic-flap contour.

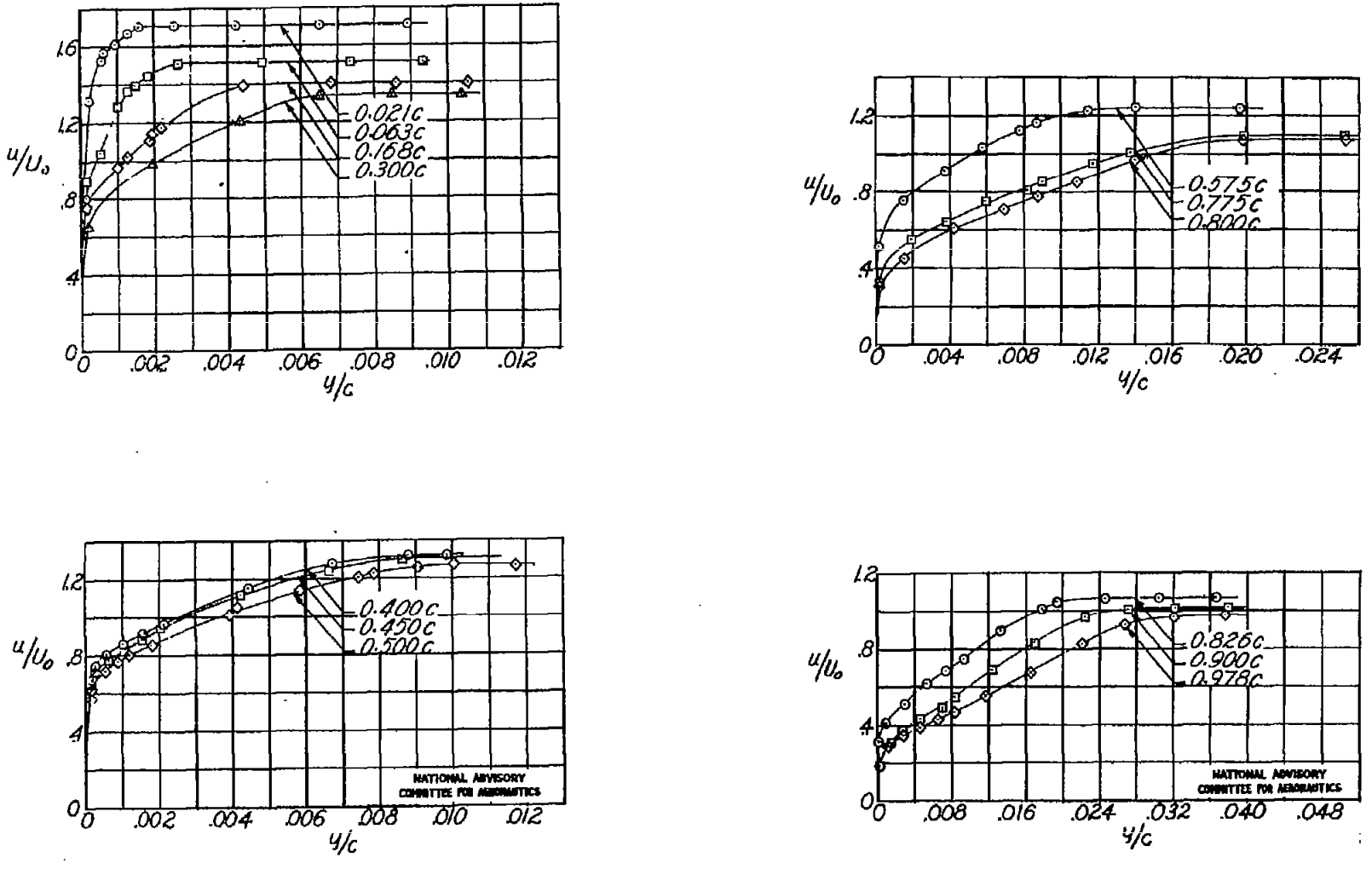

Figure 17.- Velocity profiles for the NACA 65_1-012 airfoil at $\alpha_U = 6^\circ$, $\delta = 0^\circ$, with free transition. Basic-flap contour.

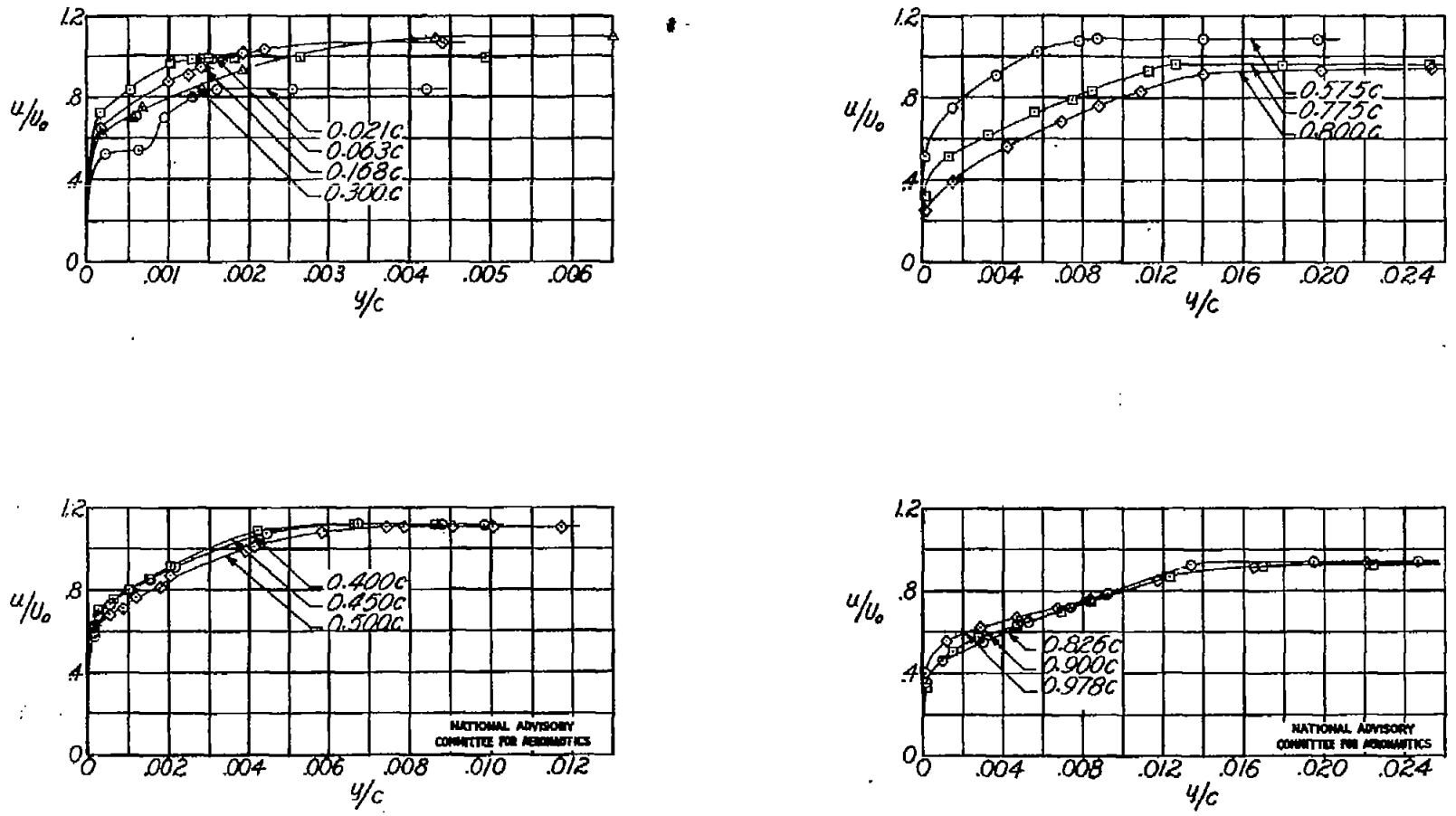

Figure 18.- Velocity profiles for the NACA 65_1-012 airfoil at $\alpha_U = 0^\circ$, $\delta = -6^\circ$, with transition strips at the leading edge. Basic-flap contour.

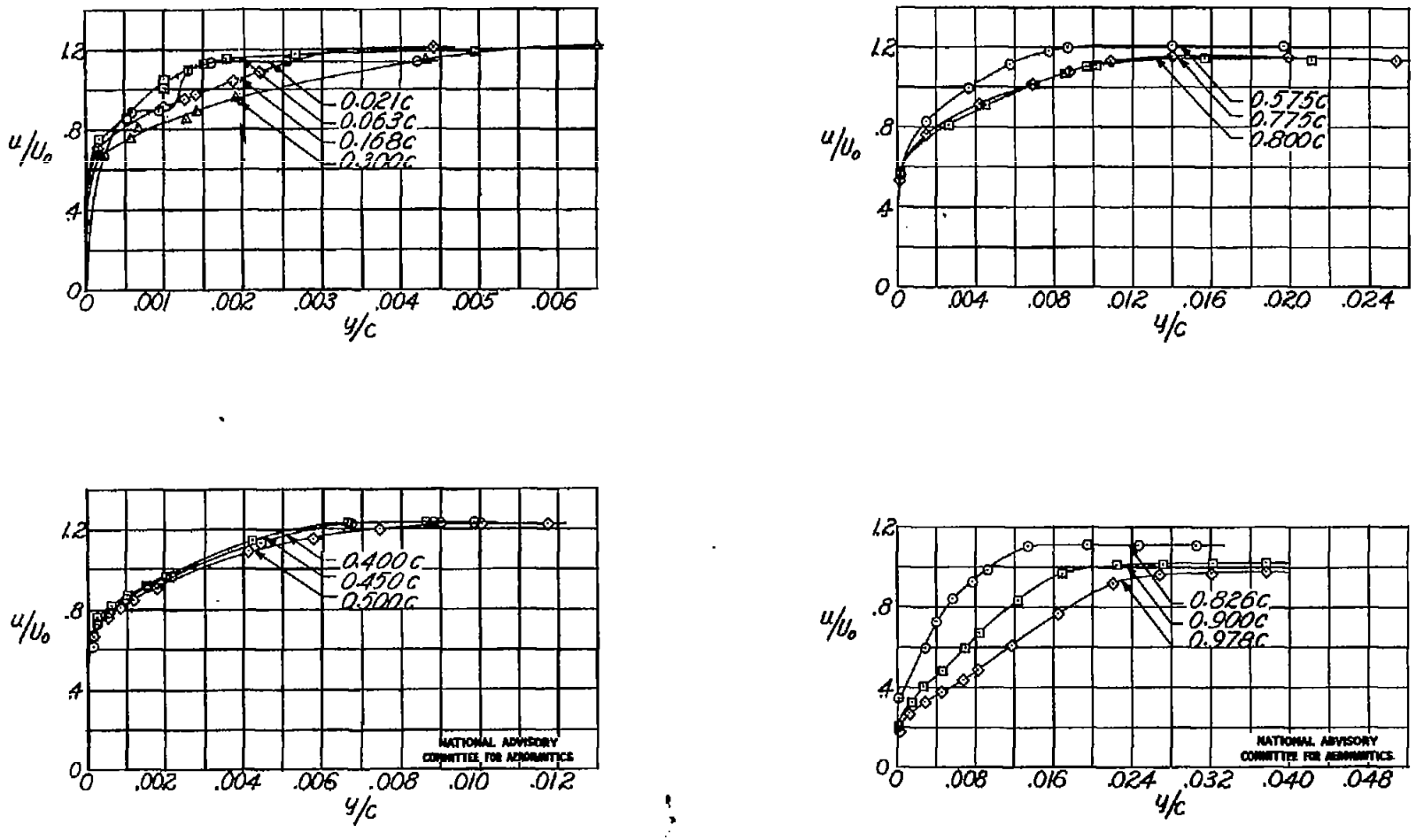

Figure 19.- Velocity profiles for the NACA 65_1-012 airfoil at $\alpha_U = 0^\circ$, $\delta = 6^\circ$, with transition strips at the leading edge. Basic-flap contour.

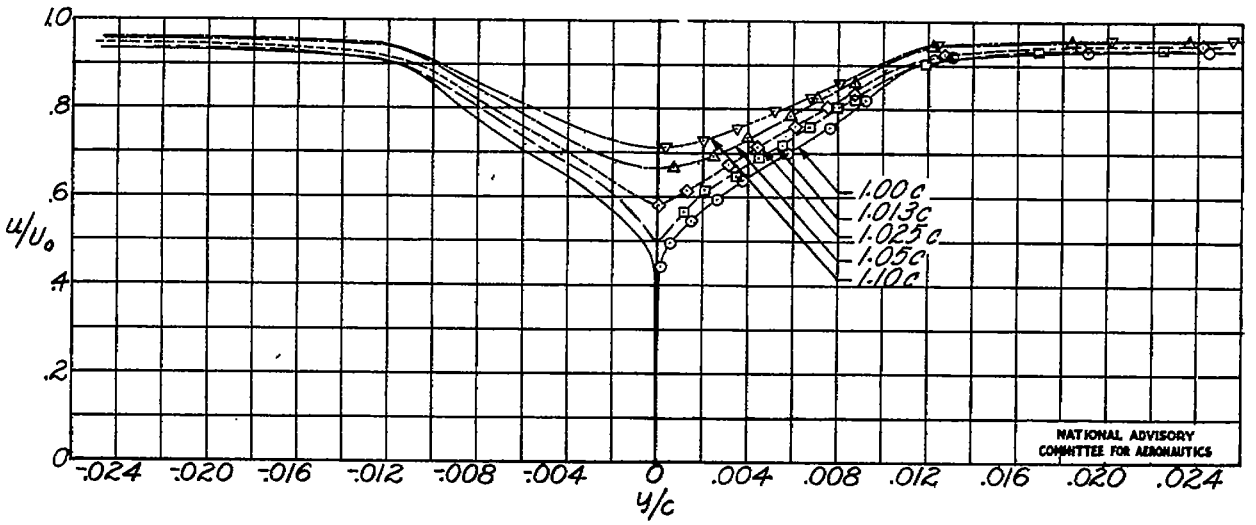

Figure 20.- Wake velocity profiles for the NACA 65_1-012 airfoil at $\alpha_U = 0^\circ$, $\delta = 0^\circ$, with transition strips at 0.50c. Basic-flap contour.

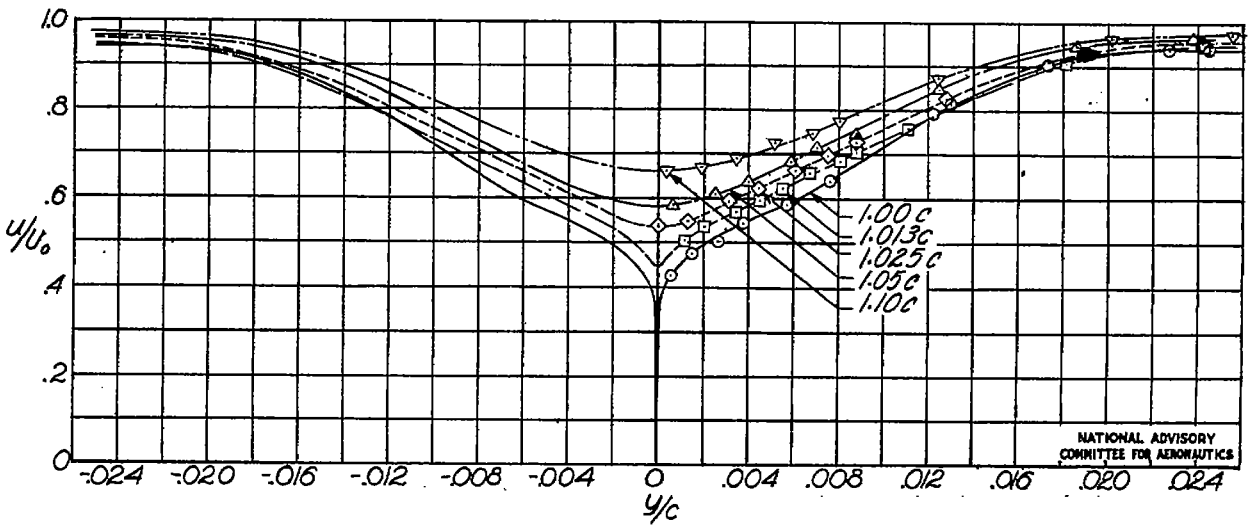

Figure 21.- Wake velocity profiles for the NACA 65_1-012 airfoil at $\alpha_U = 0^\circ$, $\delta = 0^\circ$, with transition strips at the leading edge. Basic-flap contour.

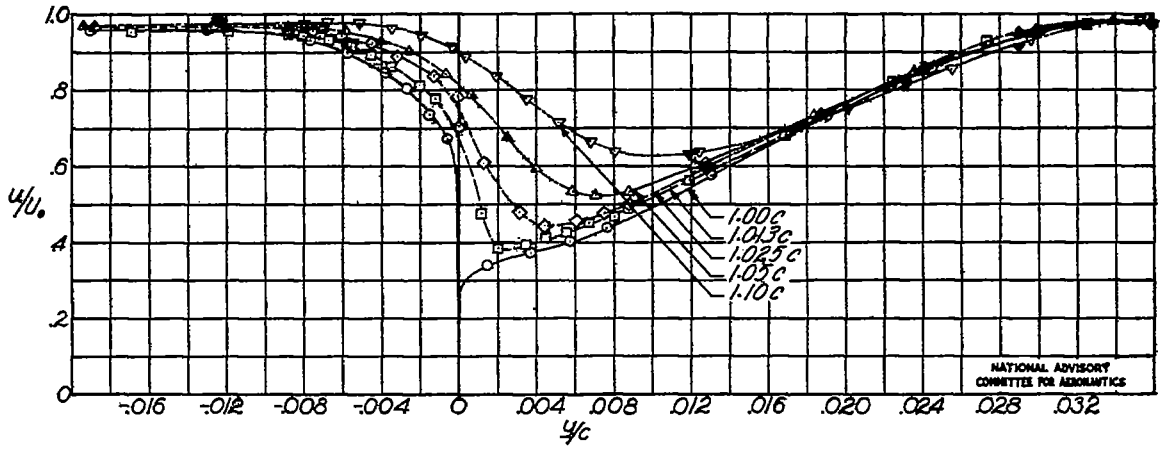

Figure 22.- Wake velocity profiles for the NACA 65_1-012 airfoil at $\alpha_U = 6^\circ$, $\delta = 0^\circ$, with free transition. Basic-flap contour.

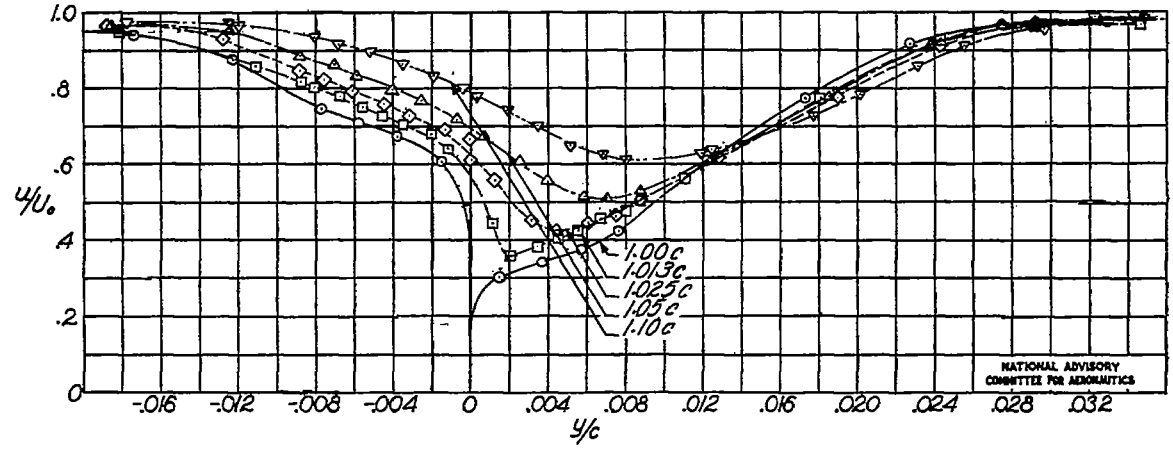

Figure 23.- Wake velocity profiles for the NACA 65_1-012 airfoil at $\alpha_U = 0^\circ$, $\delta = 6^\circ$, with transition strips at the leading edge. Basic-flap contour.

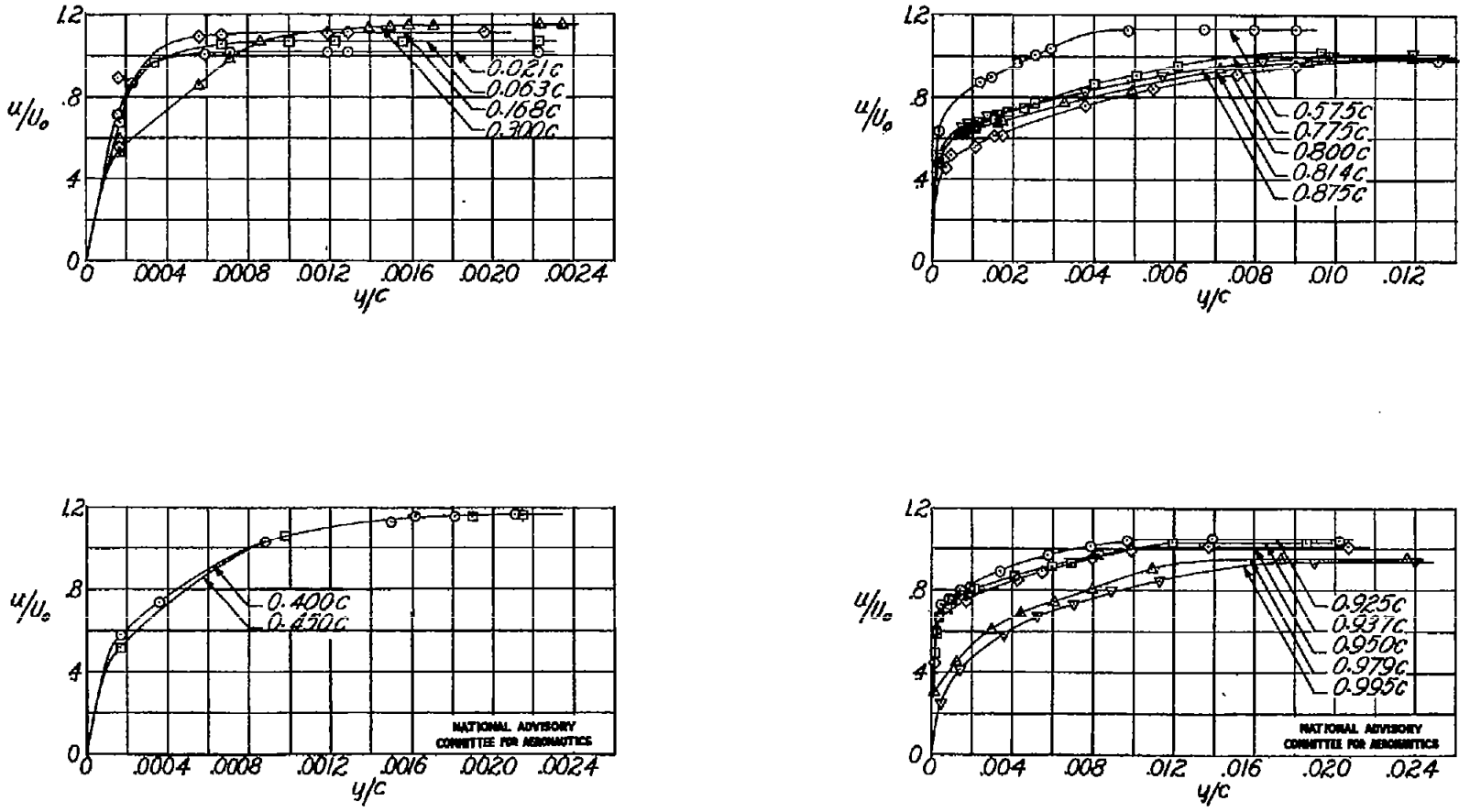

Figure 24.- Velocity profiles for the NACA 65_1-012 airfoil at $\alpha_U = 0^\circ$, $\delta = 0^\circ$, with transition strips at 0.50c. Modified-flap contour.

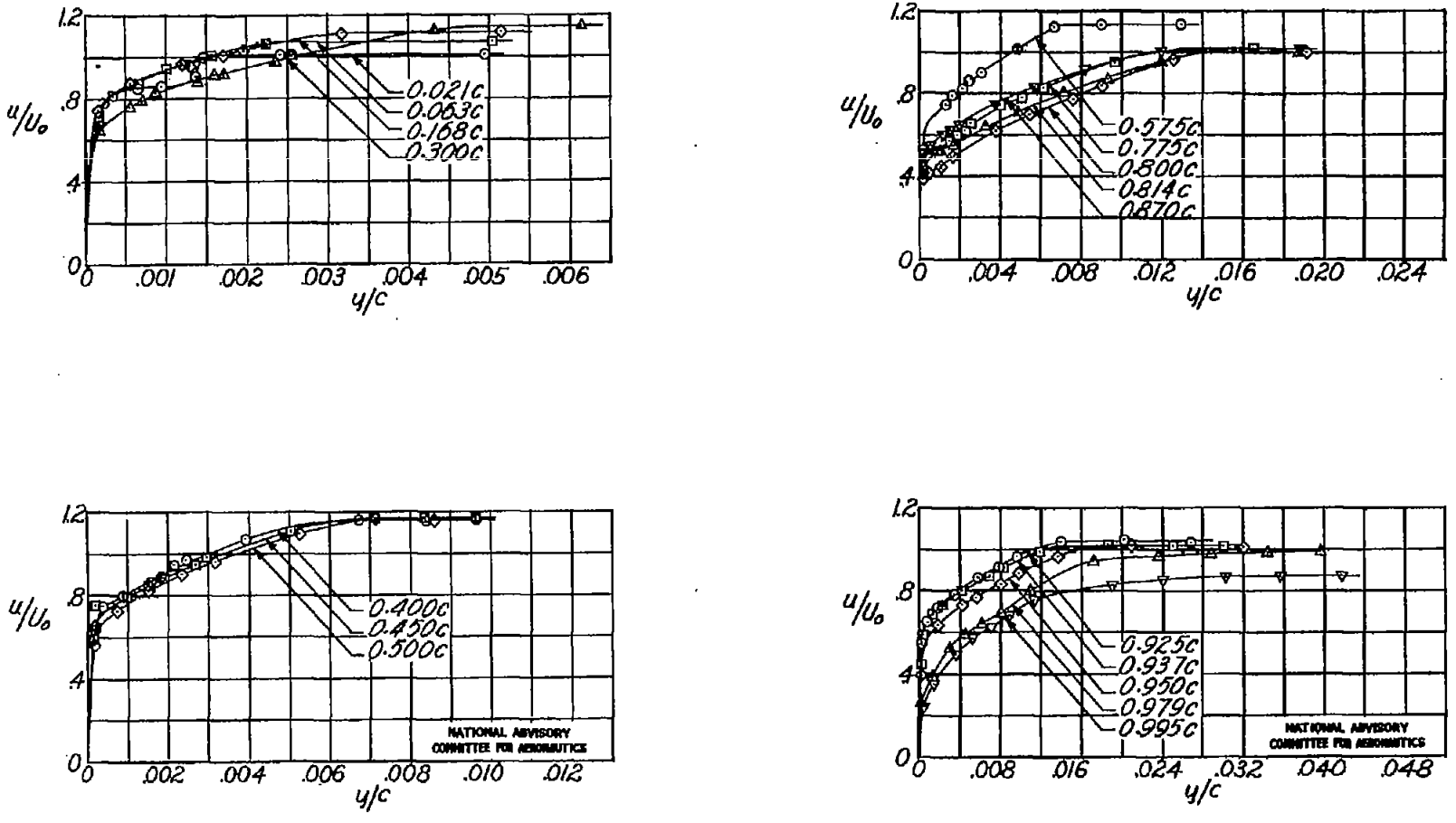

Figure 25.- Velocity profiles for the NACA 65_1-012 airfoil at $\alpha_U = 0^\circ$, $\delta = 0^\circ$, with transition strips at the leading edge. Modified-flap contour.

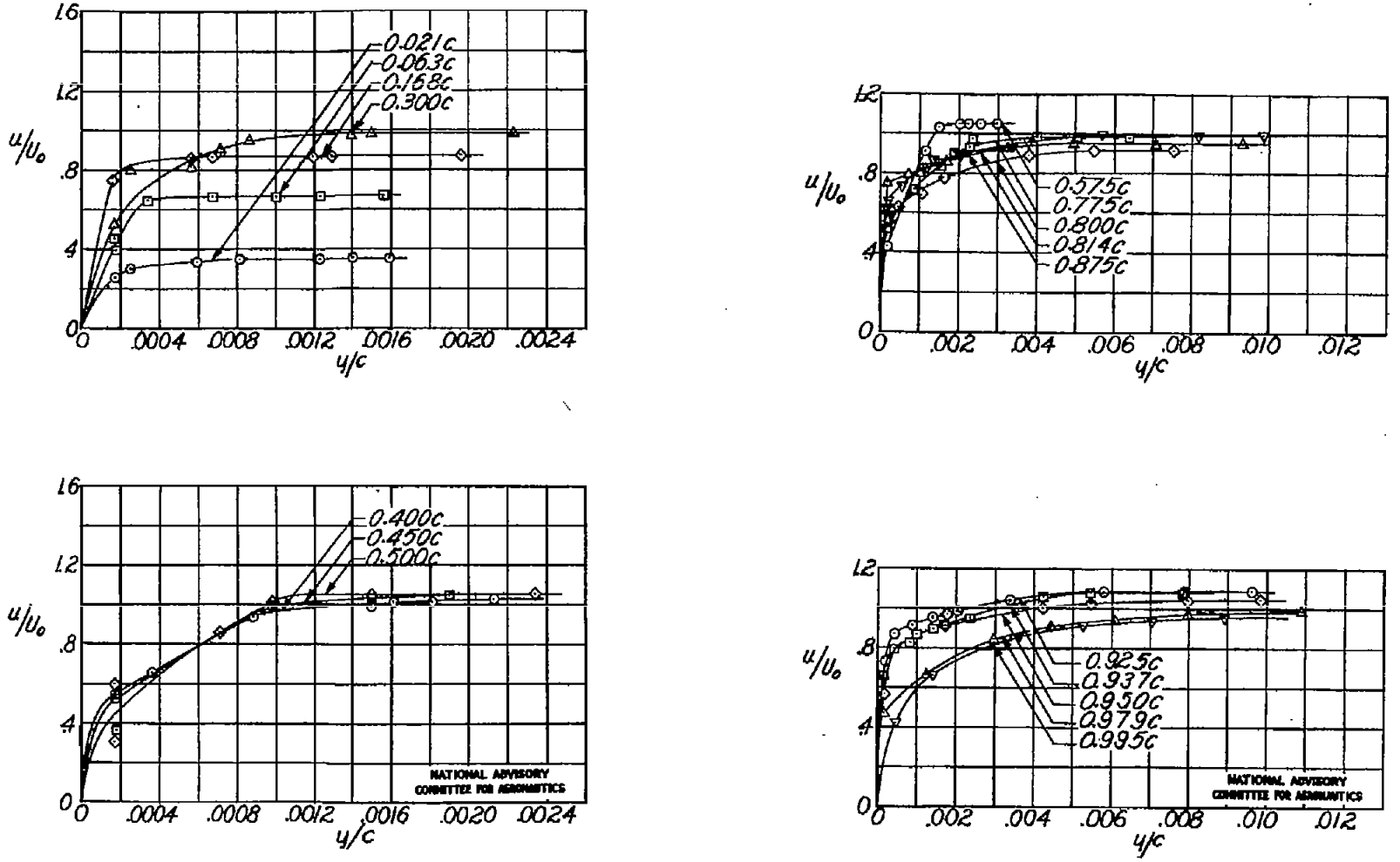

Figure 26.- Velocity profiles for the NACA 65_1-012 airfoil at $\alpha_U = -6^\circ$, $\delta = 0^\circ$, with free transition. Modified-flap contour.

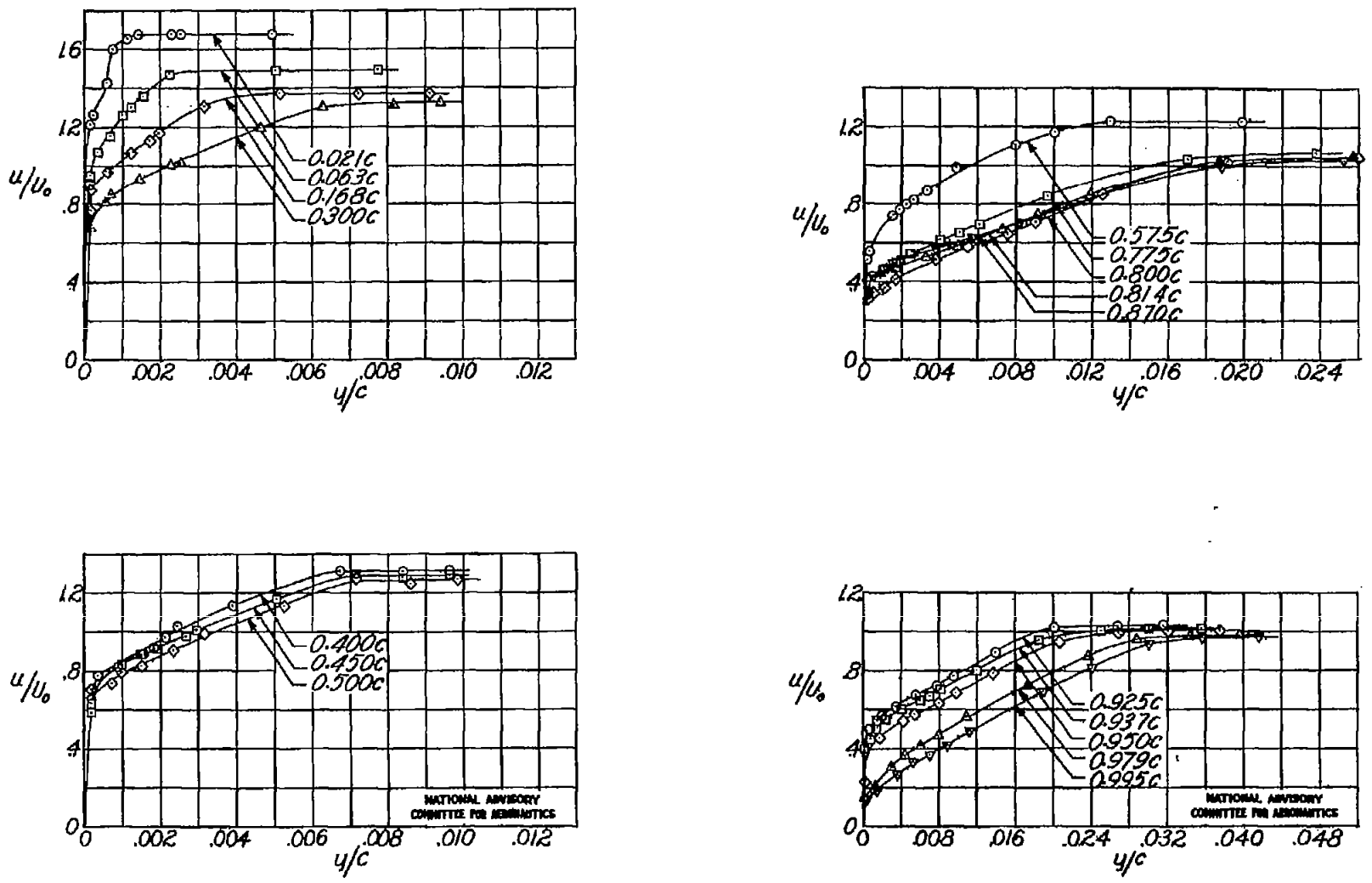

Figure 27.- Velocity profiles for the NACA 65_1-012 airfoil at $\alpha_U = 6^\circ$, $\delta = 0^\circ$, with free transition. Modified-flap contour.

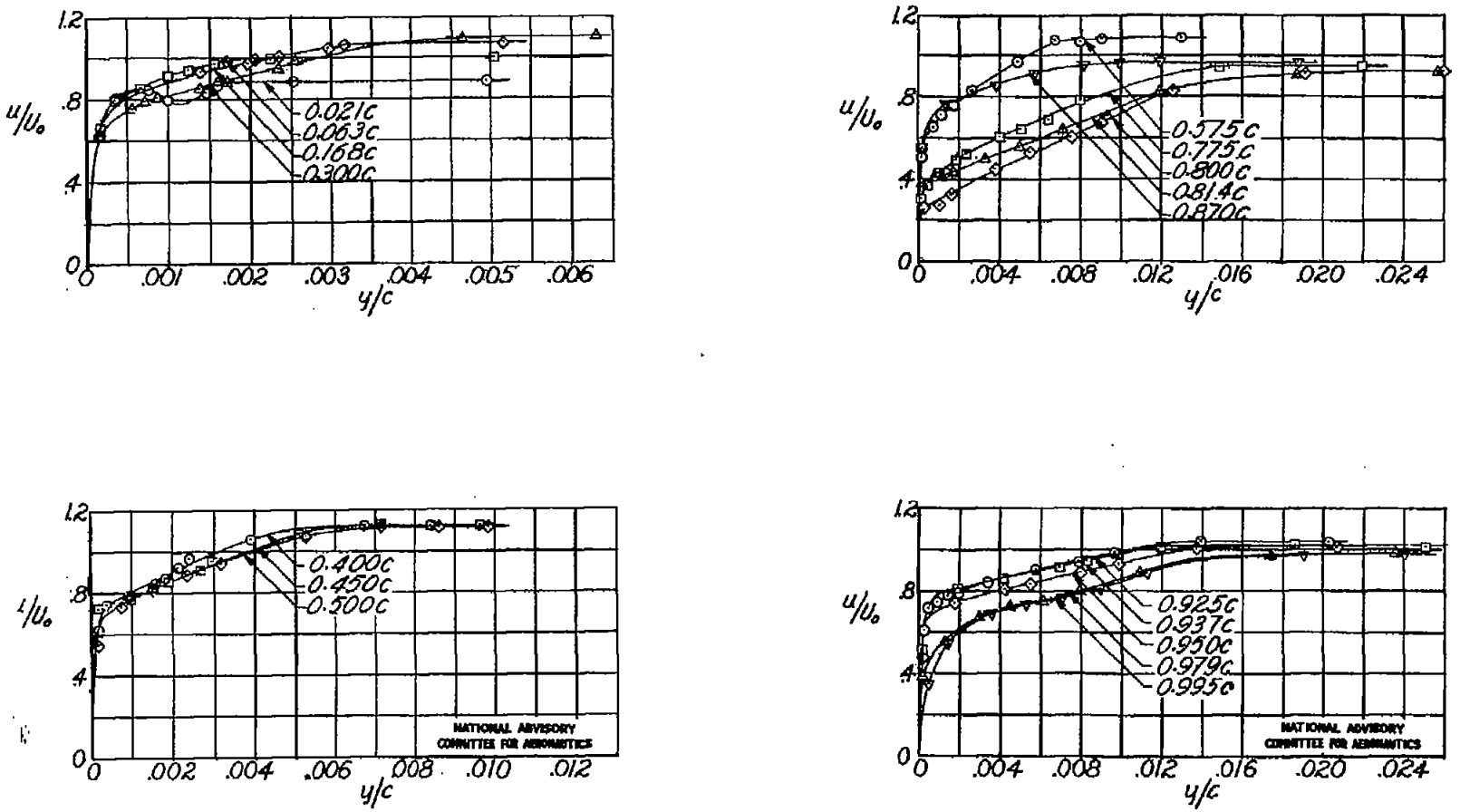

Figure 28.- Velocity profiles for the NACA 65_1-012 airfoil at $\alpha_U = 0^\circ$, $\delta = -6^\circ$, with transition strips at the leading edge. Modified-flap contour.

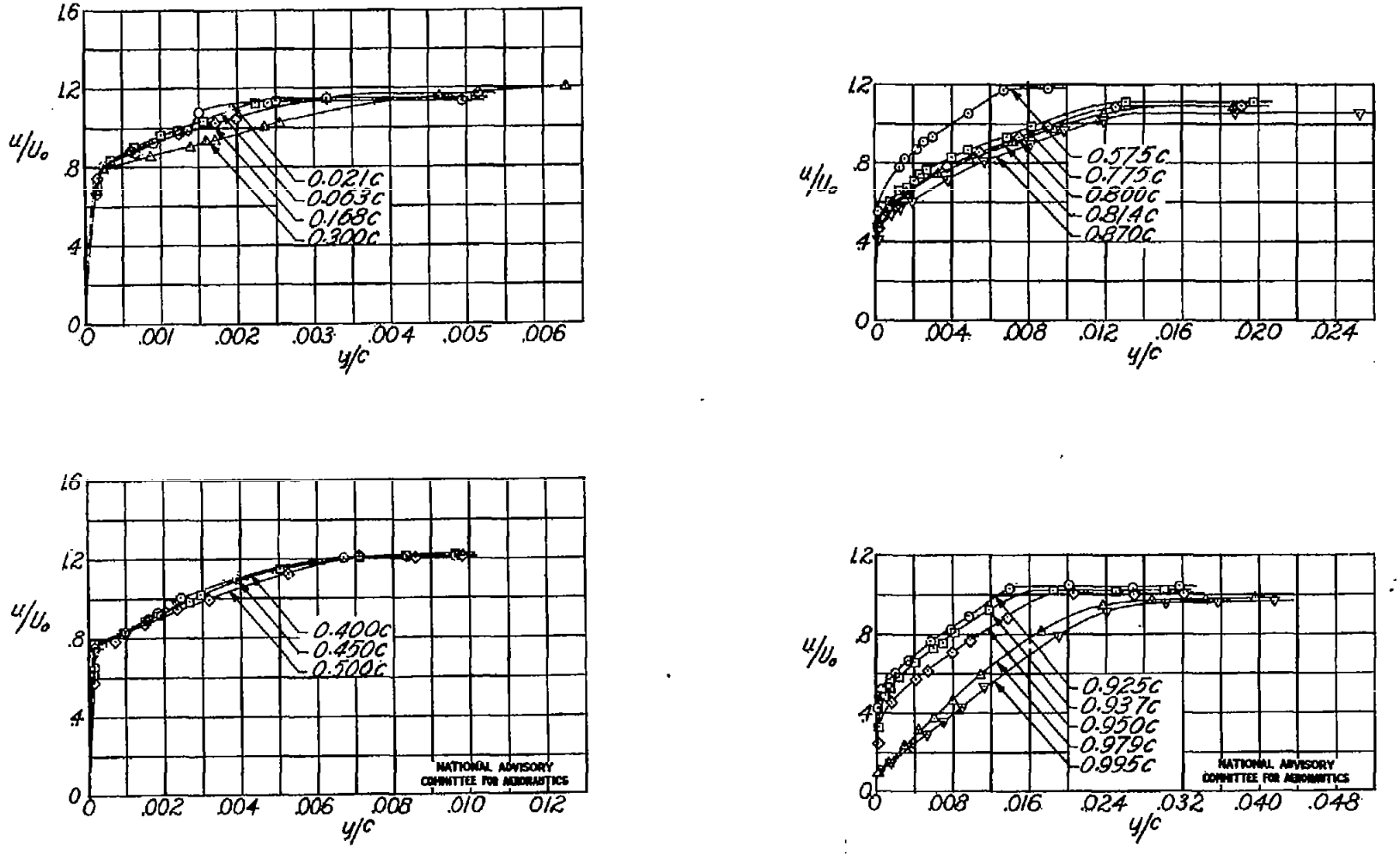

Figure 29.- Velocity profiles for the NACA 65_1-012 airfoil at $\alpha_U = 0^\circ$, $\delta = 6^\circ$, with transition strips at the leading edge. Modified-flap contour.

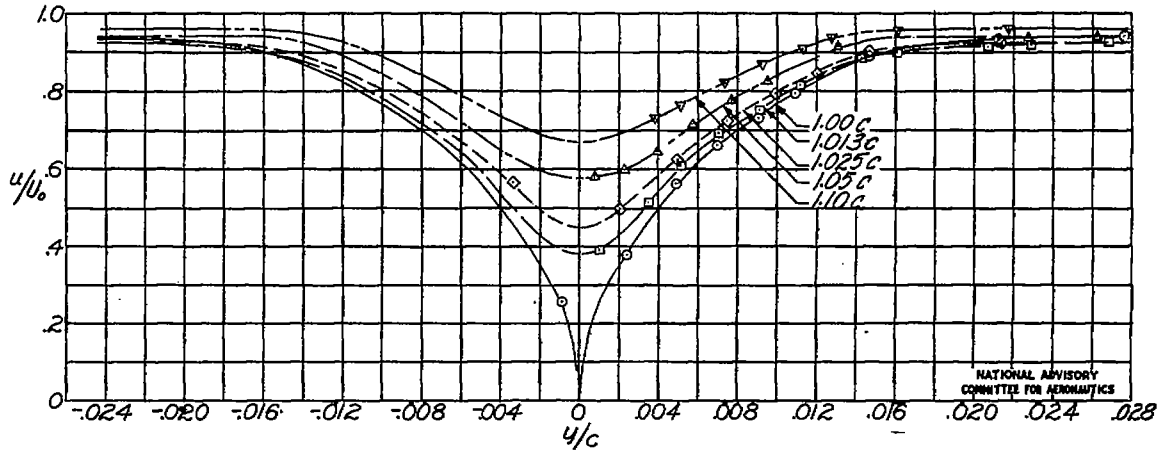

Figure 30.- Wake velocity profiles for the NACA 65_1-012 airfoil at $\alpha_U = 0^\circ$, $\delta = 0^\circ$, with transition strips at 0.50c. Modified-flap contour.

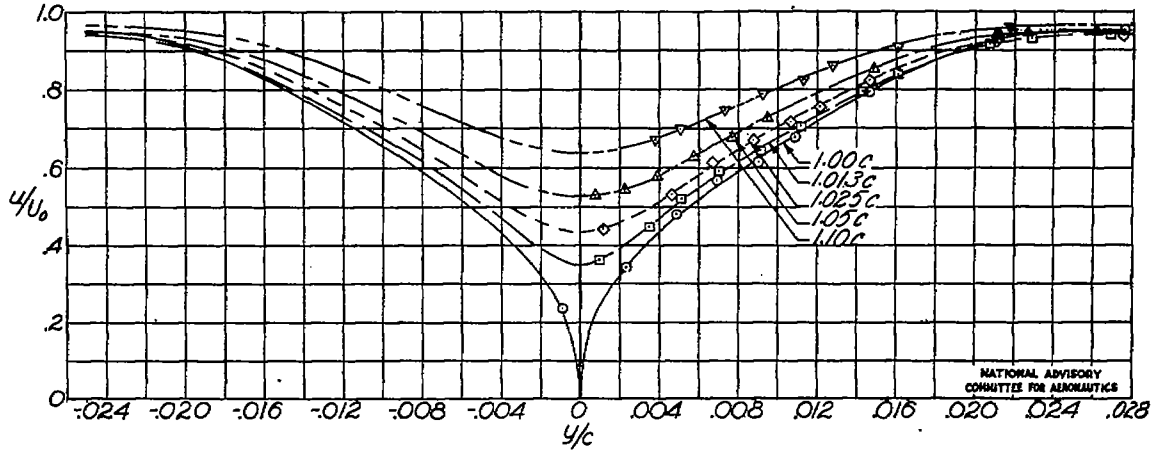

Figure 31.- Wake velocity profiles for the NACA 65_1-012 airfoil at $\alpha_U = 0^\circ$, $\delta = 0^\circ$, with transition strips at the leading edge. Modified-flap contour.

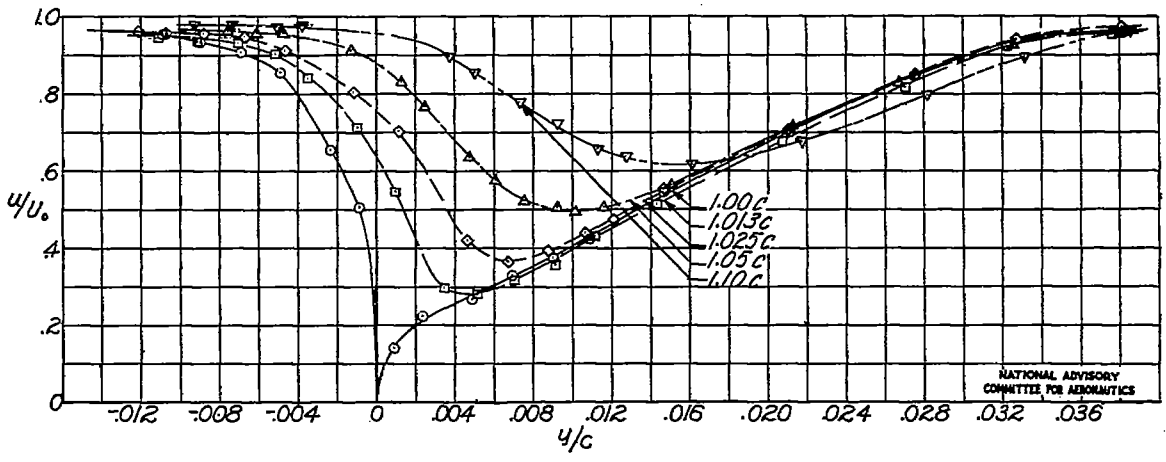

Figure 32.- Wake velocity profiles for the NACA 65_1-012 airfoil at $\alpha_U = 6^\circ$, $\delta = 0^\circ$, with free transition. Modified-flap contour.

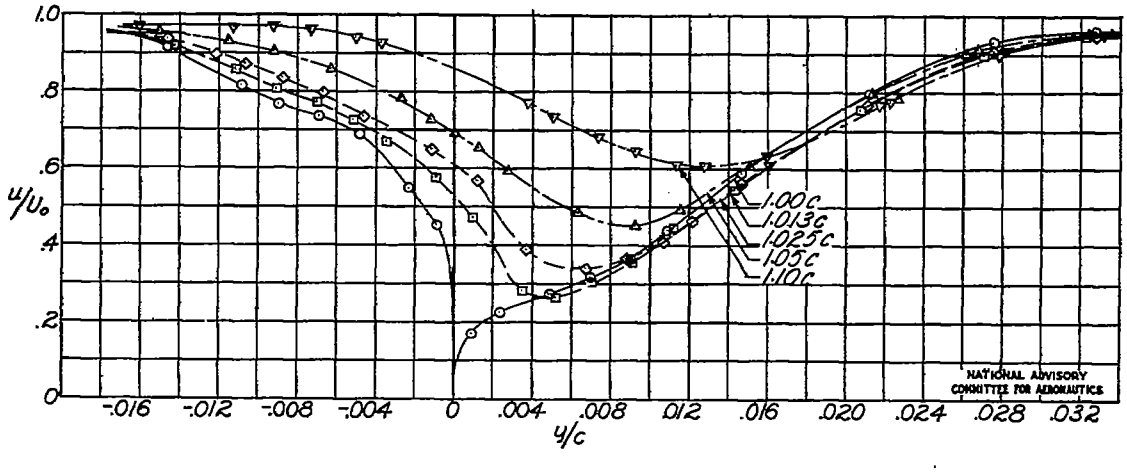

Figure 33.- Wake velocity profiles for the NACA 65_1-012 airfoil at $\alpha_U = 0^\circ$, $\delta = 6^\circ$, with transition strips at the leading edge. Modified-flap contour.

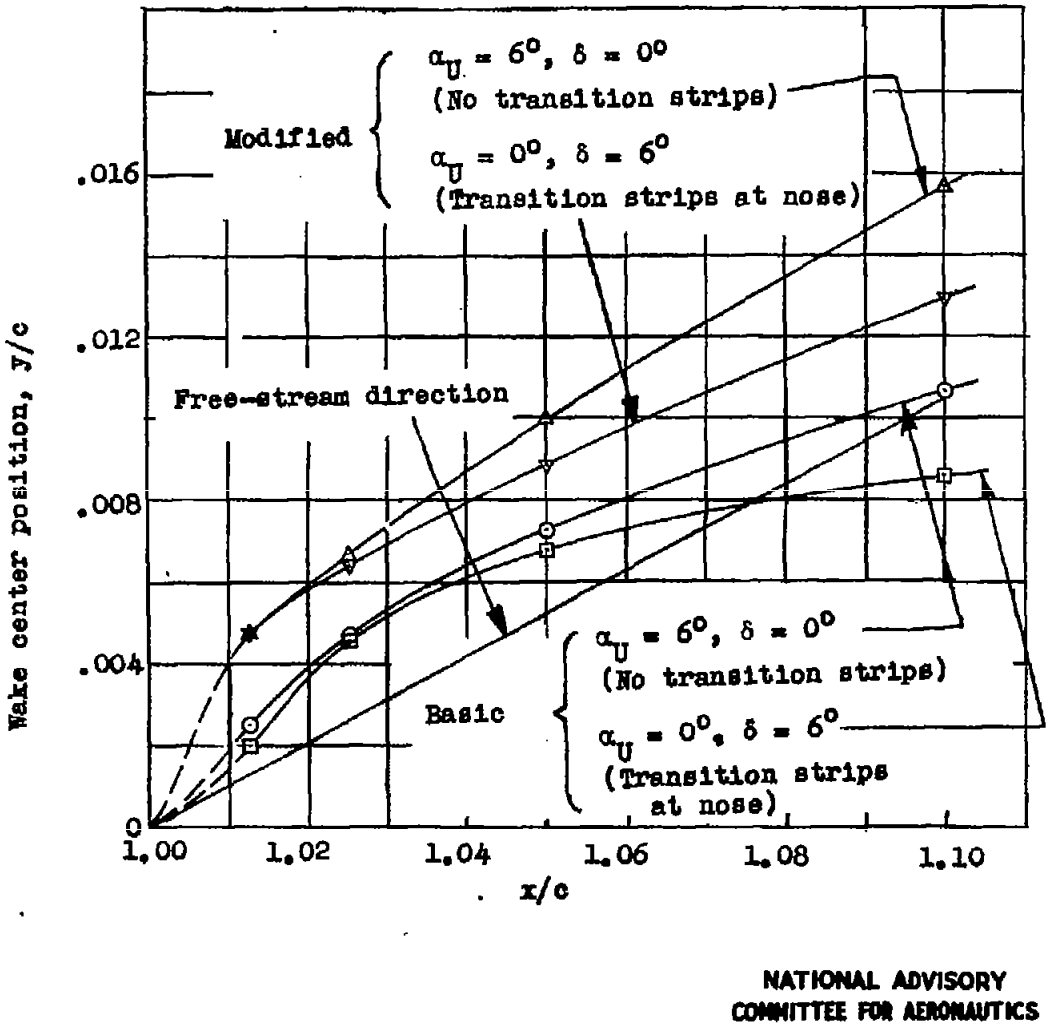

Figure 34.- Vertical position of minimum wake velocity for the NACA 65_1-012 airfoil. Basic- and modified-flap contours.

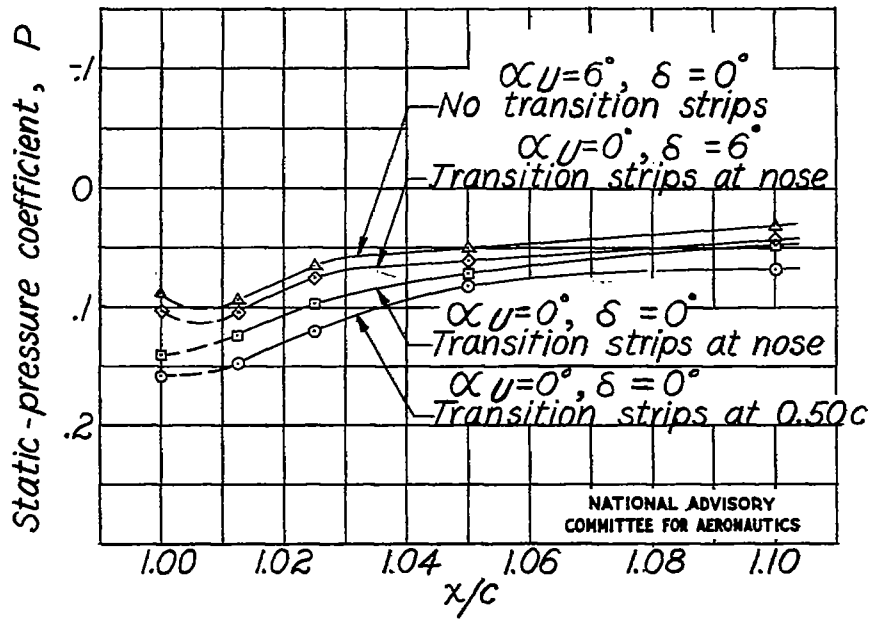

(a) Basic

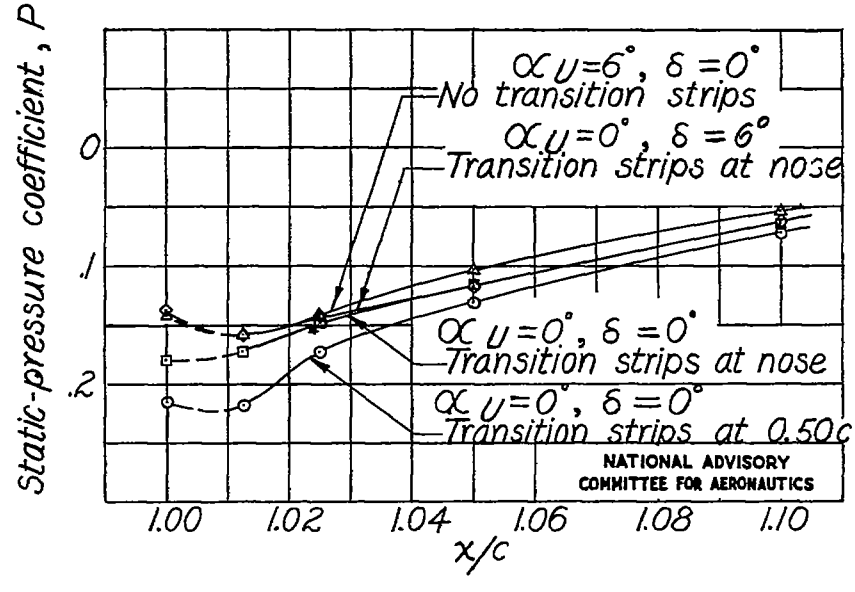

(b) Modified.

Figure 35.- Static pressure at the position of minimum velocity in the wake of the NACA 65_1-012 airfoil. Basic- and modified-flap contours.

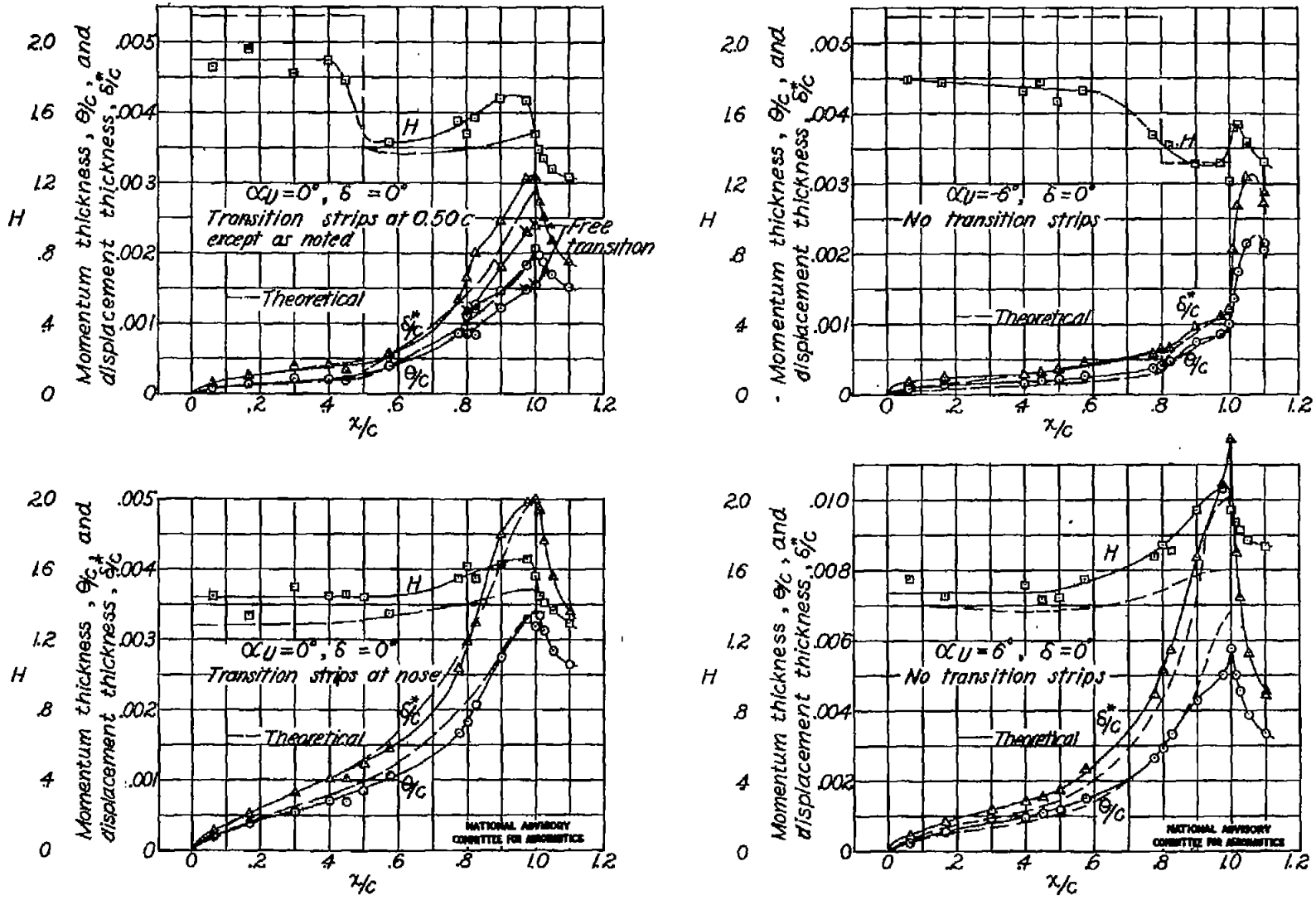

Figure 36.- Comparison of theoretical and measured boundary-layer parameters for the NACA 65_1-Q12 airfoil. Basic-flap contour.

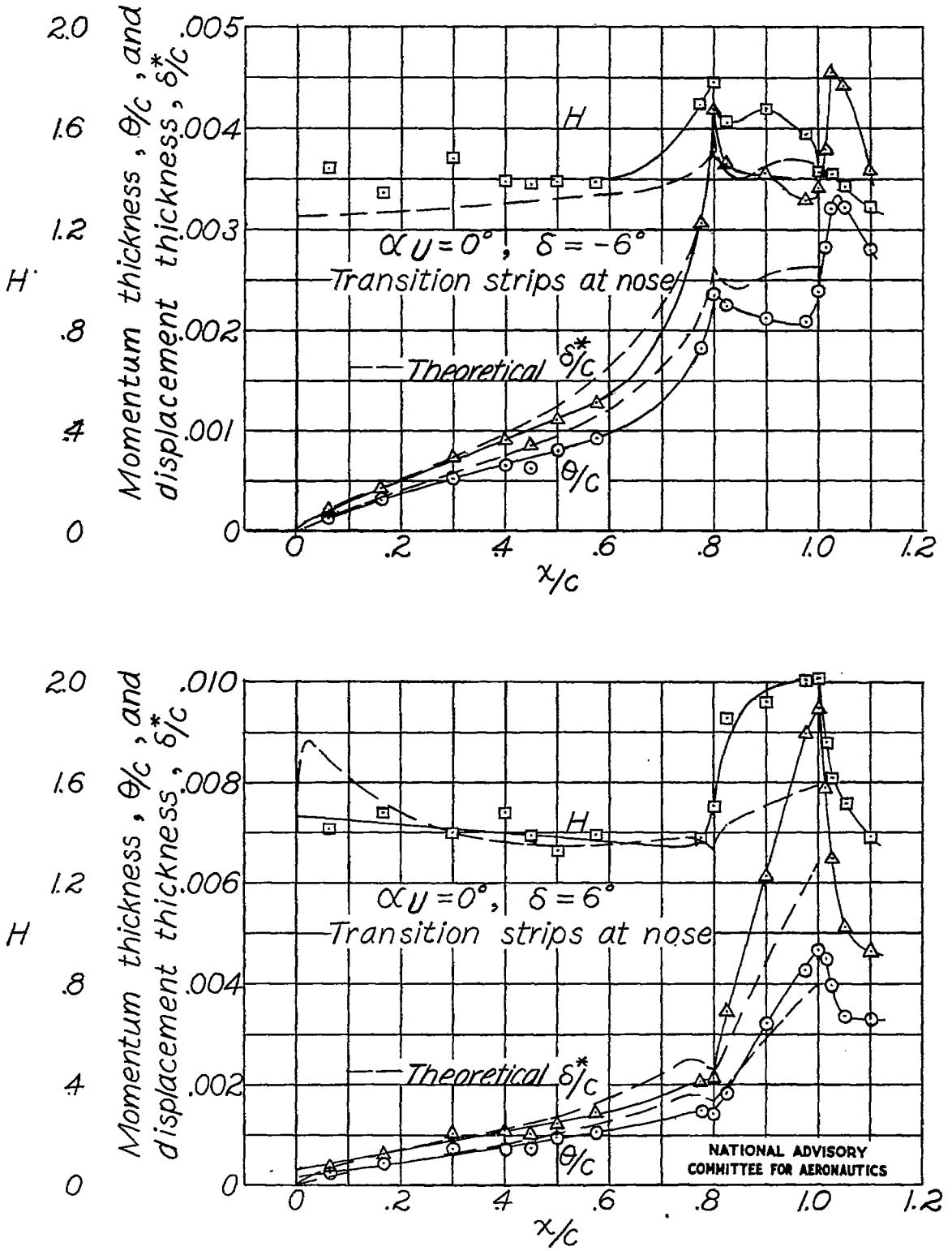

Figure 36.- Concluded.

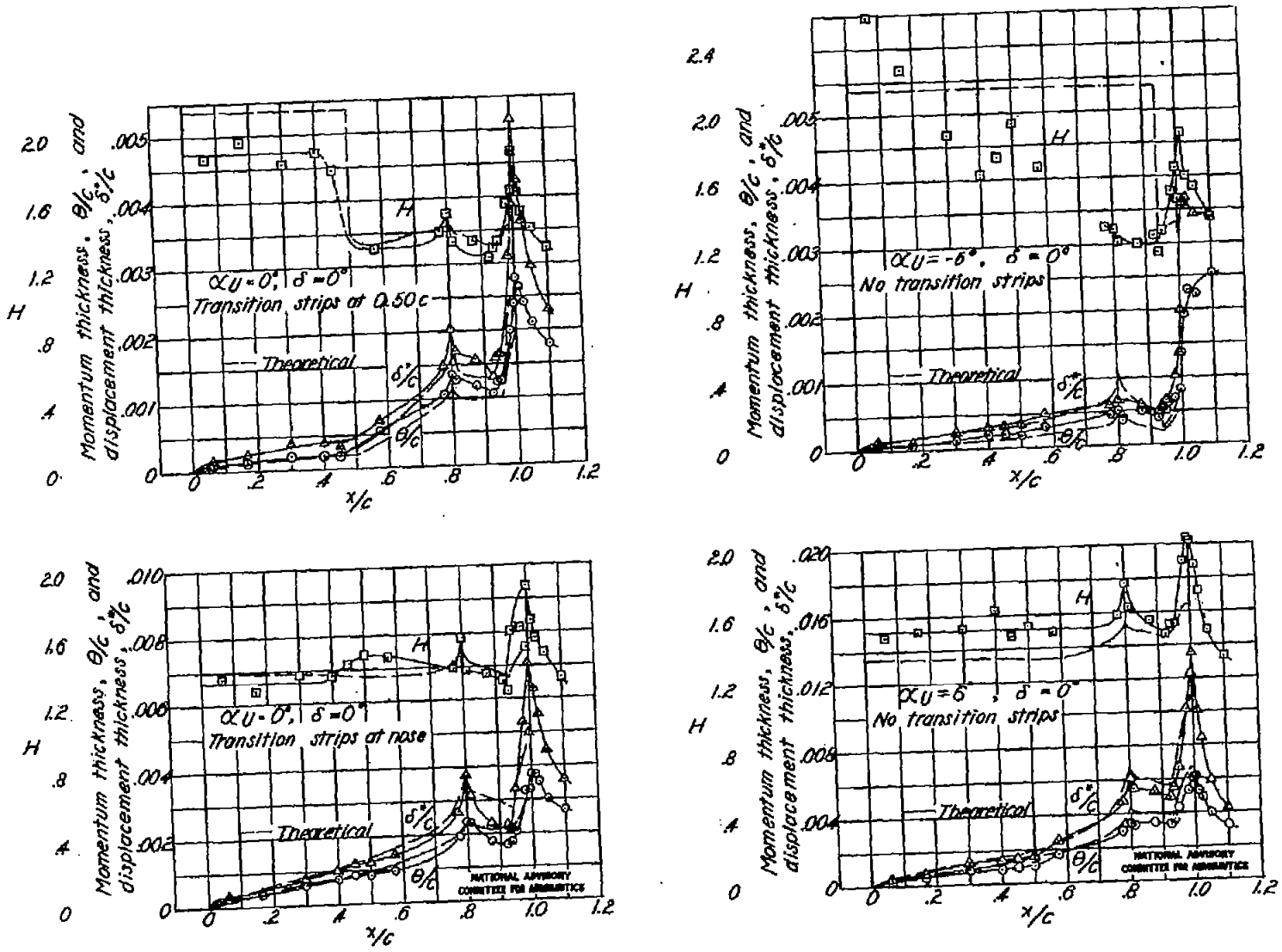

Figure 37.- Comparison of theoretical and measured boundary-layer parameters for the NACA 65_1-012 airfoil. Modified-flap contour.

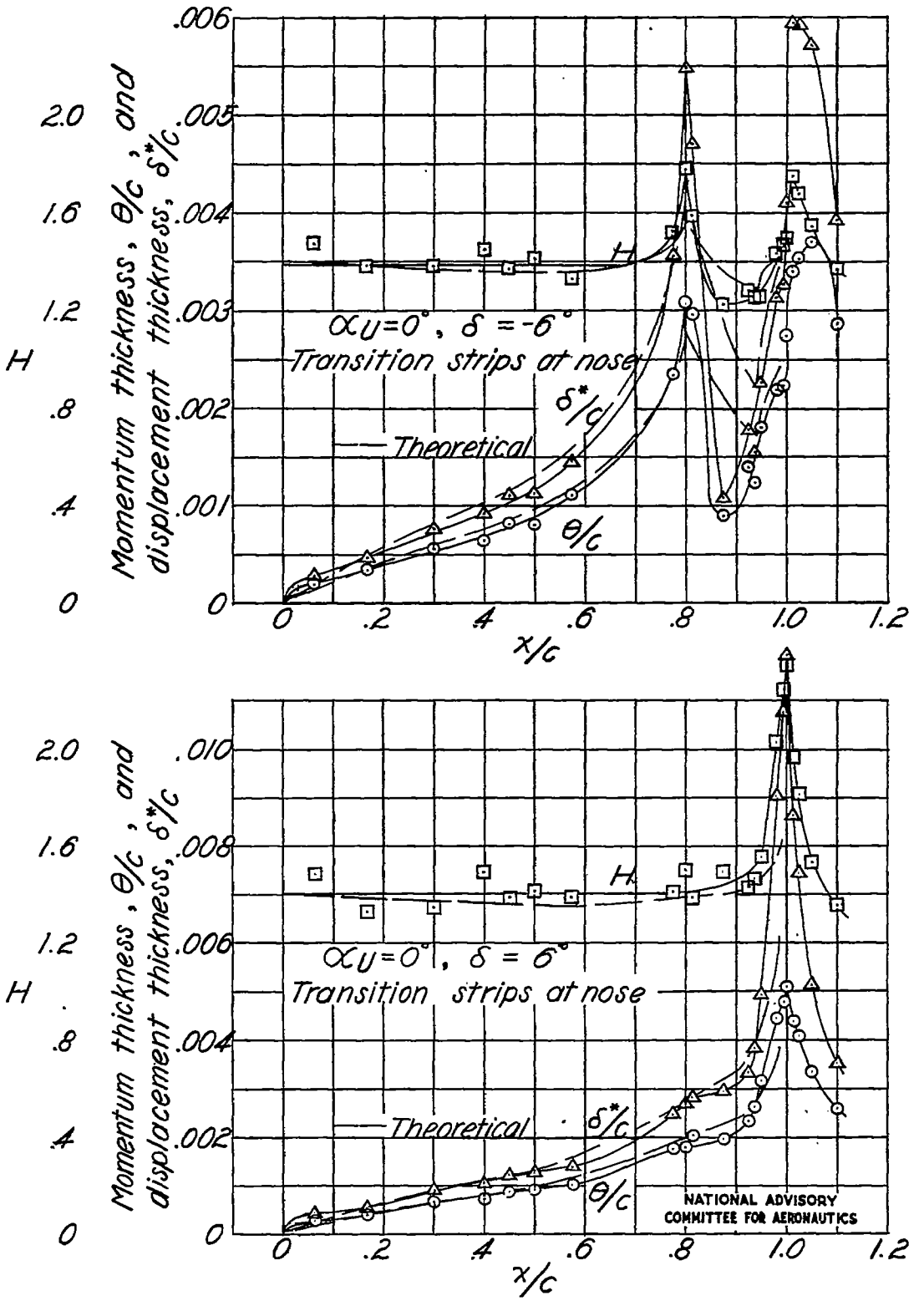

Figure 37.- Concluded.

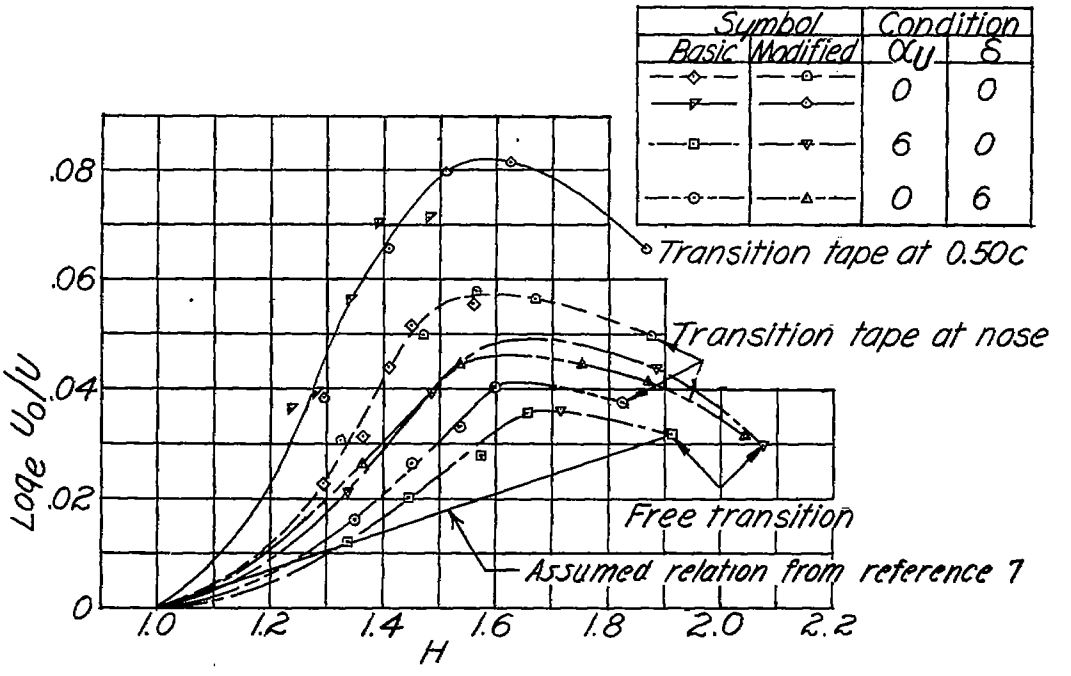

(a) Shape parameter, H.

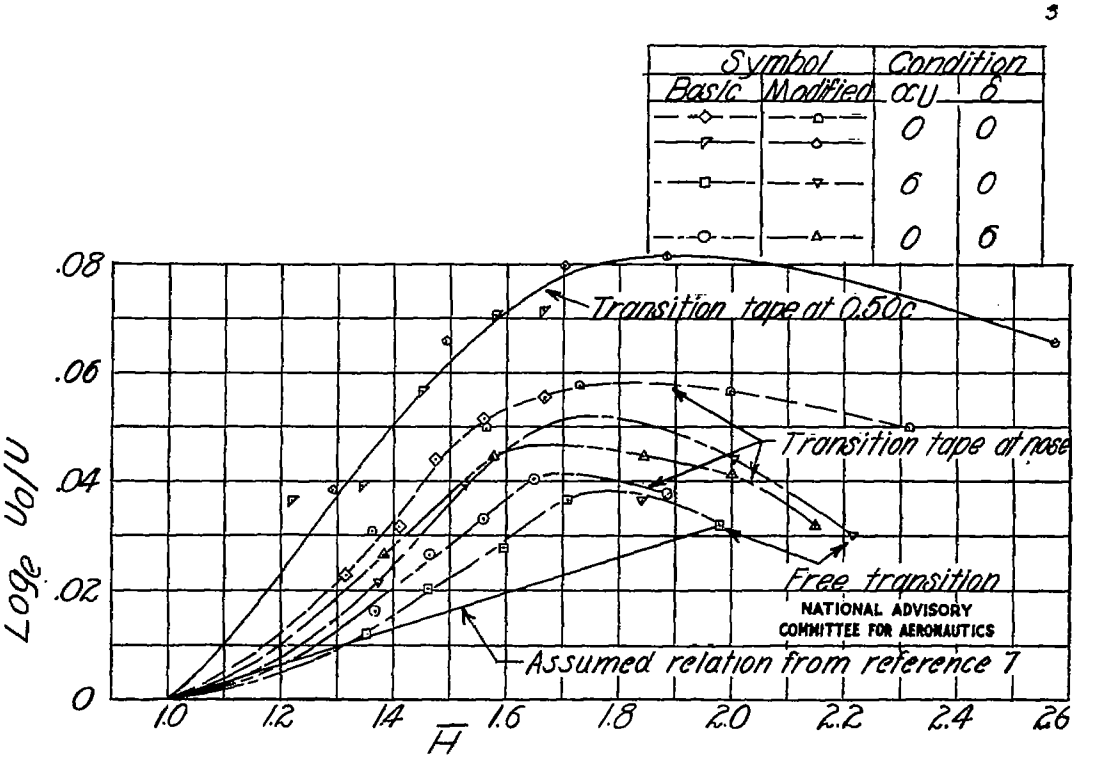

(b) Shape parameter, $\overline{H}$.

Figure 38.- Relation between velocity at the edge of the wake and the boundary-layer-shape parameter for the basic- and modified-flap contours.

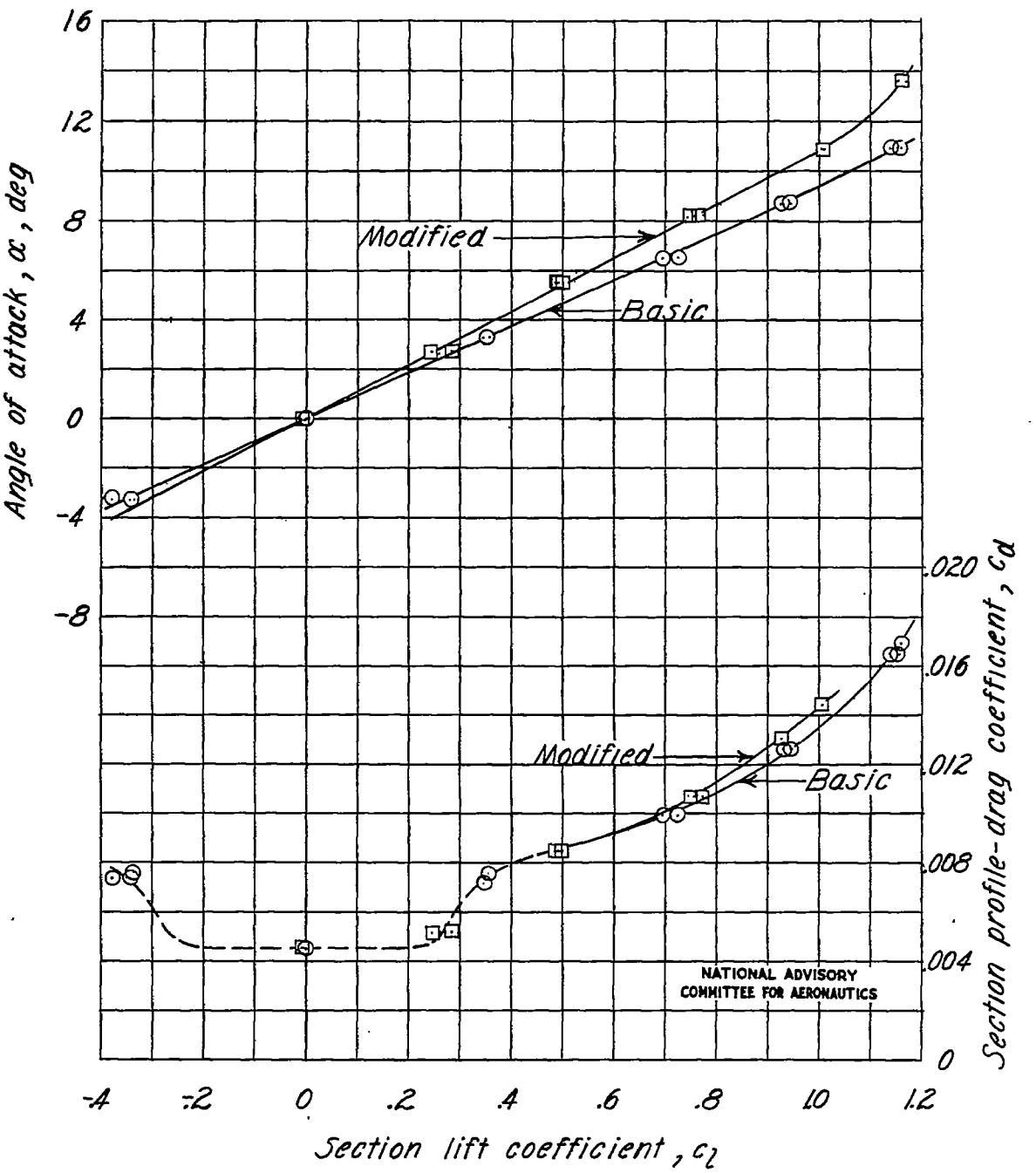

Figure 39.- Lift and drag characteristics of the NACA 65_1-012 airfoil with a basic and a modified flap. Free transition; $R = 4.64 \times 10^6$, $\delta = 0^\circ$.

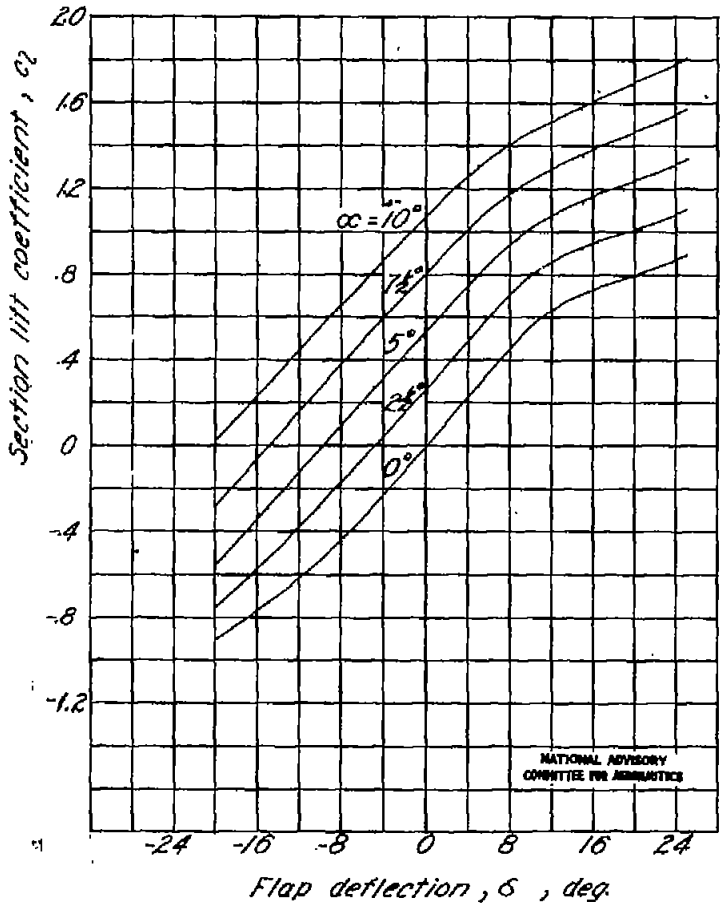

(a) Basic.

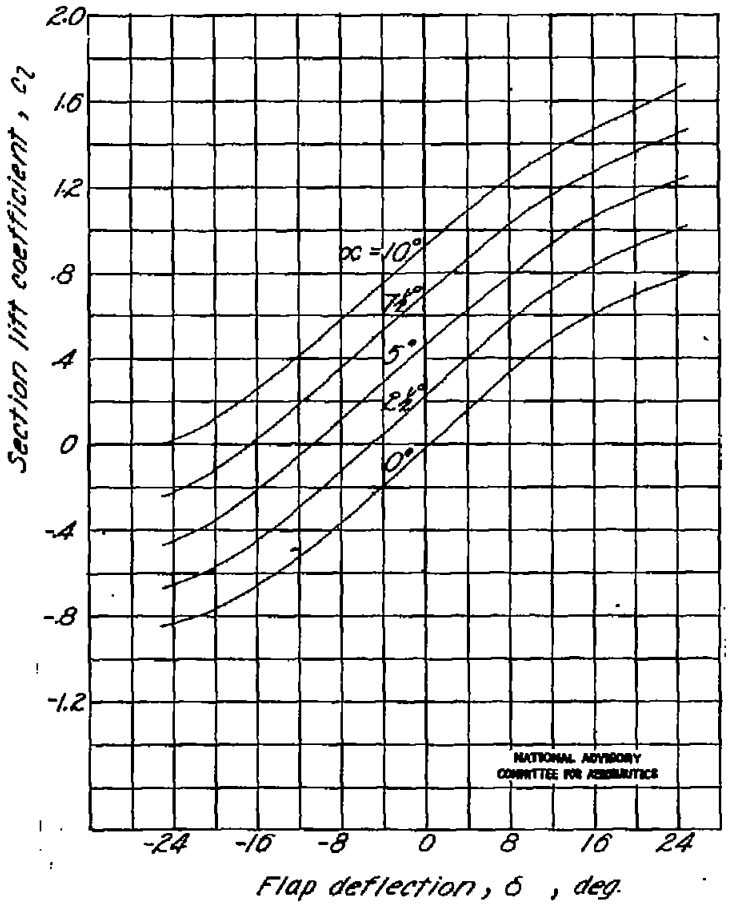

(b) Modified.

Figure 40.- Variation of section lift coefficient with flap angle for the NACA 65_1-012 airfoil with a basic and a modified flap. Free transition.

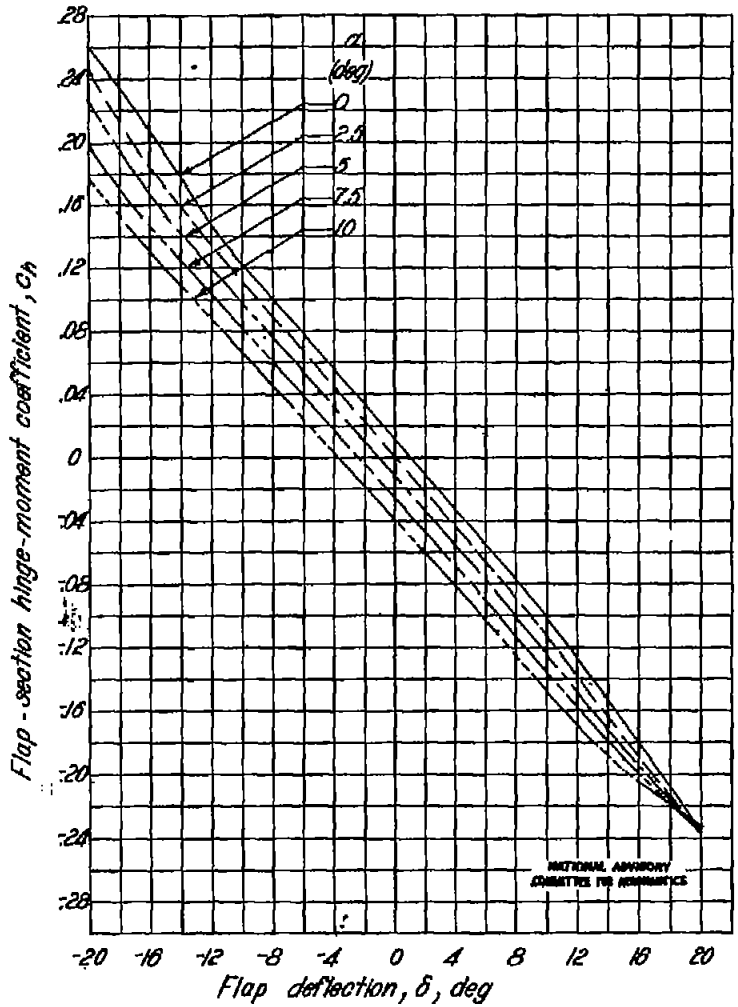

(a) Basic.

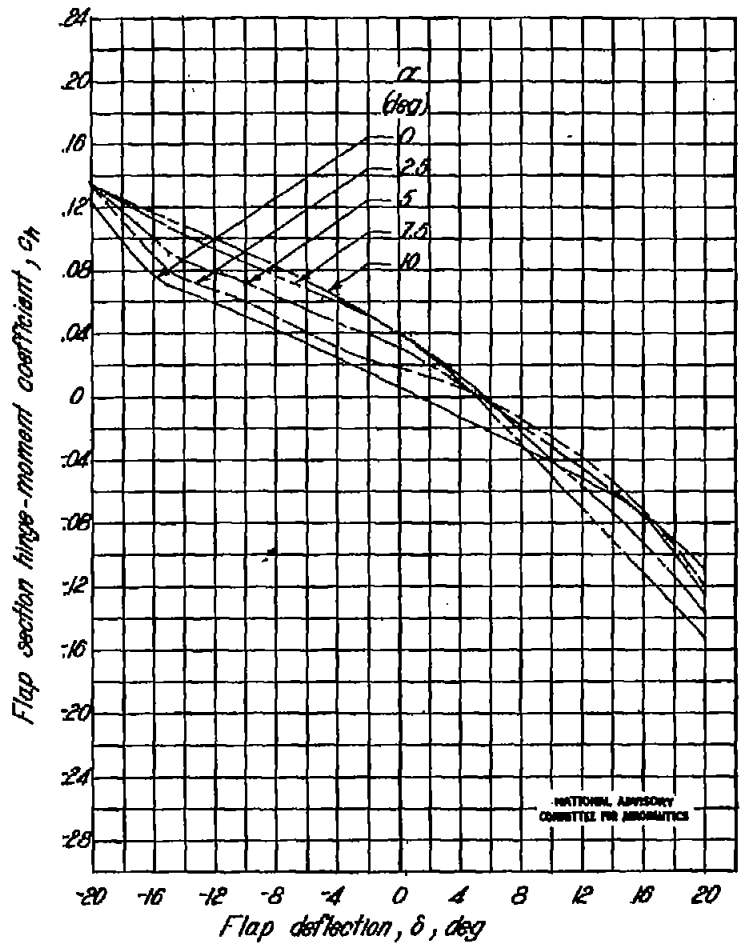

(b) Modified.

Figure 41.- Variation of flap section hinge-moment coefficient with flap deflection for the NACA 65_1-012 airfoil with a basic and a modified flap. Free transition.

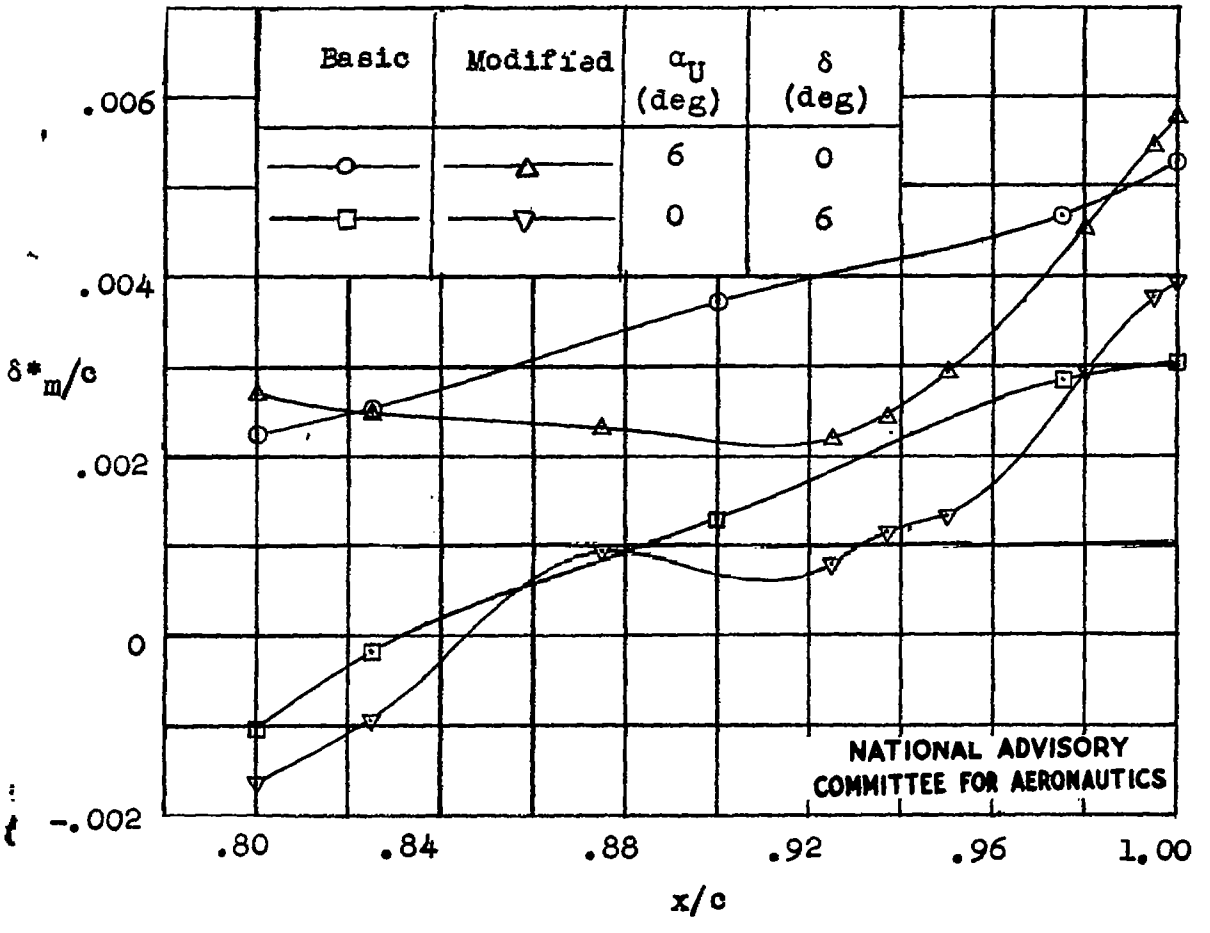

Figure 42.- Comparison of the effective-camber change on the NACA 65_1-012 airfoil. Basic- and modified-flap contours.